Technology Collaboration Programme
by IEA

International Energy Agency
Photovoltaic Power Systems Programme

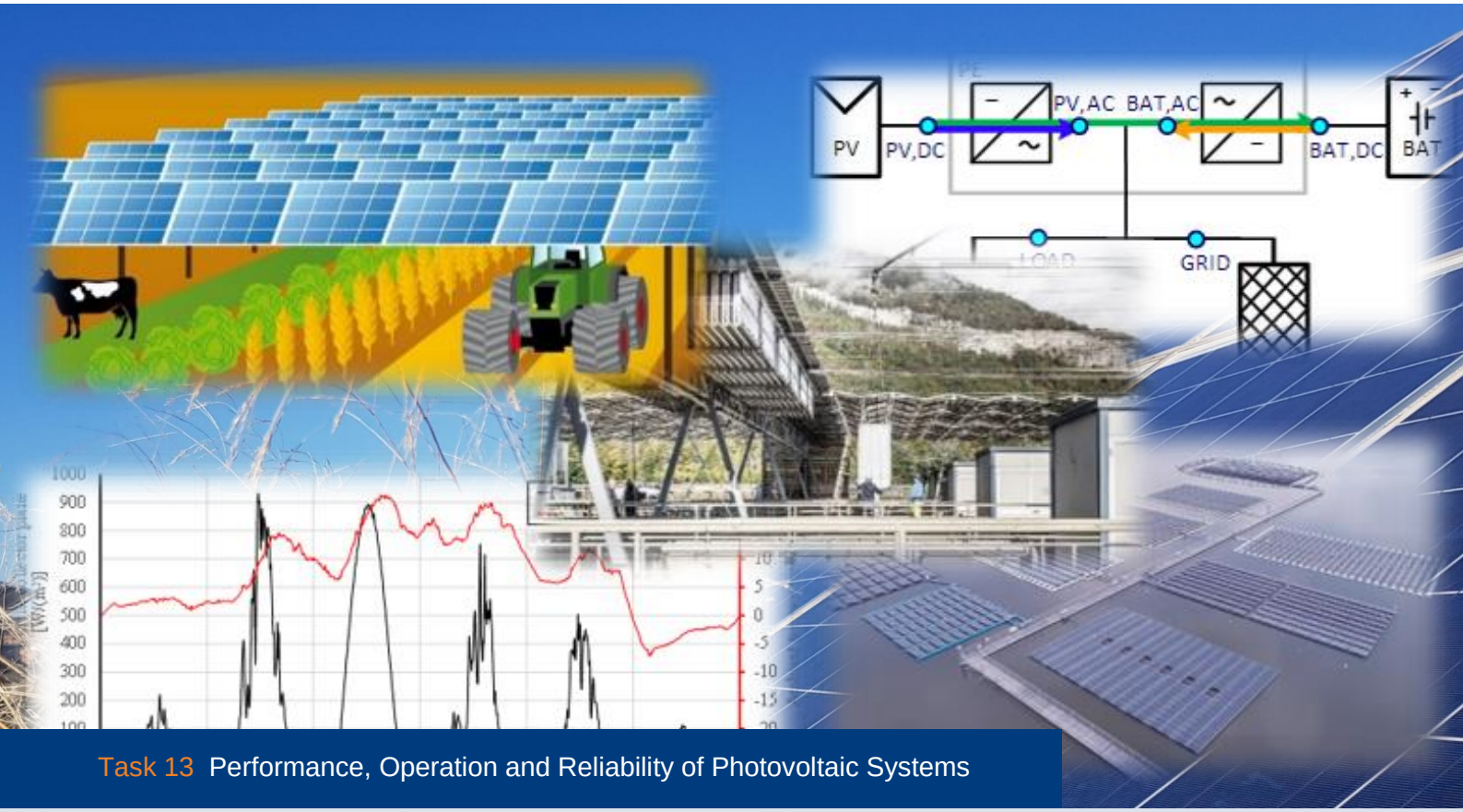


Task 13 Performance, Operation and Reliability of Photovoltaic Systems

PVPS

# Performance of New Photovoltaic System Designs

2021

Report IEA-PVPS T13-15:2021

# What is IEA PVPS TCP?

The International Energy Agency (IEA, founded in 1974, is an autonomous body within the framework of the Organization for Economic Cooperation and Development (OECD). The Technology Collaboration Programme (TCP) was created with a belief that the future of energy security and sustainability starts with global collaboration. The programme is made up of 6.000 experts across government, academia, and industry dedicated to advancing common research and the application of specific energy technologies.

The IEA Photovoltaic Power Systems Programme (IEA PVPS) is one of the TCP's within the IEA and was established in 1993. The mission of the programme is to "enhance the international collaborative efforts which facilitate the role of photovoltaic solar energy as a cornerstone in the transition to sustainable energy systems." In order to achieve this, the Programme's participants have undertaken a variety of joint research projects in PV power systems applications. The overall programme is headed by an Executive Committee, comprised of one delegate from each country or organisation member, which designates distinct 'Tasks,' that may be research projects or activity areas.

The IEA PVPS participating countries are Australia, Austria, Belgium, Canada, Chile, China, Denmark, Finland, France, Germany, Israel, Italy, Japan, Korea, Malaysia, Mexico, Morocco, the Netherlands, Norway, Portugal, South Africa, Spain, Sweden, Switzerland, Thailand, Turkey, and the United States of America. The European Commission, Solar Power Europe, the Smart Electric Power Alliance (SEPA, the Solar Energy Industries Association and the Cop- per Alliance are also members.

**Visit us at: www.iea-pvps.org**

# What is IEA PVPS Task 13?

Within the framework of IEA PVPS, Task 13 aims to provide support to market actors working to improve the operation, the reliability and the quality of PV components and systems. Operational data from PV systems in different climate zones compiled within the project will help provide the basis for estimates of the current situation regarding PV reliability and performance.

The general setting of Task 13 provides a common platform to summarize and report on technical aspects affecting the quality, performance, reliability and lifetime of PV systems in a wide variety of environments and applications. By working together across national boundaries we can all take advantage of research and experience from each member country and combine and integrate this knowledge into valuable summaries of best practices and methods for ensuring PV systems perform at their optimum and continue to provide competitive return on investment.

Task 13 has so far managed to create the right framework for the calculations of various parameters that can give an indication of the quality of PV components and systems. The framework is now there and can be used by the industry who has expressed appreciation towards the results included in the high-quality reports.

The IEA PVPS countries participating in Task 13 are Australia, Austria, Belgium, Canada, Chile, China, Denmark, Finland, France, Germany, Israel, Italy, Japan, the Netherlands, Norway, Spain, Sweden, Switzerland, Thailand, and the United States of America.



**COVER PICTURE**

Exemplary graphical overview of subtask 1.3 topics. (Sources: Fraunhofer ISE, ISFH, dhp technology, SPF Institute for Solar Technology, SERIS)

**ISBN** 978-3-907281-04-8: Report IEA-PVPS T13-15:2021 Performance of New Photovoltaic System Designs

INTERNATIONAL ENERGY AGENCY

PHOTOVOLTAIC POWER SYSTEMS PROGRAMME

IEA PVPS Task 13

Performance, Operation and Reliability of Photovoltaic Systems

# Performance of New Photovoltaic System Designs

Report IEA-PVPS T13-15:2021

April 2021

ISBN 978-3-907281-04-8

# AUTHORS


**Main Authors**

Franz Baumgartner, Zurich University of Applied Science (ZHAW), Zurich, Switzerland

Mike Green, Green Power Engineering, Ra'anana, Israel

Matthias Littwin, Institute for Solar Energy Research Hamelin (ISFH), Emmerthal, Germany

Wilfried van Sark, Utrecht University (UU), Utrecht, Netherlands

**Contributing Authors**

Cyril Armand Allenspach, Zurich University of Applied Science (ZHAW), Zurich, Switzerland

Evelyn Bamberger, SPF Institute for Solar Technology, Rapperswil, Switzerland

Christof Biba, SPF Institute for Solar Technology, Rapperswil, Switzerland

Christopher Deline, National Renewable Energy Laboratory, (NREL), Golden, CO, USA

Roger French, Solar Durability and Lifetime Extension Research Center (SDLE), Case Western Reserve University (CWRU), Cleveland, OH, USA

Daniel Gfeller, Bern University of Applied Science (BFH), Bern, Switzerland

Sara Mirbagheri Golroodbari, Utrecht University (UU), Utrecht, Netherlands

Marc Köntges, Institute for Solar Energy Research Hamelin (ISFH), Emmerthal, Germany

Christian Messner, Austrian Institute of Technology GmbH, Center for Energy (AIT), Vienna, Austria

Urs Muntwyler, Bern University of Applied Science (BFH), Bern, Switzerland

Rosmarie Neukomm, Bern University of Applied Science (BFH), Bern, Switzerland

Daniel Riley, SANDIA National Laboratory (SNL), Livermore, CA, USA

Davide Rivola, Scuola universitaria professionale della Svizzera italiana (SUPSI), Manno, Switzerland

Joshua Stephenson Stein, SANDIA National Laboratory (SNL), Albuquerque, NM; USA

Max Trommsdorff, Fraunhofer Institute for Solar Energy Systems (ISE), Freiburg, Germany

**Editors**

Matthias Littwin, Institute for Solar Energy Research Hamelin (ISFH), Emmerthal, Germany

Ulrike Jahn, TÜV Rheinland, Cologne, Germany

# TABLE OF CONTENTS

# ACKNOWLEDGEMENTS

This paper received valuable contributions from several IEA-PVPS Task 13 members and other international experts. Many thanks to:

Thomas Schott, Bern University of Applied Science (BFH), Bern, Switzerland

This report is supported by the State of Lower Saxony, Swiss Federal Office of Energy (SFOE) under contract number 8100073, project number SI/501788 supporting the IEA PVPS Task 13 actions, Swiss competence center for Energy research (future grids SCCER-FURIES), United States Department of Energy Office (DOE), Office of Energy Efficiency and Renewable Energy, IEA-ISGAN SIRFN is being carried out as part of the IEA research cooperation on behalf of Austrian Federal Ministry for Climate Action, Environment, Energy, Mobility, Innovation and Technology (BMK), The Netherlands Enterprise Agency (RVO), Green Power Engineering Ltd., Netherlands Ministry of Economic Affairs and Climate (EZK) and German Federal Ministry of Economic Affairs and Energy (BMWi) under grant number 0324304A, 0324304B, 0324304C project “Joint project: Task13-3 - Management and participation in Task 13 'Performance, Operation and Reliability of Photovoltaic Systems' Phase 2018 - 2021 within the Photovoltaic Power Systems (PVPS) Programme of the International Energy Agency (IEA).

# LIST OF ABBREVIATIONS

| Abbreviation | Description |
|---|---|
| AC | Alternating current |
| agri | Agrivoltaics |
| APV | Agrivoltaics, or agrophotovoltaics |
| ARENA | Australian Renewable Energy Agency |
| ASTM | ASTM International, formerly known as American Society for Testing and Materials, is an international standards organization |
| BAT2AC | Discharge power path from the battery to AC |
| BOS | Balance of system, non-PV-module components in a PV system |
| BSW | German Solar Industry Association |
| BVES | German Energy Storage Association |
| c-Si | Crystalline silicon |
| CCT | Concise cycle test |
| CEC | California Energy Commission |
| DC | Direct current |
| DHW | Drink hot water |
| DKE | German Commission for Electrical, Electronic & Information Technologies |
| DUT | Device under test |
| elec | Electrical |
| EMS | Energy management system |
| EN | European Norm |
| FONA | Research for Sustainable Development, funding framework of the German Federal Ministry of Education and Research |
| FPV | Floating photovoltaic |
| FTCC | Floating, tracking, cooling, concentrating |
| GCP | Grid connection point |
| GM | Ground-mounted |
| HHL | Household load |
| IEA | International Energy Agency |
| IEC | International Electrotechnical Commission |
| IR | Infrared |
| KPI | Key performance indicator |
| LED | Light emitting diode |
| LTM4611 | DC/DC micro module regulator |

| | |
|---|---|
| LV | Low voltage |
| max | Maximum |
| MI | Microinverter |
| MIE | Module integrated electronic |
| MLPE | Module level power electronic |
| MOSFET | Metal-oxide-semiconductor field-effect transistor |
| MPP | Maximum power point |
| MPPT | Maximum power point tracker |
| MWT | Metal wrap through technology for crystalline silicon solar cells |
| nom | Nominal |
| OC | Open circuit |
| PAR | Photosynthetic active radiation |
| PAT | Performance acceptance test |
| POA | Plane of array |
| PV | Photovoltaic |
| PV2AC | Power path PV power for direct load coverage and grid feed-in |
| PV2BAT | Power path PV power for battery charging (AC system PV2BAT consists of PV2AC and AC2BAT) |
| PVC | Polyvinyl chloride |
| PVsyst | Software package for the study, sizing and data analysis of complete PV systems |
| Ref | Reference |
| SAS | Solar array simulator |
| SC | Short cut |
| SI | String inverter |
| SOC | State of charge of a battery |
| STC | Standard test conditions |
| UV | Ultraviolet |
| ZENIT | Software tool developed by Fraunhofer ISE, to simulate the overall electrical yield of a photovoltaic system implementing chain of loss models |

# LIST OF SYMBOLS

| Symbol | Description | Unit |
|---|---|---|
| *AMa* | Airmass | - |
| *C* | State of charge of a battery | kWh |
| $C_0$ | Unitless empirical coefficient describing the linear relationship between the irradiance and the PV AC module output power, typical values near 1 | - |
| $C_1$ | Unitless empirical coefficient describing the logarithmic relationship between the irradiance on the PV AC module output power | - |
| $E_{Bat}$ | Energy the battery storage system supplied during the coffee making process | kWh |
| $E_{consumption}$ | Total energy consumption | kWh |
| $E_{grid\text{-}feed\text{-}in}$ | Electric energy supplied to the grid | kWh |
| $E_{grid\text{-}purchase}$ | Electric energy from the grid | kWh |
| $R_{net}$ | Grid purchase ratio | % |
| $E_{HH}$ | Household electricity (without heat pump). | kWh |
| $EN_{AC}$ | Measured AC electrical generation of the PV system | kW |
| $E_{Nespresso}$ | Energy totally used for coffee making by the coffee machine | kWh |
| $E_{POA}$ | Broadband POA irradiance incident upon the module which reaches the active PV material. $E_{POA}$ is estimated from measured broadband POA irradiance by accounting for the module losses due to specular reflection and/or acceptance of diffuse irradiation. | W/m² |
| $E_{PV\text{-}yield}$ | Produced PV electricity, measurement on the DC and AC lines; the AC current measurement is used for the energy balance. | kWh |
| $E_{ref}$ | Reference POA irradiance | W/m² |
| $E_{supplied}$ | Amount of energy fed into the system | kWh |
| $E_{used}$ | Amount of energy from PV used to cover the load and fed into the grid | kWh |
| $E_{use}$ | Total useful energy demand for household electricity, domestic hot water and space heating | kWh |
| $f_1$ | Empirical unitless function which modifies the PV AC module output power as a function of absolute (pressure corrected) airmass relative to the reference absolute airmass | - |
| $G_{POA}$ | Measured plane of array irradiance | W/m² |
| $G_{STC}$ | Irradiance at standard test conditions (1 000 W/m$^2$) | W/m² |
| *i* | a given point in time | - |
| *I* | Current | A |

| | | |
|---|---|---|
| $LER$ | Land equivalent ratio | - |
| $LL$ | Land losses | - |
| $M$ | Voltage boost ratio | - |
| $N$ | Total number of DC/DC optimizers in a system | - |
| $n_g$ | Number of solar cells in a cell group $N_G$ | - |
| $N_G$ | Number of cell groups in a PV module | - |
| $P$ | Power | W |
| $P_1$ | PV AC module power in typical operation state | W |
| $P_2$ | PV AC module power in self-limiting state | W |
| $P_3$ | PV AC module power in low-irradiance state | W |
| $P_{AC,max}$ | Maximum AC output power of a PV AC module | W |
| $P_{Bat,AC}$ | Charge condition-dependent maximum charge power for AC-coupled battery systems | W |
| $P_{Bat,AC'}$ | AC-side excess PV power | W |
| $P_{Bat,PV}$ | Charge condition-dependent Maximum charge power from PV for DC-coupled battery systems | W |
| $P_{Bat,PV'}$ | DC-side excess PV power | W |
| $P_{BAT2AC}$ | Discharge power from the battery to cover the Load | W |
| $P_{Grid}$ | Exchange power with the grid | W |
| $P_{Load}$ | Electrical load at grid connection point | W |
| $P_{LOAD,DC}$ | Required DC PV power to cover the load | W |
| $P_{max}$ | Maximum power | W |
| $P_{NT}$ | Consumed active AC power by an PV AC module | W |
| $P_{out,mean,N}$ | Mean output power of all $N$ DC/DC optimizers in a system | W |
| $P_{out,Opt}$ | Output power of the DC/DC optimizer $Opt$ | W |
| $P_{PV,AC'}$ | Possible invertible PV output | W |
| $P_{PV,DC}$ | Output of the PV generator | W |
| $P_{PV2Bat}$ | PV power for battery charging | W |
| $P_{PV2Bat,AC}$ | Excess PV power consumed by the AC-coupled battery | W |
| $P_{PV2Bat,DC}$ | Excess PV power consumed by the DC-coupled battery | W |
| $P_{PV2LOAD}$ | Direct load coverage | W |
| $PR$ | Performance ratio | % |
| $P_{SPV}$ | Battery losses | W |
| $P_{STC}$ | Summation of installed modules' power rating from flash test data | W |
| $P_{VB}$ | Power consumption of the PV inverter, battery converter and power meter at the Grid Connection Point | W |
| $Q_{DHW}$ | Domestic hot water energy demand | kWh |
| $Q_{SH}$ | Space heating energy demand | kWh |

| | | |
|---|---|---|
| $R_{gen}$ | Ratio of PV yield to total electrical energy consumption | % |
| $R_{self\text{-}con}$ | Self-consumption ratio | % |
| $R_{suff}$ | Level of independence from the external power grid | % |
| $SMF$ | Shade mitigation factor | % |
| $T_C$ | Cell temperature of the PV AC module | °C |
| $T_0$ | Reference cell temperature of the PV AC module, usually 25°C | °C |
| $U$ | Voltage | V |
| $\gamma_{AC}$ | Response of the PV AC module's power output to change in cell temperature | 1/°C |
| $\varepsilon_{self\text{-}consumption}$ | Share of self-consumption | % |
| $\varepsilon_{self\text{-}sufficiency}$ | Degree of self-sufficiency | % |
| $\eta$ | Conversion efficiency | % |
| $\eta_{avg,wgt}$ | Average weighted efficiency | % |
| $\eta_{AC2BAT}$ | Conversion efficiency from AC to battery | % |
| $\eta_{BAT2AC}$ | Conversion efficiency from battery to AC | % |
| $\eta_{DC/AC}$ | Conversion efficiency from DC to AC | % |
| $\eta_{DC/DC\ EURO\ \&\ CEC}$ | EURO and CEC conversion efficiency from DC to DC | % |
| $\eta_{DC/DC,max\ avg}$ | Maximum averaged conversion efficiency from DC to DC | % |
| $\eta_{DC/DC,power\ wgt}$ | Power weighted conversion efficiency from DC to DC | % |
| $\eta_{Opt}$ | Efficiency of the DC/DC optimizer *Opt* | % |
| $\eta_{PV2AC}$ | Inverter efficiency from PV to AC | % |
| $\eta_{PV2BAT}$ | Conversion efficiency from PV to battery | % |
| $\eta_{Sys}$ | System efficiency | % |
| $\eta_{Total\ max\ avg}$ | Maximum averaged conversion efficiency of a total system | % |
| $\eta_{Total\ power\ wgt}$ | Power weighted conversion efficiency of a total system | % |
| $\eta_{Total\ EURO\ \&\ CEC}$ | EURO and CEC conversion efficiency of a total system | % |

# EXECUTIVE SUMMARY

The goal of this document is to provide a compendium of new performance characterization methods for new photovoltaic (PV) system designs as a reference. New methods are described and explained by laboratory tests up to case studies. While performance characterization is more than evaluating efficiency of a component or a system in certain operating points, the results account for multi-dimensional usage and benefits. These assessments are intended to provide well-founded and comparable key figures in order to enable new PV system designs to move faster into new fields of application.

This report gives a short introduction into current standards and definitions regarding performance characterization of PV systems as a starting point. New PV system components and complex new systems with PV are then described with their respective performance characterization methods. Where currently no performance characterization methods for complex PV systems particularly with multiple functions exist, their design and their performance, energetically and regarding multi-dimensional usage benefits, are presented and described by means of showcases.

PV systems are not only PV modules and PV inverters in an optimally oriented system which produce as much electrical energy as possible. Current PV systems may provide a dual or even a triple use. However, as varied as the use of each system and each PV installation is, as different is the approach of performance evaluation.

The market of PV system components for special applications e.g. partially shaded operating conditions, or foldable or floating PV is growing. For all kinds of these PV systems, the Performance Ratio (*PR)* can be calculated. This *PR* in the PV sector just relates the energy yield of ideal PV systems to the real energy yield of real PV systems operated at a certain place. The *PR* cannot rate non-energy benefits of PV systems, components or installations.

Then again, the key performance indicator KPI for PV installation investment decisions often is the energy yield respecting *PR* only. Often, *PR* is used because measurement schemes are unknown or do not exist to evaluate the multiple benefits of the PV system. In the design phase of a certain PV installation the PV energy yield can only be calculated via simulation if the PV components' behaviour under different operating conditions is known. However, manufacturers of Balance of System (BOS) components often provide less meaningful performance figures in their datasheets which are not appropriate input data for a PV component or PV system simulation.

Starting from this point, this report provides measurement protocols to characterize single new PV system components with the goal of providing simulation models, figures for the model parameterization and the goal of obtaining meaningful performance indicators besides the *PR*. For multi-Maximum-Power-Point-Tracker (MPPT) inverters, a measurement protocol is proposed based on existing standards for the efficiency assessment of string inverters. In the new measurement protocol adjustments for the existing protocol are introduced and validated. In the case of PV Module Level Power Electronics (MLPE), their performance under different representative shaded operating conditions of their respective PV module is more meaningful than their weighted EURO or California Energy Commission (CEC) efficiency. For the PV module micro inverter, DC/DC optimizer, or in general, MLPE equipped PV system installations and particularly shade resilient PV module designs measurement protocols and figures as a performance indicator to rate their specific beneficial operation are presented. They enable the

comparison of new PV system components and designs with their advanced functions and benefits.

The PV battery system characterization is discussed in four steps. At first, with a simple test showing the inertia of a PV battery storage system the need of more meaningful performance indicators besides the nominal storage capacity and maximum efficiency is demonstrated. In the second step, the efficiency guideline for PV storage systems is discussed. Here, a measurement protocol is introduced which enables to systematically assess performance relevant figures from PV battery storage systems. In a third step, a dynamic PV battery storage simulation model is introduced which can be parameterized by the performance relevant figures assessed, according to the previously introduced efficiency guideline. All of these figures enable to parameterize PV battery system simulation models in a more sufficient way than the often-found figures of the maximum efficiency or the maximum capacity in datasheets. In the fourth step, simulations with that way parameterized dynamic PV battery storage model enables for individual PV system performance assessment by means performance indicators established in the sector of PV battery storage system.

Furthermore, the concise cycle test (CCT) a measurement protocol for the performance assessment of whole energy supply systems for single family or semi-detached houses in a Hardware-in-the-Loop testbench is introduced. This CCT allows for a performance assessment in a reasonably short time of six days without any previous examinations of the devices to be tested. Finally, we introduce the new key performance indicator grid purchase ratio. It allows a system assessment even if inefficient electric applications are used in the system under test.

Performance indicators for complex new systems with PV have to consider their multiple-usage benefits, e.g. additional yield or benefit, economically or regarding social acceptance. The performance indicators are as manifold as the multiple-usage of a certain PV system installation may be. As an example, in the area of parallel agricultural and PV usage (APV) the Land Equivalent Ratio (*LER*) shall be mentioned here. It indicates how efficient the parallel double-usage of a field is compared to two parallel single usage fields with the same total area.

For foldable PV systems, the multiple-usage performance can be rated, for example by the amount of steel and respective $CO_2$ emissions saved by its light weight structure, as operation during heavy wind or snow load conditions is avoided. A showcase with a foldable PV installation over wastewater treatment basins with respective performance indicators is given in the report. The variety of multiple-usage of foldable PV makes it difficult to determine a certain set of performance indicators which can be generally applied.

For floating PV (FPV) systems also, the multiple-usage benefits depend on their certain environmental operating conditions (e.g. reduced algal growth). A KPI is the PV module operating temperature which, besides the irradiation, is influenced by the wind speed. However, the pure presence of a waterbody beneath the PV modules does not imply lower PV module operating temperatures compared to land-based PV systems in the same area. Currently, there is no commonly applicable use case for rating an FPV performance characterization. Therefore, further research has to be carried out to find valid use cases and performance indicators for FPV.

For all performance characterization methods and performance indicators introduced in this report no standards exist currently. Although, some are closer to an existing standard multi-MPPT inverter) or on the way to a standardization process (PV storage systems). In the case of floating PV and foldable PV research and development are just at the beginning of the way to standardized performance characterization.

The work on this report has shown, that the development of a uniform performance indicator for all kinds of new PV components or new complex systems with PV will hardly be possible. Nevertheless, a framework should be developed which allows to normalize different performance indicators to make them comparable.

# 1 INTRODUCTION

New photovoltaic (PV) system designs are being developed to increase the value of the energy produced by either lowering the installation costs, increasing the efficiency or adding functions to the system. Some of these innovations include advanced power electronics to optimize the performance ratio of PV systems. Some new PV systems have additional functions, such as coupling PV energy with storage and power grid, including storage for electromobility, agricultural PV, and floating PV systems. For most of the mentioned new system components and double function systems, no standards exist on how to characterize and normalize the performance of the system or parts in the PV system. The International Energy Agency Photovoltaic Power Systems Technology Collaboration Programme's Task 13 (IEA PVPS Task 13 Subtask 1.3 group with over 15 PV experts from six countries) addresses these performance aspects. Performance is a measure of how well something meets expectations compared to a reference. We present new characterization methods for "New PV System Designs" to determine performance factors and indicators for the performance and the usability of new systems or new system parts. Where no methods are available on the performance, pros and cons will be explained by case studies. In these case studies, performance experiences with innovative PV systems are collected and summarized. The characterization methods and case studies cover not only technical but also economic aspects.

The energetic performance of a system is always defined as a ratio of energy input and output of a component or a system. In general, it is not possible to give one figure for the performance. Typically, the performance is a function of external and internal conditions and time. In some cases, the definition of a performance factor is possible, if the component or system is depending on well-known internal or external factors but without time dependence. In this case, a typical distribution of the conditions is used to calculate a performance factor. However, the more the performance is depending on not well known external or internal conditions or even on foregoing external or internal conditions, it becomes more and more complex to define a useful performance of the system. Additional complexity is gained if the performance cannot only be expressed by energetic units because other values should be considered in parallel. In these cases, multiple key performance factors become necessary if the performance of a system has partially opposing optimization targets or multiple typical applications exist.

**Table 1: Definitions and applicability assessment of performance definitions.**

| Name | Description | Allows for | |
|---|---|---|---|
| | | Calculation for one use case | Comparison of one use case |
| **Performance factor** | Relation between output to input for one special use case. | X | X |
| **Performance indicator** | Relation between output to input for one use case with an unknown additional factor or monotonically increasing (decreasing) function. | | X |

The aim of a key performance factor is to characterize and compare a component or system for a typical use case and one important optimization goal. Therefore, (key) performance factors are only useful if they robustly describe the energetic (usability, cost) performance of a

system. To do this, they must meet a number of conditions. Firstly, the performance must be assessed in situations that describe the typical technical application as close as possible. Secondly, the factors must be as robust as possible against deviations in the application. The key performance factor must represent the input to output ratio of a given application. This avoids complex simulations of the systems for energetic or even usability comparisons. If this is not possible we try to give key performance indicators (KPI) which at least allow statements such as the higher/lower the performance indicator is the more useful (better), seeTable 1.

# 2 STANDARDS AND DEFINITIONS

## 2.1 Current standards for performance characterization of new system components

### 2.1.1 Component level

For planning decisions of PV systems, the definition of a meaningful efficiency is important to characterize the components. The standards EN 50530 [1] and the IEC 61683 [2] serve as examples for efficiency definitions of inverters and microinverters. The Standard EN 50530 specifies a measurement procedure to determine the weighted EURO efficiency of grid-connected PV (micro)inverters as well as the IEC 61683 specifies the California Energy Commission (CEC) efficiency. If new components like multi-maximum power point tracker (MPPT) string inverter or PV AC-modules are to be investigated new and extended methods must be applied as introduced in chapter 3.1.

### 2.1.2 Performance definition for PV systems with additional function

In the following we present the most important performance definitions used in this report. On system level several ratios can be considered to rate a PV system´s performance. As an example, the performance ratio *PR* of a standard PV system is given by

$$PR = \frac{\sum_i EN_{AC,i}}{\sum_i P_{STC}\left(\frac{G_{POA,i}}{G_{STC}}\right)} \quad (1)$$

with

- $EN_{AC}$ = measured AC electrical generation (kW)
- $P_{STC}$ = summation of installed modules' power rating from flash test data (kW)
- $G_{POA}$ = measured irradiance in the plane of array (POA) (W/m$^2$)
- $i$ = index of a set of measurement results at the same time
- $G_{STC}$ = irradiance at standard test conditions (STC) (1000 W/m$^2$) [3].

In this case one assumes that all energy generated by the inverter of the PV system is fully consumed by electrical applications.

For a net coupled PV system with and without a Battery the degree of self-consumption is given by

$$\varepsilon_{selfcon} = \frac{\sum_i P_{PV\text{-}self\text{-}con,i}}{\sum_i P_{PV\text{-}AC,i}} \quad (2)$$

and the degree of self-sufficiency (autarky) is given by

$$\varepsilon_{selfsuf} = \frac{\sum_i P_{PV\text{-}self\text{-}con,i}}{\sum_i P_{AC\text{-}Load,i}}. \quad (3)$$

The system efficiency $\eta_{Sys}$ describes the PV energy used $E_{used}$ to cover the load and fed into the grid in relation to the amount of energy fed into the local (e.g. household) system $E_{supplied}$

$$\eta_{\mathrm{Sys}} = \frac{E_{\mathrm{used}}}{E_{\mathrm{supplied}}}. \tag{4}$$

# 3 PERFORMANCE CHARACTERIZATION OF NEW PV SYSTEM COMPONENTS

## 3.1 Specific characterization methods for system components

### 3.1.1 New performance characterization methods for multi-MPPT PV inverters

The current standard for characterization of the overall efficiency of PV inverters [1] was first released in 2010. At that time, multi-MPPT (maximum power point tracker) PV inverters were not widely-used. Therefore, the standard did not focus on the specific characteristics of PV inverters with more than one MPP (maximum power point) tracker. Today however, multi-MPPT PV inverters have become a market standard. To obtain a complete characterization of these devices, new test methods are necessary. Therefore, new test profiles for multi-MPPT PV inverters are proposed [4].

A good multi-MPPT PV inverter should be able to track the MPP on each input even if these MPPs have completely different voltage or current values. To characterize this feature, the proposed test profiles emulate heterogeneous input conditions on the inverter's MPP trackers. They are based on the linear ramp profiles for the characterization of the dynamic MPPT efficiency according to EN 50530 [1]. However, the ramps on the different inputs are not synchronous. With this approach, it is possible to simulate the whole range from completely homogeneous to very inhomogeneous input conditions in a reasonably short amount of time. The ramps simulate a change in irradiance between 100 W/m$^2$ and 800 W/m$^2$ in 150 seconds, which results in a gradient of 4⅔ W/(m$^2$·s).

The simulated *P-U* characteristics are also modeled according to EN 50530 [1]. They are scaled so that the MPP at Standard Test Conditions (STC) would be at the rated voltage and power of the corresponding MPP tracker (which do not necessarily have to be the same on each of the inverter's inputs). The cell temperature is assumed to be constantly at 25°C. At first, there is a lead time of 300 seconds with 800 W/m$^2$ of simulated irradiance, which allows the inverter under test to turn on and stabilize on the MPP. Then, the simulated irradiance at the first MPP tracker falls to 100 W/m$^2$ in 150 seconds. It remains at this level for 150 seconds and then rises back to 800 W/m$^2$ in another 150 seconds. The simulated irradiance on the second MPPT follows the same course, but with a delay of 300 seconds. This means that the simulated irradiance on the second MPPT starts to fall at the same time as the simulated irradiance on the first MPPT starts to rise again. Consequently, the profile on each following MPPT (if present) will follow his previous MPPT's profile with a delay of 300 seconds. This test sequence is done twice. Figure 1 shows the proposed test profile for four MPPTs.

If the inverter under test has more than four MPP trackers, to keep the test short, the profile of the first MPP tracker will also be applied to the fifth MPP tracker, the profile of the second MPP tracker will also be applied to the sixth MPP tracker and so forth. The test can therefore be extended to an arbitrary number of MPP trackers. As the size of the simulated PV array is defined in relation to the nominal power of the corresponding MPP tracker, the test procedure is even flexible enough for inverters with MPP trackers of different sizes.

Even though the proposed test is simple and short, it allows a good characterization of the inverter under test in situations, when one MPP tracker runs with a power much lower than the others.

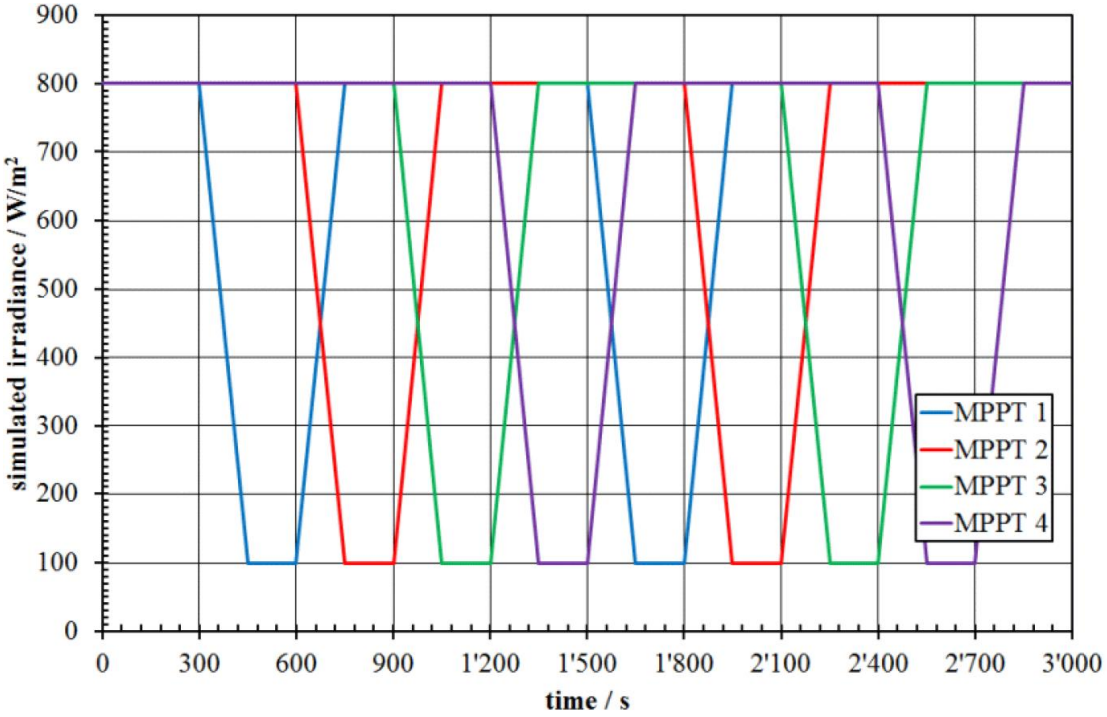


**Figure 1: Test profile for PV inverters with four MPP trackers [4].**

In fact, it could already be shown that under inhomogeneous conditions, the conversion efficiency of a multi-MPPT PV inverter is considerably smaller compared to a situation, when all inputs operate at the same voltage. This loss of efficiency occurs because under homogeneous input conditions, the device under test bypasses its input stages and performs the MPP tracking by modulation of the common DC link voltage. However, if the MPP voltage of the attached strings is no longer identical, the inverter activates its input stages which allows an individual MPP tracking on each input. Due to the additional power stages, the conversion losses are increased, and the conversion efficiency is reduced. Figure 2 shows an actual measurement of this situation, performed on an inverter with three MPP trackers.

During the first 300 seconds of the measurement, the simulated irradiance has been equal on all three MPP trackers. It is clearly visible that in this phase, the measured voltages on each MPP tracker are perfectly congruent. After this, the simulated irradiance of the first MPP tracker started its linear ramp. Shortly thereafter, the first MPP tracker tries to compensate for the now reduced MPP voltage. From this moment on, the three input voltages are no longer congruent, and the efficiency drops by about 0.4%. At $t$ = 350 s, the inverter under test tried one last time to bypass the input stages and the efficiency went up again for about 15 s. After that, the simulated MPP voltage on the first MPP tracker has drifted far enough that a common MPP tracking is no longer possible, and the inverter tracks the three inputs individually.

A loss of efficiency of 0.4% might not sound too bad. However, considering that the manufacturers of PV inverters fight for every tenth percent of efficiency, this is already a serious loss – a loss which cannot be detected by the current test standards. It also means that the devices conversion losses go up by 25% (2% instead of 1.6%). Consequently, the power dissipation is also increased by 25%, which leads to a considerable heating of the components. In this case, the heatsink of this passively cooled PV inverter under full load became too hot to be touched by bare hand even if the ambient was at room temperature! A higher temperature will always have a negative impact on the device's lifetime. Therefore, it is imperative that such effects must be unveiled by tests which aim to obtain a good characterization of such devices.

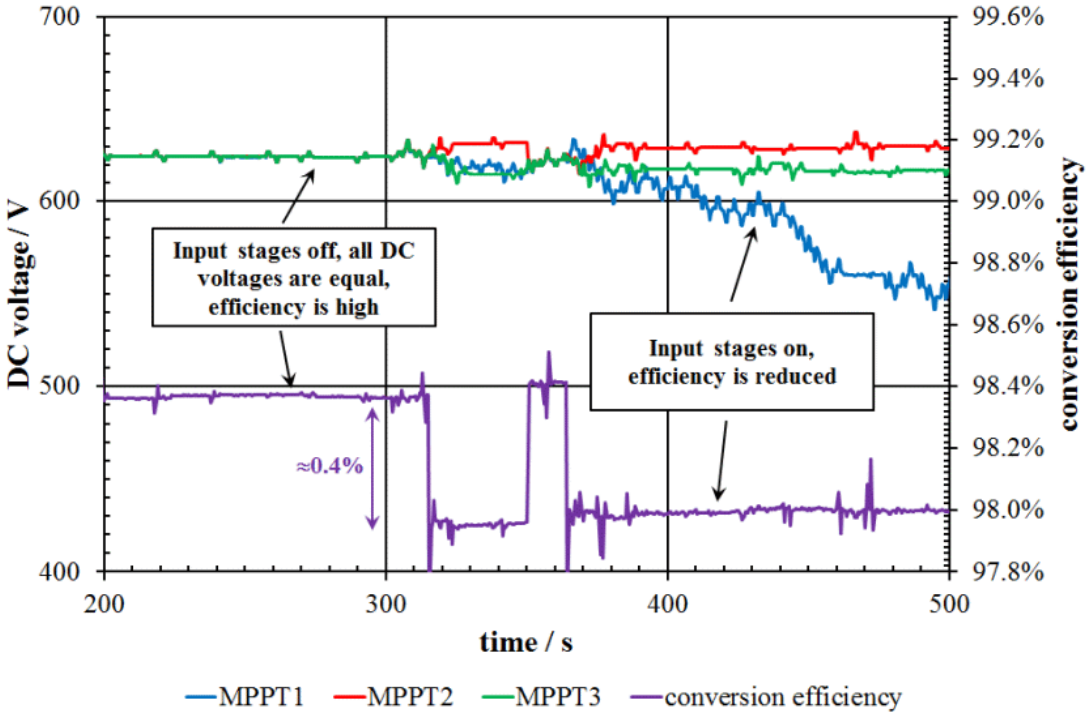


**Figure 2: Efficiency loss under inhomogeneous conditions [4].**

The proposed test profiles adjust existing test methods [1] to make PV inverter efficiency a reliable performance indicator also for multi-MPPT PV inverter.

### 3.1.2 Characterization methods for DC/DC smart modules

The measurement of PV modules under standard test conditions is governed by IEC 60904-1 [5], allowing for indoor flash testing and outdoor / continuous illumination characterization. The embedding of module-level or sub-module DC/DC optimizers into the junction box of modules was initially proposed to improve performance under partial shading conditions [6]. However, market adoption followed more swiftly as a response to updated building electrical codes designed to improve safety of emergency personnel responding to rooftop fires [7]. In many situations where the module-level DC power optimizer is an integral part of the module either embedded in the PV laminate or in parallel with bypass diodes in the junction box, characterization of the module without the effects of the DC/DC converter is impossible.

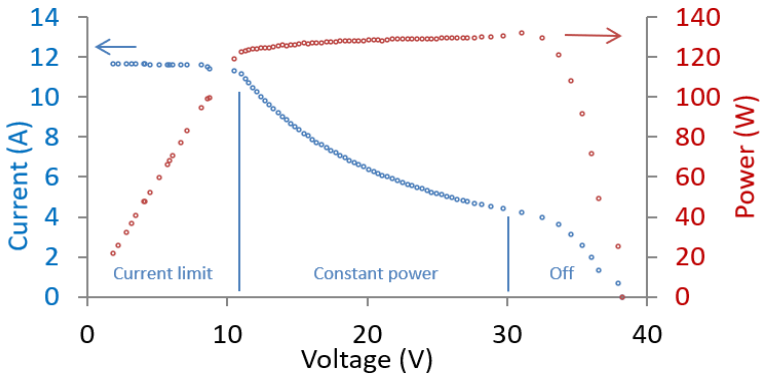


**Figure 3: Buck converter DC response [8].**

The response of a smart module depends in part on the power converter topology (e.g. buck, buck/boost), which describes the range in which the conversion is active. For a 'buck' converter, a constant-power regime is entered for module voltage < $U_{MPP}$, until a maximum current limit is reached, shown in Figure 3. Other practical limits such as current, voltage and power maxima affect the DC/DC response range. A 'buck-boost' converter will respond similarly, except with a second constant-power range for operating voltage > $U_{MPP}$ to the maximum voltage limit of the device [9].

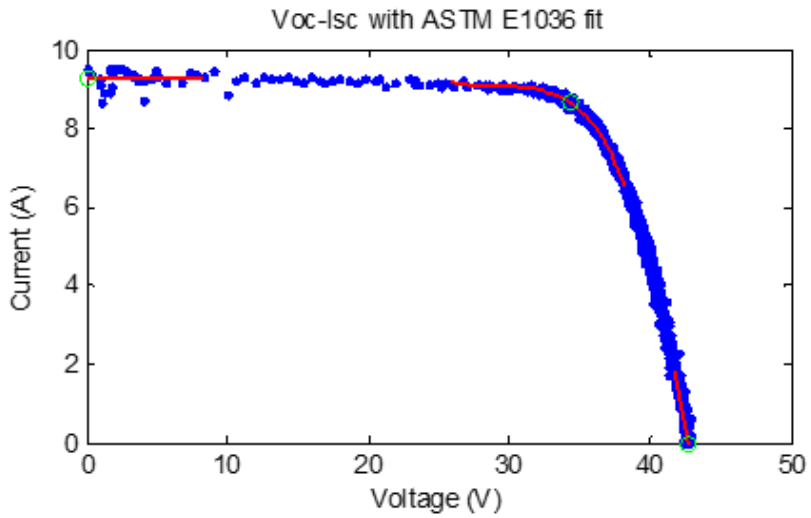


**Figure 4: The *IU* curve of the Maxim VT8012 smart module in 'flash mode' [10].**

This type of characteristic makes it difficult to extract useful module parameters, e.g. for factory characterization and binning of modules. Therefore, some DC/DC devices include a 'flash mode' allowing indoor flash measurements, assuming the sweep direction occurs from $U_{OC}$ to $I_{SC}$. Although the characteristic looks closer to a normal *I-U*-sweep, as discussed by [8] high frequency noise is typically present which requires filtering and linear fits to extract $I_{SC}$, $U_{OC}$ and $P_{MPP}$ values, see Figure 4.

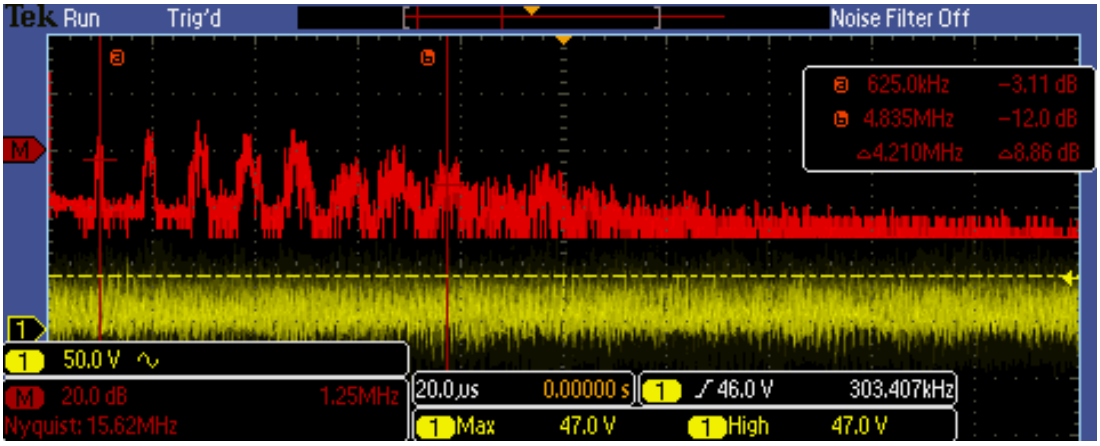


**Figure 5: High-frequency response between 625 kHz – 4 MHz of the smart module under outdoor illumination [10].**

In this case, application of ASTM E1036 [11] was successful, which calls for linear fits for $U$ < 0.2 $U_{OC}$ and I < 0.2 $I_{SC}$, along with a 4th order fit to the *P-U* curve between 0.75 $U_{MPP}$ < $U$ < 1.15 $U_{MPP}$. This was successful in filtering out the effects of the 625 kHz frequency of the buck

converter Figure 5. Other characterization requirements for smart modules include efficiency assessment of the DC/DC optimizer itself. This can be conducted largely according to the methods outlined for inverters in EN 50530 / IEC 62891 [1], [12].

However, for DC/DC converters an important free parameter that impacts conversion efficiency is voltage boost ratio *M*. Typically stated maximum efficiency values are for conditions *M* = 1, however operation in practice depends on module string length and fixed DC link voltage of the inverter depicted in Figure 6 [13]. This factor is overlooked in the conversion efficiency standards mentioned above, and merits consideration.

A final consideration concerns measuring the energy gain of DC/DC optimizer under partial-shade conditions. No standard exists to describe and quantify the impact of DC/DC optimizers under shade conditions. Therefore, a protocol has been developed to compare field results under controlled shading conditions both with and without DC/DC optimizer [14], [15]. In this procedure, a 62% opaque mesh screen is drawn across two side-by-side systems in 1.5-cell increments, measuring the relative performance for both a string-inverter and MLPE-equipped system (Figure 7 (a)).

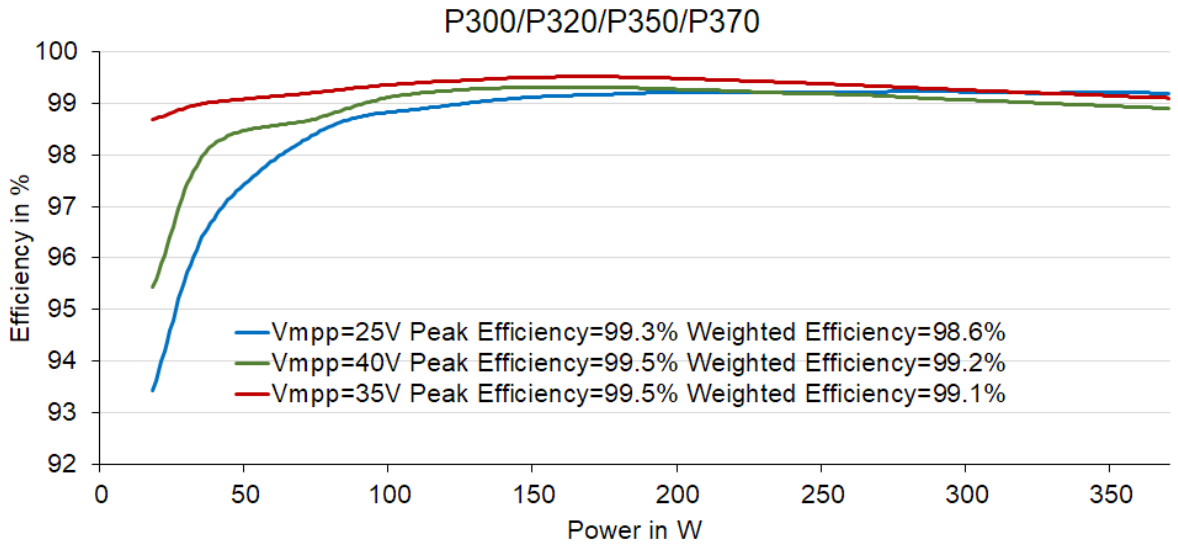


**Figure 6: Conversion efficiencies of SolarEdge module power optimizers. Courtesy of SolarEdge, data from [16].**

During this procedure the relative performance for both an only string-inverter (Reference) and an additionally DC/DC optimizer-equipped system (Maxim) is measured. Each system has two portrait-oriented PV module strings which are connected in parallel to a single MPP tracker. The Maxim PV modules integrate six DC/DC optimizers, one per PV module substring. Both in parallel connected module strings of each system are shaded after each other. Figure 7 (b) shows the resulting performance of this shading process and compares the difference in shading loss between the two systems at each shading condition. The red line shows the shade dependent performance of the reference system, the blue line represents the Maxim system.

To rate the benefit of the DC/DC optimizer equipped string the shade mitigation factor (SMF)

$$SMF = \frac{E_{\mathrm{DUT}} - E_{\mathrm{Ref}}}{E_{\mathrm{unshaded}} - E_{\mathrm{Ref}}} \quad (5)$$

was introduced. $E_{unshaded}$ represents the energy yield of a PV module in unshaded operation. $E_{Ref}$ represents the energy yield of a shaded standard module and $E_{DUT}$ represents the energy yield of PV module with DC/DC optimizers.

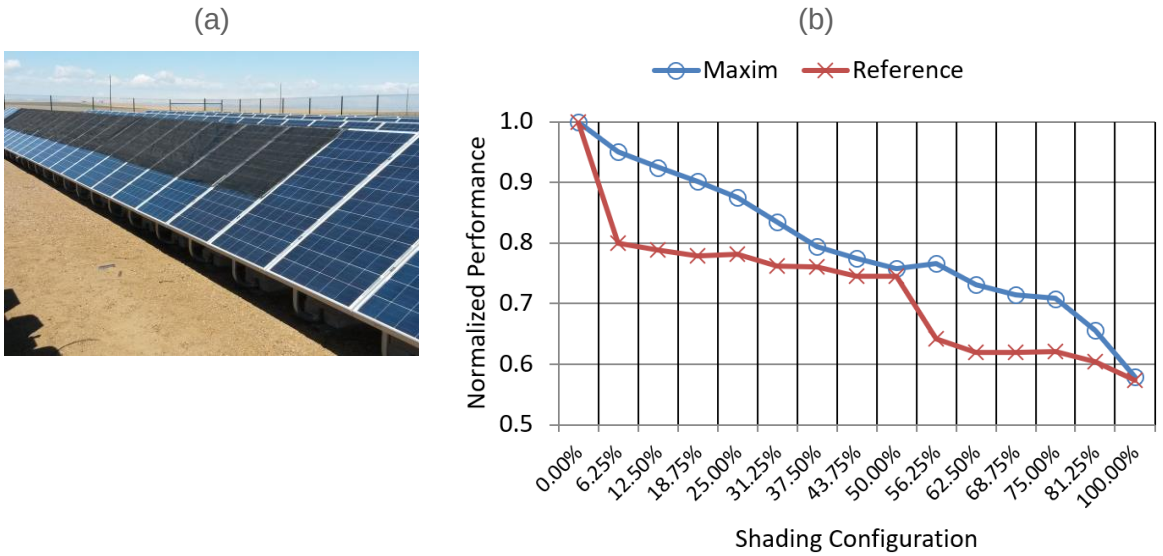


**Figure 7: (a) Two side-by-side systems, one connected to a conventional string inverter and one with DC/DC optimizer installed. Shading with 62% opaque fabric. In the foreground one of two PV module strings equipped with DC/DC optimizers and shaded is shown. (b) Difference in performance loss for the two system configurations with and without substring wise DC/DC optimizer under two portrait-oriented PV module strings subsequent shaded in 1.5 cell increments** [14]**.**

A final composite shade mitigation score is calculated via the frequencies of each shade configuration. Typical Shade Mitigation Factors of 30% - 40% are calculated, indicating that for typical residential shading, roughly ⅓ of the shading loss can be recovered by the investigated DC/DC smart modules [17], [14].

A measurement protocol for characterizing the performance of DC/DC optimizers under shading conditions has been developed. Also, the Shade Mitigation Factor (*SMF*) was introduced to quantify the impact DC/DC operation under shading conditions. Input data measurement data from specific use cases or simulation data from specific use cases. There are no standardization processes regarding this topic, yet.

### 3.1.3 New performance characterization methods for AC Modules

The use of microinverters provides flexibility of installation and safety due to lower system voltages to PV installers and owners, particularly in small residential systems. When used as distinct components in a system, the PV module and microinverter may be characterized individually with methods such as IEC 61853 [18] and EN 50530 [1].

An AC Module fully integrates the PV module with a microinverter such that there are no external DC connections. This integration of PV module directly with microinverter eliminates or hinders the ability to characterize each component separately. Instead, the fully-integrated

AC Module must be characterized as a whole. In 2015, Sandia National Laboratories developed a method for testing, characterizing, and modeling AC Modules [19].

At any given time, the AC module operates in one of three distinct states; the low-irradiance state, the self-limiting state, or the typical operation state.

The AC module operates in a low-irradiance state whenever there is insufficient irradiance to power the inversion electronics and the module may consume a small amount of active power from the electrical grid. The power in this state, $P_3$, is determined as

$$P_3 = -1 * P_{NT} \quad (6)$$

Here, $P_{NT}$ is the consumed active AC power in watts, and the power $P_3$ is always negative to indicate that the AC module consumes power in this low irradiance state. $P_{NT}$ may be obtained by specification sheets or determined empirically by measuring power consumption when the module is not illuminated.

The microinverters within PV modules generally have some output power level at which they begin to limit their output; this state is commonly known as “clipping”. In this self-limiting state, the output AC power remains constant despite changes in irradiance which allow the PV panel to produce more DC power. The power produced in this state is determined as

$$P_2 = P_{AC,max} \quad (7)$$

The value of $P_{AC,max}$ may be reported on a specification sheet or, preferably, determined empirically.

While the self-limiting power of the AC module is presented as a constant, if the modeler determines that the self-limiting power of the AC module is a function of other input variables, the self-limiting power equation may be replaced with a more accurate model.

While operating in the typical operation state the active power of the AC module changes as a function of irradiance, PV cell temperature, and solar spectrum. While operating in this state, the active AC power is represented as the product of a reference power and a series of normalized scaling factors.

$$P_1 = P_{AC,ref} * f_1(AMa - AMa_{ref}) * [C_0 * \frac{E_{POA}}{E_{ref}} + C_1 * In(\frac{E_{POA}}{E_{ref}})] * [1 + \gamma_{AC} * (T_C - T_0)] \quad (8)$$

where:

- $P_{ACref}$ is the AC power under reference conditions $E_{ref}$, $AMa_{ref}$, and $T_0$, in watts
- $f_1$ is an empirical unitless function which modifies the PV AC module output power as a function of absolute (pressure corrected) airmass relative to the reference absolute airmass
- $C_0$ is a unitless empirical coefficient describing the linear relationship between the irradiance and the PV AC module output power, typical values near 1
- $C_1$ is a unitless empirical coefficient describing the logarithmic relationship between the irradiance on the PV AC module output power
- $E_{POA}$ is the broadband POA irradiance incident upon the module which reaches the active PV material, in W/m$^2$. $E_{POA}$ is estimated from measured broadband $G_{POA}$ irradiance by accounting for the module losses due to specular reflection and/or acceptance of diffuse irradiation.
- $E_{ref}$ is the reference POA irradiance in W/m$^2$

- $\gamma_{AC}$ is the PV AC module's power output dependency to change in cell temperature in units of 1/°C
- $T_C$ is the cell temperature of the PV AC module in °C
- $T_0$ is the reference cell temperature of the PV AC module, usually 25°C

Thus, in the typical operation state, the power is modeled as a function of incident transmitted irradiance, cell temperature, and absolute airmass. Each of these factors is based on an underlying sub-model which are described in more detail in [19]. The use of normalized scaling factors to adjust a reference power allows for further development of the model to include other inputs that are not considered in this work or to utilize different sub-models to obtain more accurate scaling factors.

With the performance of the AC module defined in three distinct operating states, the model then simply determines the state in which the module is operating and uses the power model for that state.

$$P_{AC} = \begin{cases} P_1 & \text{if} \quad P_3 \leq P_1 \leq P_2 \\ P_2 & \text{if} \quad P_1 > P_2 \\ P_3 & \text{if} \quad P_1 < P_3 \end{cases} \tag{9}$$

To determine the reference conditions, reference performance, and sub-model performance parameters, Sandia measured the module's active power production in outdoor conditions over a period of several weeks with the AC module mounted on a 2-axis solar tracker. A series of tests, designed to isolate the performance parameters of each specific sub-model, are performed on each AC module. While testing is explained in [19], we present a summary of the tests here.

- Thermal test to determine module temperature coefficients. The module power is measured as it is cooled to ambient temperature and then allowed to heat via solar irradiance while remaining normal to the sun.
- Self-consumption test to determine the amount of active power consumed by the module in low irradiance conditions. The module power is measured during low irradiance conditions.
- Angle-of-incidence test to determine the effect of solar incident angle on module power production. The module power and solar incident angle are measured while the module is rotated away from the sun.
- Electrical performance test to determine the effect of changing solar irradiance, solar spectrum, wind speed, and ambient air temperature. The module is tracked normal to the sun for several days to weeks as its power is measured. A range of different weather conditions are desired.

This testing allowed for the AC module to be measured under a wide range of incident irradiance, spectra, and temperature to derive model parameters that predict AC module active power to within ±2% which Figure 8 and Figure 9 confirm.

Figure 10 shows the measured and modelled power from an AC PV module on a cold, breezy, partly clouded day. Prior to sunrise, the module operates in the low-power state, where the AC module consumes approximately 0.6 watts of active power. As the sun rises and illuminates the AC module, it begins producing active AC power according to the incident irradiance and module temperature. In the middle of the day, the AC module is limiting its output power, producing a constant amount of power, regardless of increasing incident irradiance.

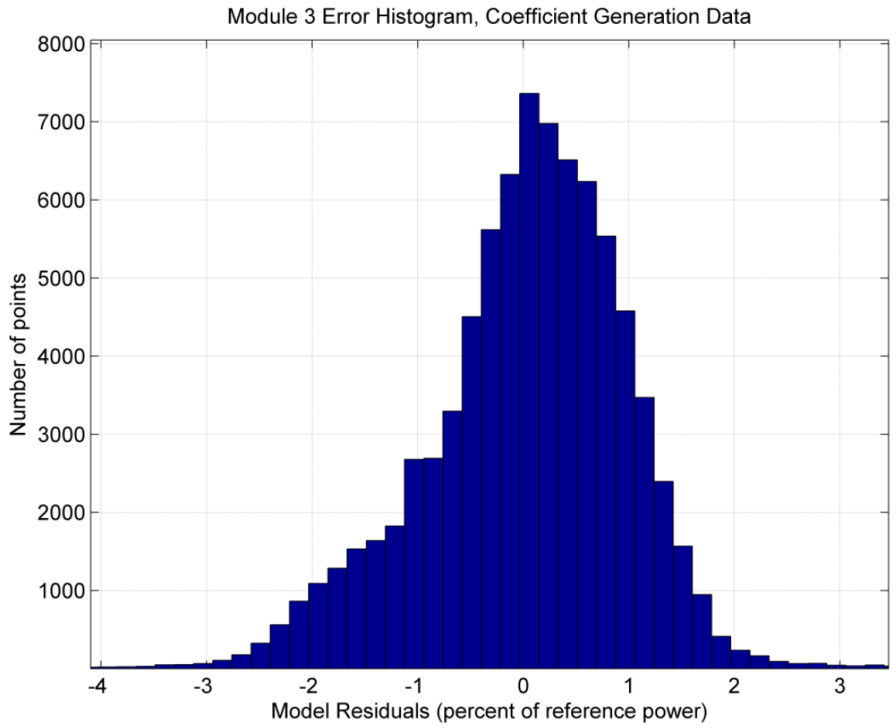


**Figure 8: PV AC module model residuals on data used within the parameter estimation data set [19].**

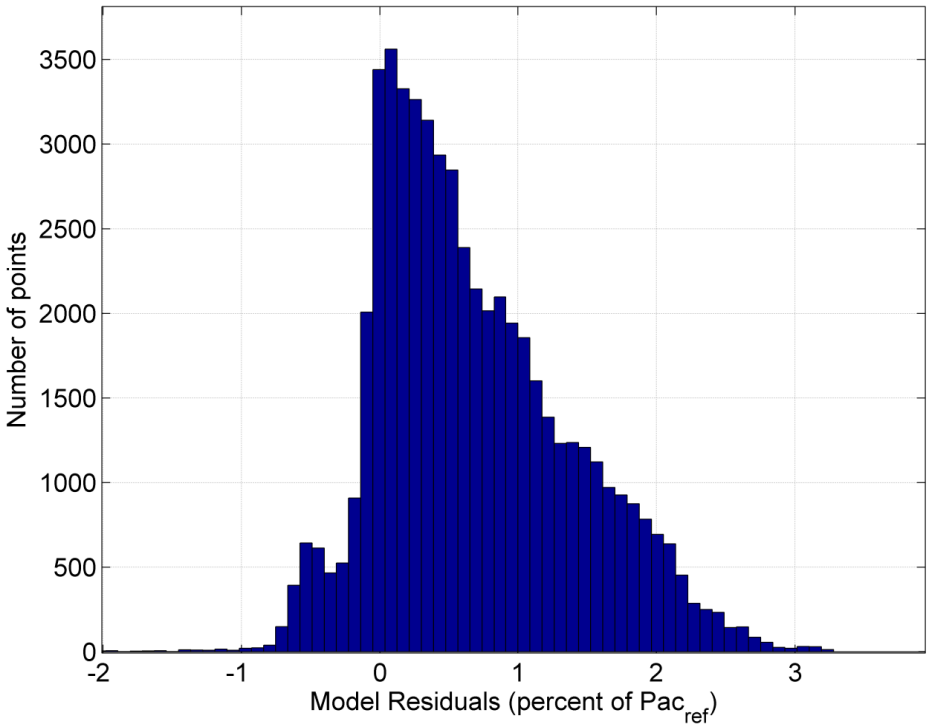


**Figure 9: Histogram of model power residuals over 9 days for a fixed-tilt PV AC module, daytime data only [19].**

While Sandia National Laboratories conducted performance testing outdoors, indoor performance testing of AC modules may be possible. However, due to the lag and self-

consumption of power within the attached microinverter, a continuous light source would be required and some performance characteristics could need to be estimated if they could not be measured directly via indoor testing.

The testing and analysis produce a performance model for each AC PV module. The models developed by Sandia were tested and validated over 9 days, during which the AC module was held at a fixed tilt while its power was measured. During the validation period, the model produced a (daytime) root mean square error (RMSE) less than 1% and predicted the total power generation within 1.4%.

The described measurement protocol and simulation model for PV AC modules enables to conduct simulations for specific use cases. With the generated results like time series of the PV AC module´s AC power or the energy yield performance indicators for the specific use case can be calculated.

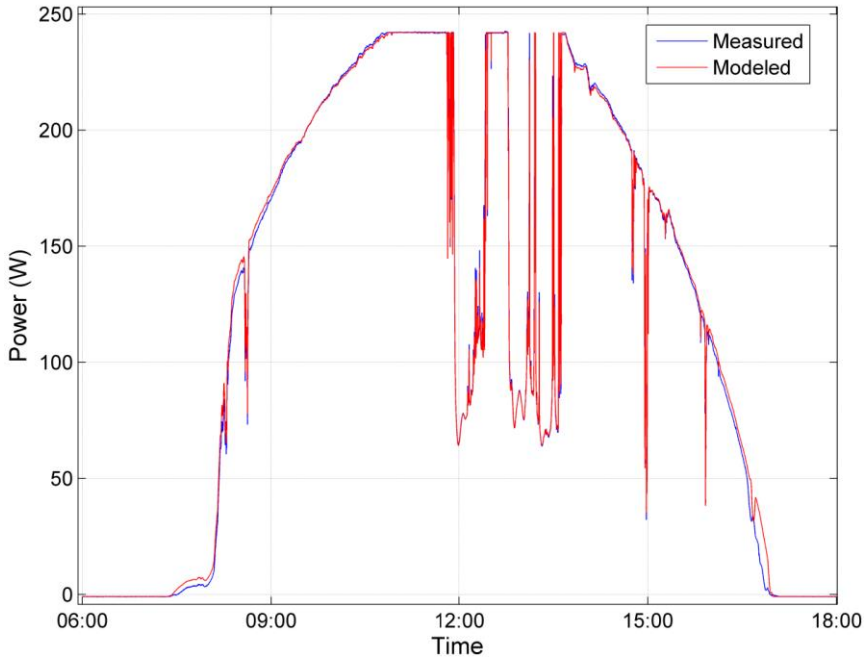


**Figure 10: Measured and modelled power from a fixed-tilt PV AC module on a cold, breezy, partly cloudy day [19].**

### 3.1.4 Modul-Level Power Electronics under indoor performance tests

Due to the electrical wiring of conventional PV systems with string inverters and their centralized maximum power point tracking (MPPT), partial-shading conditions have a great impact on the reduced performance of those systems. Module-level power electronics (MLPE) e.g. microinverters or power optimizers (DC/DC-converter) apply individual MPPT for each PV module. Thus, the annual system performance will increase, if the total MLPE efficiency for the unshaded events is not significantly lower compared to sting inverter. Claims of two-digit number percentage of performance gain of MLPE relative to standard string inverters could not be verified by intensive indoor lab test at ZHAW for typical roof shading conditions.

Figure 11 shows the simulated system with the PV module placement on the roof and a dormer, throwing a shadow on two PV modules in the late morning for instance. The roof inclination is 30° with a south facing module plane.


**Figure 11: Simulated system with the PV module placement on the roof with a dormer [20].**

The origin of the corresponding daily course of DC output of ten rooftop PV modules facing typical shading conditions of a dormer are a measurement run of a real system. Detailed ray tracing shading models calculate the time series of the DC current and voltage output of one individual PV module, with a spatial resolution of a single solar cell within the standard PV module of 60 cells and three bypass diodes.

Figure 12 show the *I-V* curves of one module and the graphical representations of three different shading situations with a 1%, 47% and 50% shading of one cell (marked in red).

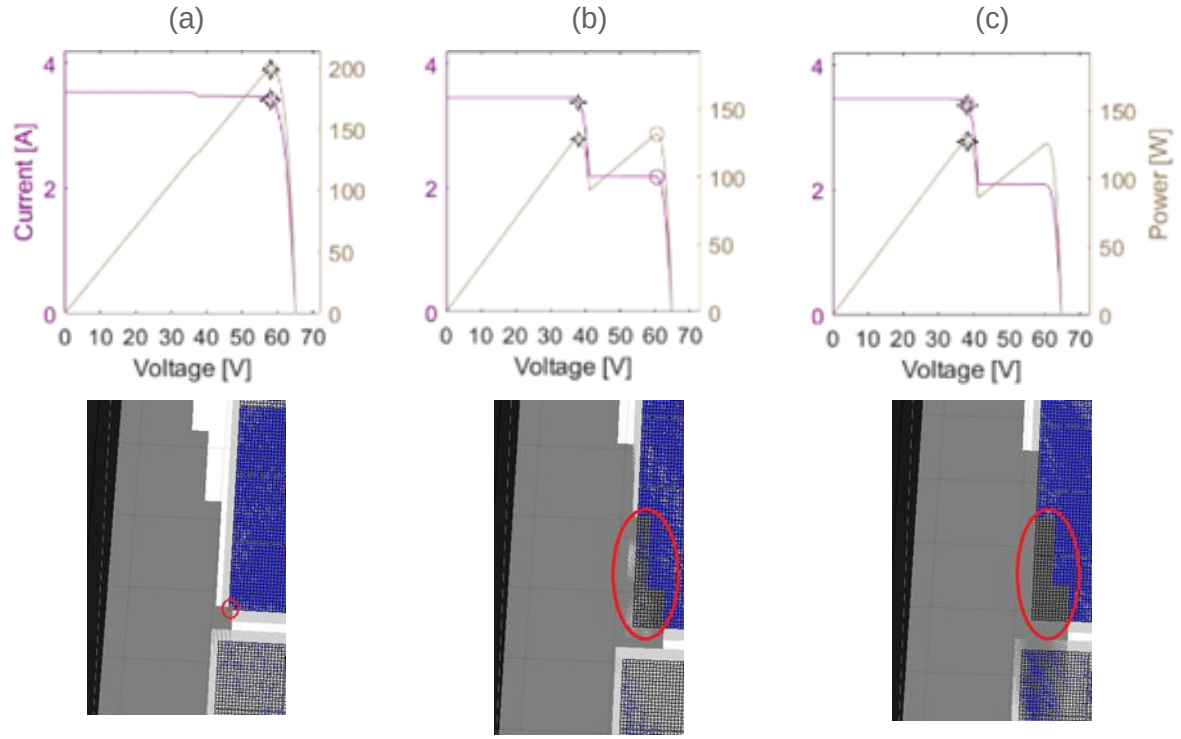


**Figure 12: *I-V* curve of one module and graphical representation of three different shading situations with (a) 1%, (b) 47% and (c) 50% shading of one cell at 1:26 pm, 1:38 pm and 1:41 pm.**

The indoor test setup uses ten serials connected commercial MLPE devices feeding the commercial DC/AC inverter. An overview of the used laboratory hardware setup is visualized

in Figure 13. Ten solar array simulators (SAS) individually controlled powering each MLPE device. To assess the performance of the power optimizer system over one day, the SAS devices received the values for $I_{MPP}$, $I_{SC}$ and $U_{MPP}$, $U_{OC}$ every 5 seconds, based on precalculated *I-V* curve values of a PV module from the system simulation. The testing was performed over 12.5 hours.

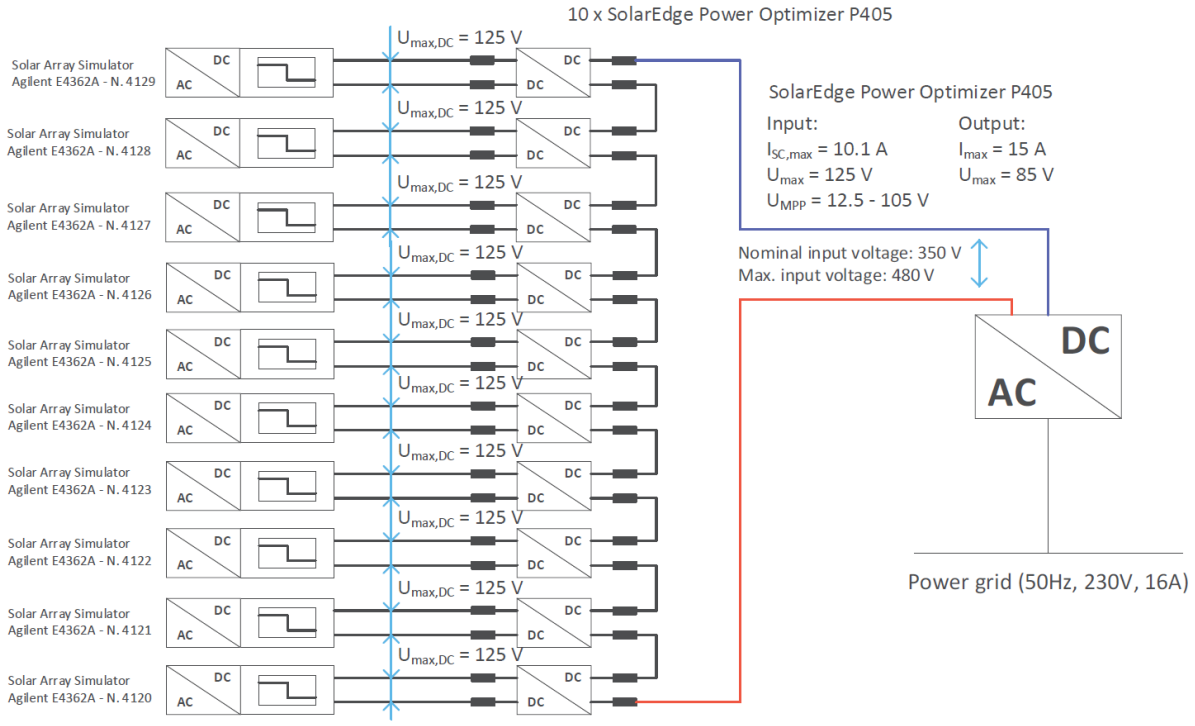


**Figure 13: Electrical lab setup to measure the performance of the MLPE system with ten power optimizers. [20]**

In Figure 14 (a), the power before and after the DC/DC conversion of the real-time irradiation test for four power optimizer is visualized, due to limited power range of the SAS devices, the curve was flattened between hour 10 and 14. Still, the effects of shading are most prominent between hour 7 and 10. Additionally, the resulting efficiency of the power optimizer is shown, whereby a plunge in efficiency in shaded conditions of approximately 5% to a value of 90% in average can be discerned.

In order to determine a performance rating of the system during realistic operating conditions, a weighted efficiency value $\eta_{avg,wgt}$ was calculated at each timestep *t* during the real-time test according to equation (10). $P_{out,Opt}$ is the output power of the DC/DC optimizer *Opt*, *N* represents the total number of DC/DC optimizers in the system, $P_{out,mean,N}$ indicates the mean output power of all *N* DC/DC optimizers and $\eta_{Opt}$ is the efficiency of the DC/DC optimizer *Opt*.

$$\eta_{avg,wgt} = \frac{1}{N} \sum_{Opt=1}^{N} \frac{P_{out,Opt}(t)}{P_{out,mean,N}} * \eta_{Opt}(t) \quad (10)$$

The resulting $\eta_{avg,wgt}$ for the assessed system is 96.79% as visualized by the dashed red line in Figure 14 (b). The efficiency can be expected to be slightly higher in the case with modules with a lower $U_{MPP}$ (i.e. lower voltage ratio).

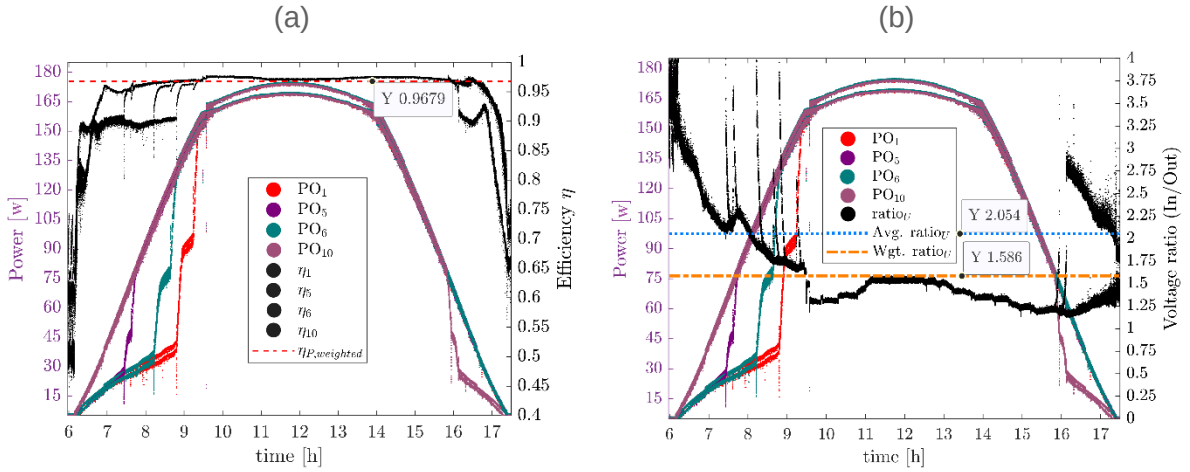


**Figure 14: (a) Plot of the real-time irradiance testing with input and output power of four MLPE power optimizers and respective efficiency values in function of time. (b) Plot of the real-time irradiance test with input and output power of four MLPE power optimizers and respective voltage ratio values in function of time.**

The measured efficiency of an individual DC/DC MLPE without the final DC/AC inverter over the input Power $P_{in}$ is given in Figure 15. Figure 16 shows the measured efficiency of an individual DC/DC MLPE without the final DC/AC inverter over the voltage ratio $U_{DC,in}/U_{DC,out}$.

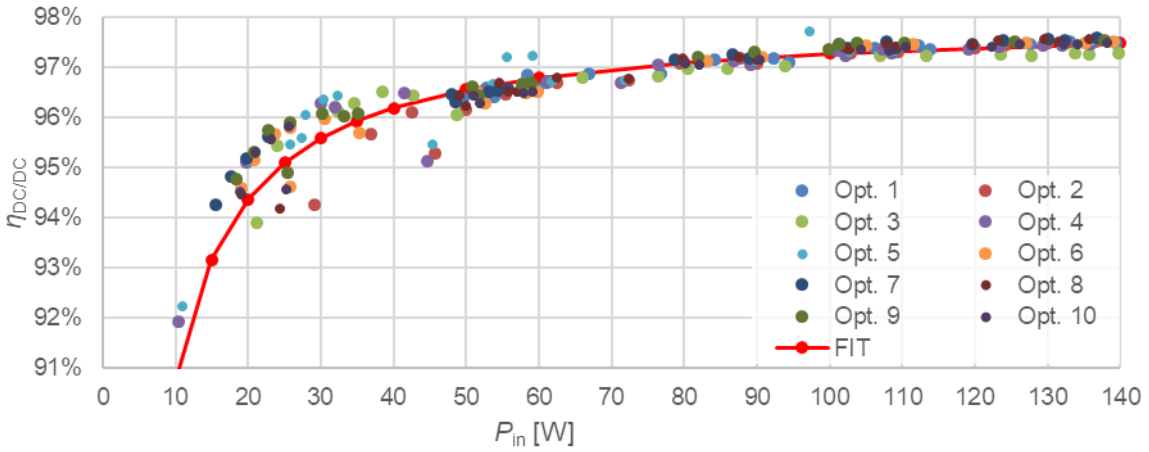


**Figure 15: Electrical setup of the analysed MLPE system with 10 optimizer and respective DC/DC efficiencies for a power range from zero to 140 Watts. Accordingly fitted function shows the approximate course of DC/DC efficiencies for the DUT Solaredge P405 in the shown power range.**

Efficiency values below 98% and for most of the real conditions below 97.5% are revealed. This is 1% below the given values in the manufactures datasheet and could by more than 2% lower than that, if the planer is not aware of the relevance of the ratio of the input and output voltage of the optimizers. Efficiency values of 97.5% and up to 98% could be reached if the ratio of DC input relative to DC output voltage is between 0.8 and 1.4. The nearly linear further decay of the efficiency will be below 93% at a ratio of 3.5. Latter is below the average efficiency of old inverters common two decades ago. It is recommended that the MLPE manufactures should give this efficiency characteristics in their datasheets, like it was done in the early days of PV inverters to show the DC voltage dependency on the DC/AC and the weighted EURO,

CEC efficiency [21],[22]. Today, PV string inverters see an 98.5% (CEC rating), up to 99% max rating and this highly relevant to compare the unshaded performance of MLPE and string systems. For the detailed analysis of the MLPE system efficiency, the fixed mode of the SAS was used to set static values in an interval of 5 seconds. In detail, a voltage range of 12 to 78 V with 2 V steps and a current range of 0.2 to 5 A with 0.1 A steps was tested and evaluated.

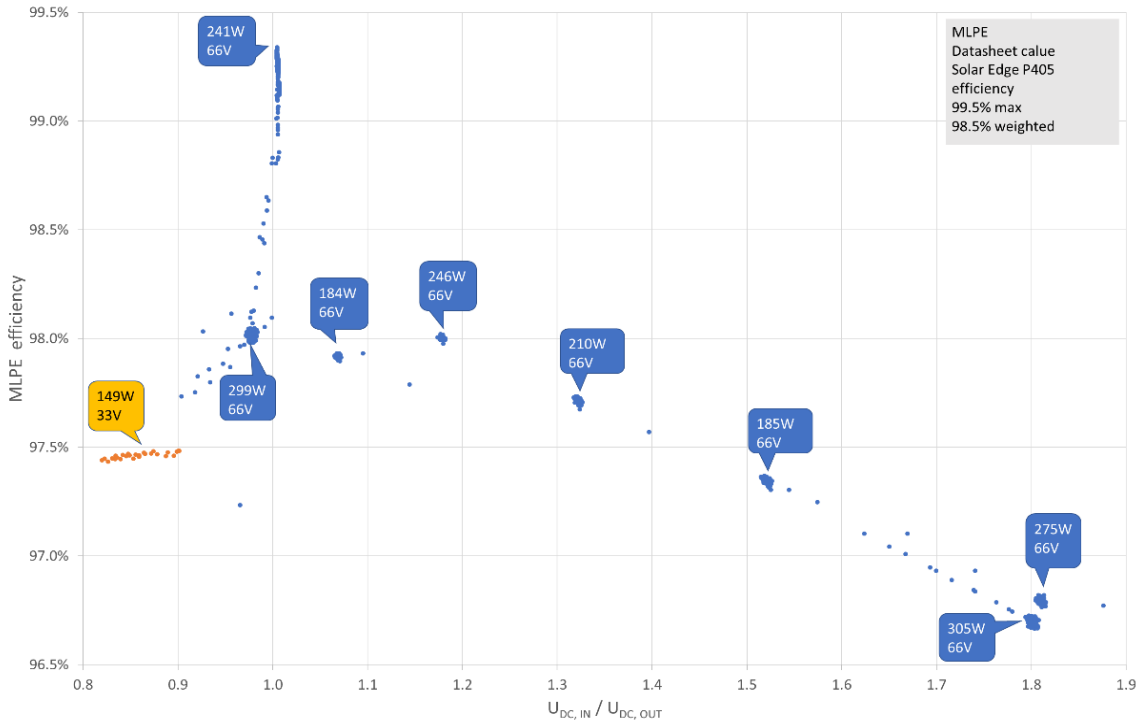


**Figure 16: Measured efficiency of one individual MLPE DC/DC converter as a function of the ratio of input and output DC voltage. The input power and input voltage are indicated during different selected shading condition during the day.**

The average efficiency value for each 1-Watt bin is visualized in Figure 17 and the maximum efficiency is found at 171 W with a value of 97.21%. The difference to the datasheet value of 2.29% is significant. However, due to the strong dependency of the efficiency of the DC/DC conversion on the input to output voltage ratio, the average values are not a general reference for every operating condition. It also depends on the absolute DC voltage level, with higher efficiency values at higher voltage (see Figure 16). Therefore, curve fitting for the measurement values for three different voltage ratios, namely, 0.6, 1.15 and 2.3, ± 0.1, were determined. As expected, the average efficiency values for a power of more than 180 W are influenced by the suboptimal voltage ratios of > 1.75. In addition, an approximated EURO and CEC efficiency was calculated, which uses the values at 90% of nominal power instead of at 100%, due to the limited power range of the SAS devices. Both values resulted in 96.61%, which is visualized in Figure 17 and indicated by the horizontal dash-dotted line. Finally, highest efficiency values of 98% was measured in a narrow field at voltage ratios of 0.99 to 1.1.

Due to the reason that the efficiency of the power optimizer varies greatly with the ratio of voltages, they were determined and visualized in Figure 17. Furthermore, the average voltage ratio is visualized with a value of 2.054 and the power weighted voltage ratio with a value of 1.586.

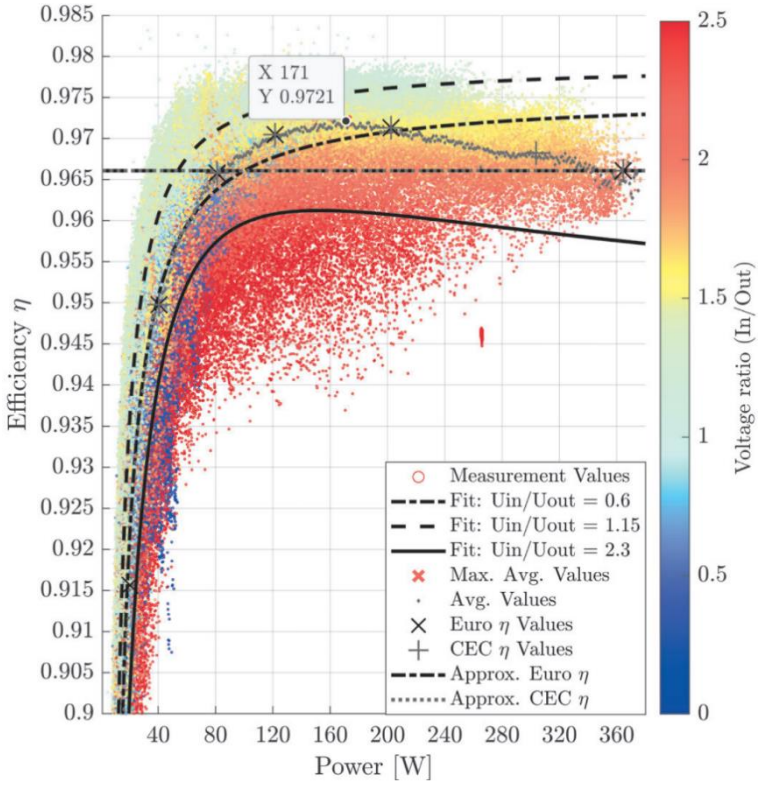


**Figure 17: Efficiency values of the DC/DC conversion of the power optimizers as a function of the input power and voltage ratio (in/out) based coloring with colour bar.**

The resulting efficiencies are only representative for a lower range of irradiance conditions. Nonetheless, a first approximation of performance of the devices were achieved and are presented in Table 2.

**Table 2: Resulting efficiency values of the devices.**

| Name | Device | Measured | Absolute difference to datasheet |
|---|---|---|---|
| $\eta_{DC/AC}$ | SE3500 | 97.40% | -0.20% |
| $\eta_{DC/DC,max\ avg}$ | P405 | 97.21% | -2.29% |
| $\eta_{DC/DC,power\ wgt}$ | P405 | 96.79% | -2.71% |
| $\eta_{DC/DC\ EURO\ \&\ CEC}$ | P405 | 96.61% | -2.89% |

Finally, the resulting efficiencies of the power optimizer and the PV-inverter were multiplied, and therefore, the total system performance estimated, which are stated in Table 3.

**Table 3: Total performance of the MLPE system.**

| Name | Resulting total system $\eta$ |
|---|---|
| $\eta_{Total\ max\ avg}$ | 94.78 % |
| $\eta_{Total\ power\ wgt}$ | 94.37 % |
| $\eta_{Total\ EURO\ \&\ CEC}$ | 94.19 % |

Due to the limited power range of the SAS devices, an increased voltage and lower current was used during the testing. This has the potential to reduce the efficiency values of the power optimizers. Still, the total system performance value (e.g. the total power weighted efficiency) shows a significant deviation of approximately -2.27% from the potential efficiency, estimated by the combined MLPE system datasheet values.

If there is a specific shading situation, the benefit of MLPE, must be determined on a case-by-case basis. There is not a general statement available for all cases. As for the simulated PV system, an additional daily yield of approximately 3.5% was calculated for the use of MLPE. The results of the simulation are stated in Table 4.

**Table 4: Simulation result of a clear-sky day with the sun path of the 20th March at Winterthur, Switzerland, and updated efficiency values for the system with MLPE.**

| System type | $\eta_{\text{Total power wgt}}$ | Simulated Daily yield |
|---|---|---|
| MLPE | 94.37% | 103.50% |
| String inverter | 97.00% | 100.00% |

In scenarios with extreme and inhomogeneous shading a MLPE system provides a significant advantage. Whereas for low shading situations, these systems are generally expected to yield less energy than conventional systems. On the other hand, the course of the shade on the module is of key importance. As for example, a shade, which is orthogonal to the cell strings (as in the simulation), will lead to significant losses in a conventional system. Accordingly, various shading situations must be examined with the indoor test facility presented in this paper and also applied by other independent laboratories.

### 3.1.5 Performance of new shade-resilient module designs

Analysis of PV energy yields of PV systems reveals in many cases that the actual yield may be lower than the expected yield. The latter is based on an appropriate description of system parameters and actual irradiance and other meteorological parameters such as ambient temperature and wind speed. A MPPT is used to optimize power generation by the PV system. Besides system or components' failures, shading is a prominent cause of performance loss, especially in the built environment, which may amount to perhaps 10% loss on an annual basis [23]. As multiple PV modules are usually connected in series to central inverters, shading-induced power losses at the module level will negatively influence the maximum attainable system power. Also, partially shaded modules and in particular cells in these modules may become reverse biased and will act as a load consuming power generated by the other, unshaded, cells. This may lead to increased cell temperatures, or hot spots [24], which may lead to faster degradation of both diode and PV module in case of partial shading. The use of bypass diodes will limit this, by bypassing shaded substrings of the solar module. Typically, three bypass diodes are used in antiparallel connection to the cells per 60/72-cell module [25], leading to power loss of 1/3, or 2/3 upon partial shading. However, adding more bypass diodes thus increasing granularity of cell groups can increase performance, especially under partial shading conditions [26]–[28].

It is obvious that optimum design in terms of string connections and use of central inverters should take potential shading effects into account. Another approach would be to apply module level power electronic which aims to optimize the maximum power of individual PV modules [29]. This has been available commercially for some years now, and system designers are

challenged to find an optimum between additional cost and additional yield, which will depend on the expected shading loss.

Mitigation of shading effects on PV performance can be classified in two groups [30]: circuit-based topologies, and modified MPPT based techniques. These are usually applied on a per-module level. For example, increasing the number of bypass diodes, or so-called total cross tied topologies, which can be fixed connections between cells in a module or adaptive connections. The latter topology requires microcontrollers that control a switching matrix, and indeed mitigate shading, but is quite complex by design, and not so fast [31]–[33]. In the following, two examples of shade mitigation strategies are described.

**Increasing module granularity**

This section gives at first a short overview of PV module topologies with different module integrated electronics. Subsequently simulation results are discussed, rating the different PV module topologies´ potential of shade mitigation.

One alternative strategy for mitigation of nonlinear shading effects is to divide the cells in the module into smaller groups of cells and apply an active bypass diode for each group of cells, instead of using a passive bypass diode [34]. An active bypass diode actually is an electrical circuit consisting of Metal-Oxide-Semiconductor Field-Effect Transistors (MOSFETs), which can be controlled via a duty cycle as control signal. Such module integrated electronics (MIEs) can be categorized in the following groups [34]: (i) conventional systems, consisting of three bypass diodes per module and a central converter to change the output voltage level; (ii) buck converters, to which normal PV modules are connected and thus the output current of the shaded module is to be controlled; (iii) buck-boost converters, in which both current and voltage are to be controlled; and (iv) voltage equalizers, which are a combination of different converters or even bidirectional converters to equalize the voltage by power processing [35]–[37].

In conventional modules, the cells are generally grouped in three groups of series connected cells and to each group one bypass diode is connected in parallel. The MPPT algorithm of the (string) inverter optimizes the generated power. MIEs using buck or buck-boost converters are potentially interesting for controlling current or voltage and current of the shaded cell group [34].

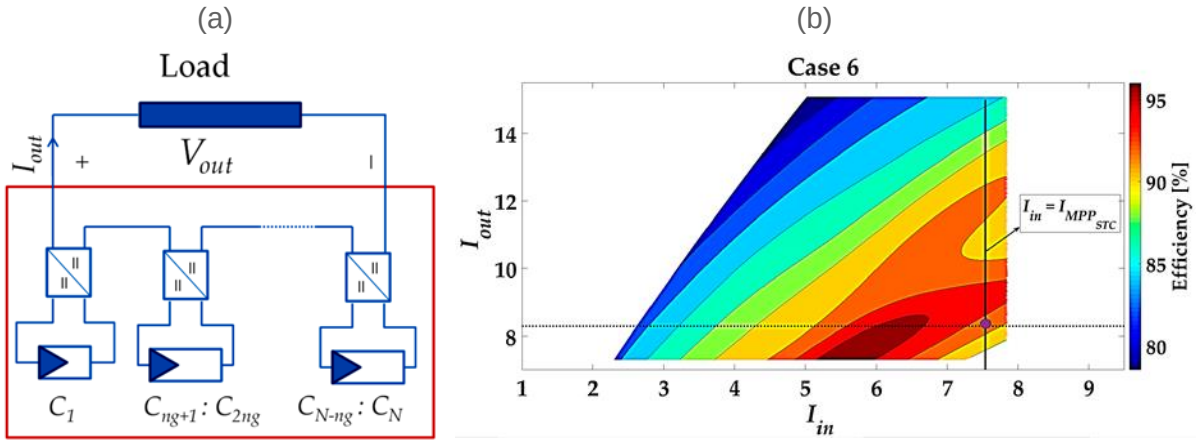


**Figure 18: (a) Smart module architecture with $n_g$ cells in $N_G$ groups with electronic circuits, (b) contour plots of efficiency as a function of input and output current for a smart module with ten groups of six cells [34].**

While in the ultimate case with ideal lossless bypass diodes one bypass diode per cell shade mitigation is optimal, this is certainly not economically and technically optimal due to losses of real bypass diodes. Hence, a compromise must be sought between the number of bypass diodes, and thus groups of series-connected cells $N_G$. Figure 18 (a) shows the principle design of a module with $n_g$ solar cells in $N_G$ groups of cells in a module [34]. Using 60 monocrystalline silicon solar cells (open circuit voltage ($V_{OC}$) of 613 mV, short circuit current ($I_{SC}$) of 7.92 A, maximum power ($P_{max}$) of 3.7 W, efficiency $\eta$ of 15.4%) and a number of DC/DC converters, in this case Linear Technology LTM4611, the optimum configuration in terms of converter efficiency has been determined. Figure 18 (b) shows the efficiency contour plots, for a module with ten groups of six cells. Specifications per group are thus: $V_{OC}$ = 3.67 V, $I_{SC}$ = 7.92 A, $P_{max}$ of 22.18 W. Because of the system topology, the output current flow of each converter is equal as all converters are connected in series. This strategy extracts as much power as each group of cells could generate, even though some groups may be very heavily shaded. In the smart module architecture all cells, even shaded ones, are thus producing power efficiently and none of the cells is bypassed.

Four different module topologies have been modelled and simulated to assess the shading mitigation potential: (1) an so called ideal module, in which for each cell a DC/DC converter is responsible to level up the current for shaded cells, (2) smart module with ten groups of six cells in which for each group a DC/DC converter is operated, (3) a module with three parallel to a DC/DC converter connected strings with each string consisting of 20 cells connected in series and a blocking diode (normally this topology is implemented for strings of PV modules instead of PV cells) and (4) a standard module with series-connected strings, operated with a DC/DC converter, consists of three series groups of 20 cells, where each group is equipped with one bypass diode.

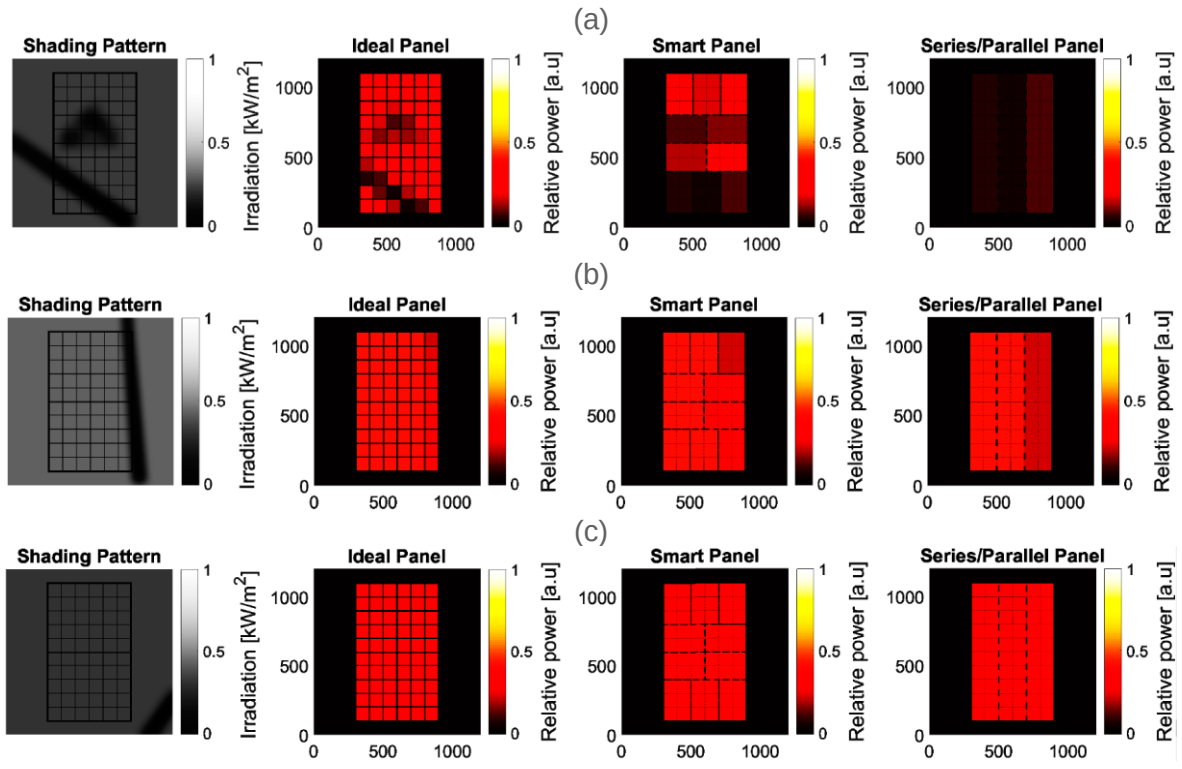


**Figure 19: Effect of different shading patterns on different module topologies, (a) combined pole and random shading pattern, (b) pole shading pattern, (c) no shade [34].**

Figure 19 shows the simulated output power for three different shading patterns on different module topologies. The power of the ideal module clearly reflects the shade that is cast on the module. This is most clear in Figure 19 (a). Current and voltage of the series/parallel module is considerably affected by the shade Figure 19 (b), in which only the edge of the module is shaded reveals that two groups of cells in the smart module are affected, and 1/3 of the series/parallel module. Module power is nearly equal when there is no shade as shown in Figure 19 (c), illustrating some loss in the smart module, see also Table 5. Table 5 compares the output power of the different introduced four module architectures under the three shading patterns show in Figure 19 (a)-(c).

**Table 5: Output power for three different shading patterns, as shown in Figure 19 [34].**

| Architecture | (a) combined pole and random shading pattern [W] | (b) pole shading [W] | (c) no shade [W] |
|---|---|---|---|
| Ideal | 48.35 | 84.23 | 116.54 |
| Smart | 18.49 | 69.00 | 108.85 |
| Series Connected | 0.84 | 30.95 | 112.35 |
| Parallel Connected | 4.51 | 62.97 | 113.42 |

Measured irradiance data is used as simulation model input, which is acquired at the Utrecht Photovoltaic Outdoor Test facility at Utrecht University campus in the center of the Netherlands recorded at 7 September 2016 (see Figure 20). The 15-minute time frame 1 is used for the simulation of (a) combined pole and random shading pattern, time frame 2 for the simulation of the pole shading and time frame 3 for simulation of no shade conditions.

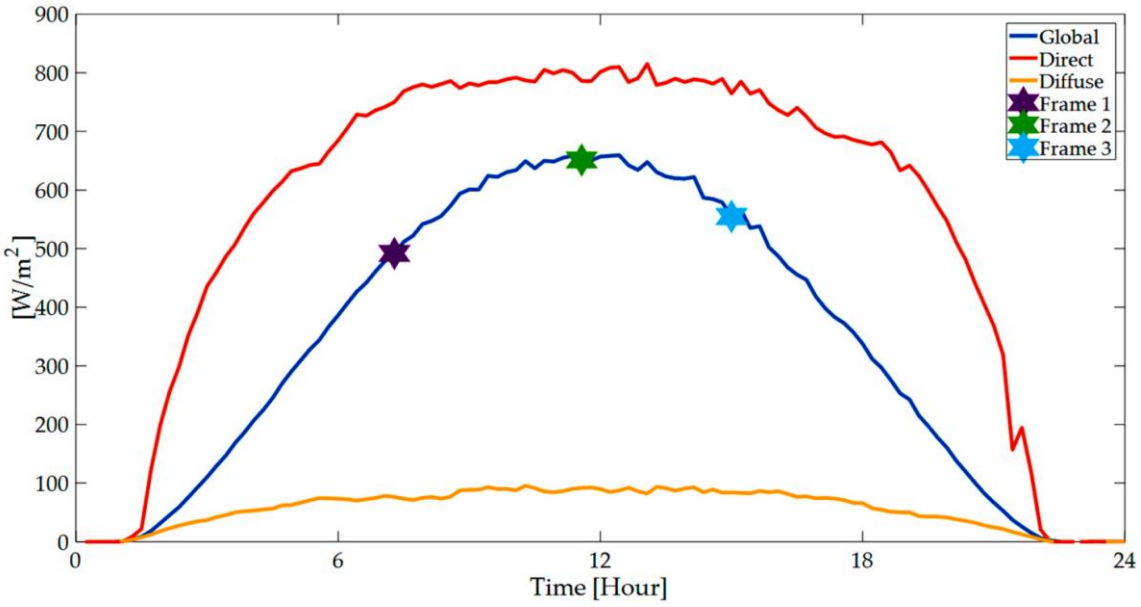


**Figure 20: Global, direct and diffuse irradiation levels on 7 September 2016 at the Utrecht Photovoltaic Outdoor Test facility at Utrecht University campus [34].**

The smart module with ten groups of six cells has been manufactured recently, using specially designed electronic circuitry based on the considerations stated above [38]. This has been tested with several shading patterns. Figure 21 illustrates the movement of the shade on the smart module during little over one hour, and which cell groups are affected. In addition, a tree with some leaves was moving due to wind in front of the module as well.

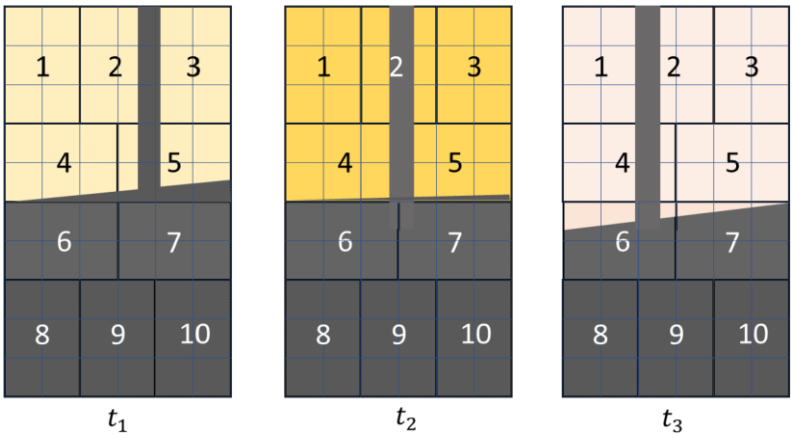


**Figure 21: Moving shading pattern during the experiments for different time frames ($0 < t_1 < 20$ mins; $20 < t_2 < 40$ mins; $40 < t_3 < 60$ mins [38].**

Figure 22 shows that groups six to ten (G6 to G10) do not generate power, while the other groups show fluctuating power, which clearly corresponds to the shading pattern. Summarizing the results, it can be inferred that the average output power in the smart module is higher than the expected average power of a conventional module with three bypass diodes. The smart module generated on average 8.13 W under a very restricted shading condition with three different shade types at maximum irradiation of 350 W/m$^2$.

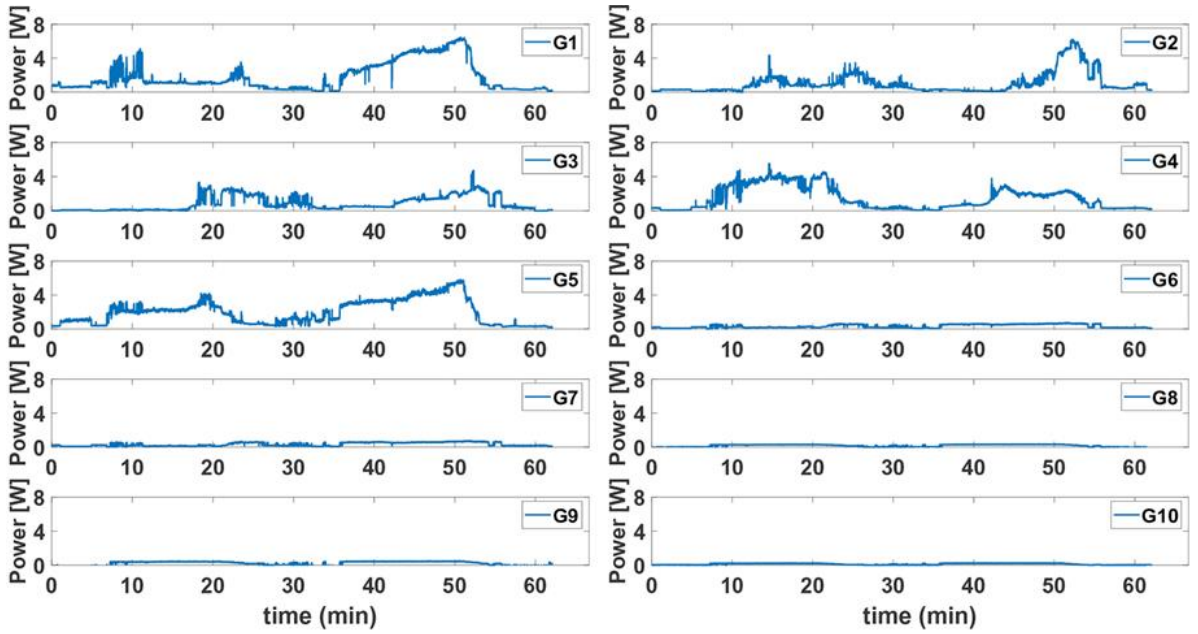


**Figure 22: Output power of the ten cell groups [38].**

However, considering the outputs from groups with severe shading a conventional panel under these testing conditions would generate only about 1.64 W, or about five times less, which is due to the bypass diodes being activated. It remains to be seen in how far annual yields would be improved for shaded PV systems.

**Increasing cell granularity, Tessera module**

In this section a real build PV module with a high cell granularity (Tessera module) is introduced and measurement results from equally shaded single PV modules (standard and Tessera, both with the same nominal power) are compared as well as measurement results from two six-module fields (standard and Tessera, all with the same nominal power). The Tessera PV module topology does not refer to the four PV module topologies introduced in the previous section.

The Tessera solar module concept [39], [40], named after 'tesserae' being used as individual tiles in ancient mosaics, makes use of small cells that are cut by laser scribing from 156 x 156 $mm^2$ silicon cells. The used cells are 6-inch metal wrap through (MWT) c-Si cells, which have been cut to produce 16 mini cells. These are interconnected in series, and connected to a bypass diode that is laminated in the back sheet. Being back contact solar cells, interconnection schemes can be designed using a conductive backsheet, which thus allows to integrate diodes, see Figure 23 (a).

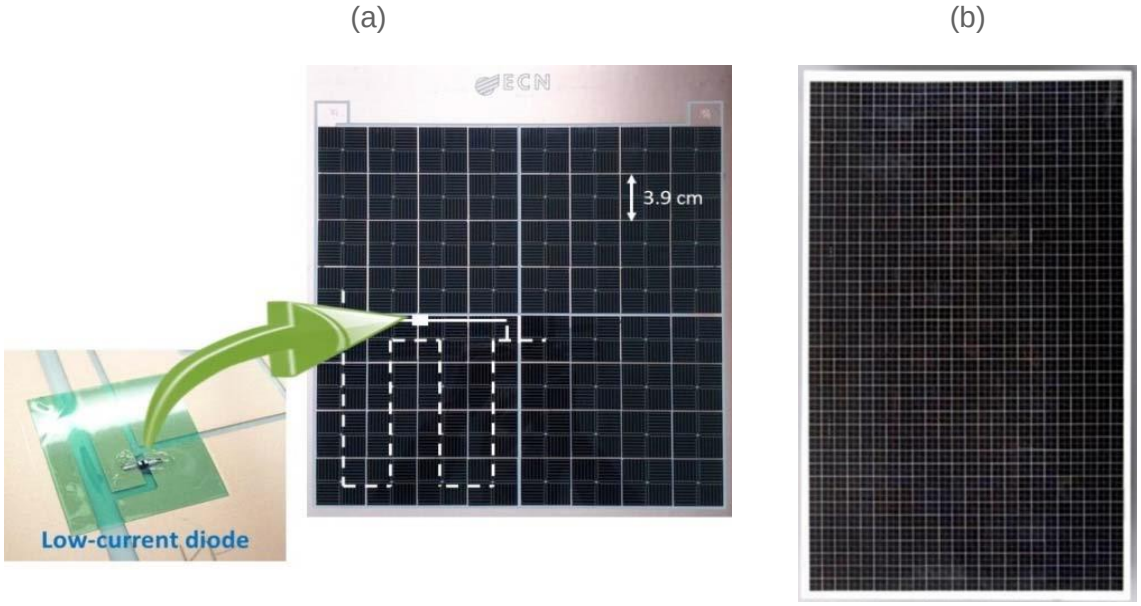


**Figure 23: (a) Building block of Tessera module concept consisting of four full size MWT cells, (b) full module of 1.6 m$^2$ consisting of 960 mini cells [24].**

Blocks of 64 mini cells can then be connected in parallel forming modules with custom size and rated power (see Figure 23 (b)). This module building block shows $V_{OC}$ of around 40 V and $I_{SC}$ of 0.6 A, under standard test conditions [40]. A standard module size of 1.6 m$^2$ comprises 15 of these module building blocks of 64 mini cells that are connected in parallel, thus yielding $I_{SC}$ of 8 A, and module rating of 265 $W_p$. Module manufacturing equipment is the same as for standard back contact modules, albeit with a small modification in the production line.

The design of the blocks is optimized for shade resilience. The sub cells can be regarded as pixels, and only a shaded pixel will be affected by the shade, and not 1/3 of a (standard) module. Because of a somewhat different output compared to a standard module, a dedicated inverter may be required. However, the voltage of the module is almost independent of shading conditions, which would make inverter design less complex [41].The performance of the Tessera module has been experimentally tested and compared to a standard module. To this end, artificial shading conditions have been applied while using a solar simulator. Note, the absence of diffuse irradiance exaggerates the results somewhat. The shade performance was defined as the ratio of maximum power obtained in a shading condition and the maximum power of a standard 3-string module. Another measure is the shade linearity. This will be 100% if a *x*% sized shade will lead to the same *x*% of power loss induced by that shading [40]. As shading conditions, a pole, a dormer and a tree have been used. Table 6 shows that the Tessera module considerably outperforms the standard module both for shade performance as well as shade linearity.

**Table 6: Effect of shading conditions on the shade performance and shade linearity of the Tessera module compared to standard module [40].**

| Shadow type | Shade performance | | Shade linearity | |
|---|---|---|---|---|
| | Standard module [%] | Tessera [%] | Standard module [%] | Tessera [%] |
| Pole | 17 | 67 | 20 | 76 |
| Dormer | 26 | 64 | 38 | 92 |
| Tree | 53 | 73 | 66 | 92 |

Obviously, the advantage of using a Tessera module rather than a standard module depends on the actual shape and size of the shading condition. A PVsyst simulation has been performed for a house with a dormer in an urban environment with trees and a lamppost, with PV modules on its roof. On an annual basis, the simulations show that a shade-induced loss of 11% is incurred for the standard module, while the Tessera module shows only 7% loss. Thus, the Tessera module shows a 4% higher energy yield compared to a standard module. This average advantage may seem low, but the simulation includes hours in the year for which no shade is cast on the modules. The yield advantage can be much higher in winter months, where shading is adversely affected PV yield (see also [23]). For example, a sunny hour in January shows a yield advantage of 24% [40].

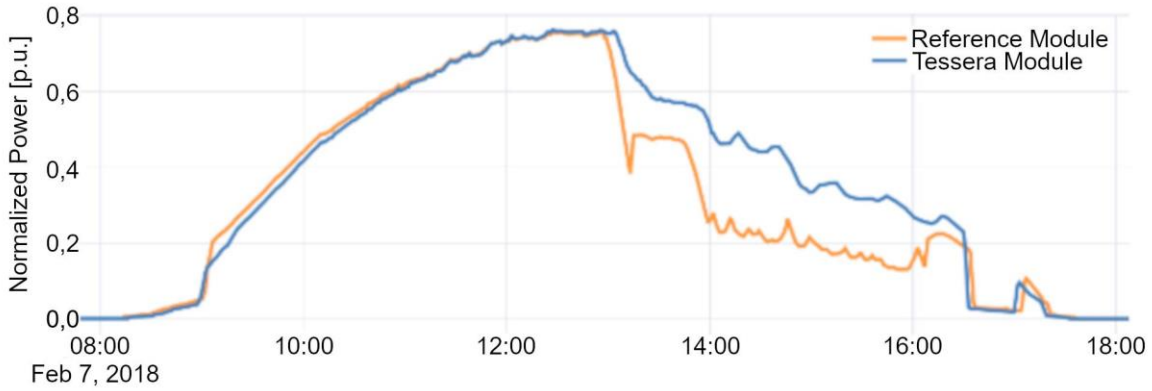


**Figure 24: Normalized power output of a Tessera and standard module under the same partial shading conditions [42].**

A field test with six 265 $W_p$ Tessera modules has been performed comparing their performance to two reference systems, all with the same orientation and tilt: one with six standard modules, also of 265 $W_p$ capacity each, connected in series to a string inverter (SI), and one with six standard modules each equipped with a microinverter (MI) [42]. The Tessera modules are also connected to individual microinverters. A pole shade has been used for assessment of partial shading effects.

Figure 24 compares the normalized power outputs of the Tessera and reference module under identical shading conditions of a day in winter. The pole affects the performance of the modules between 1 pm and 4:30 pm, while in the morning power generation is identical. For this

particular day, the Tessera module generates 15% more energy than the reference module. Interestingly, micro inverter efficiency is somewhat higher in case of the Tessera module due to the more stable voltage output of the module. The shade leads to voltage reduction of about 1/3 for the reference module.

This can also be seen in Figure 25, where DC voltage, relative power output and micro inverter efficiency for a period of six months is shown. Besides the cloud of points between ~27 V and ~37 V, for both modules, another cloud of points is visible around 20 V. All in all, inverter efficiency is 2-3% higher in case of the Tessera module [42].

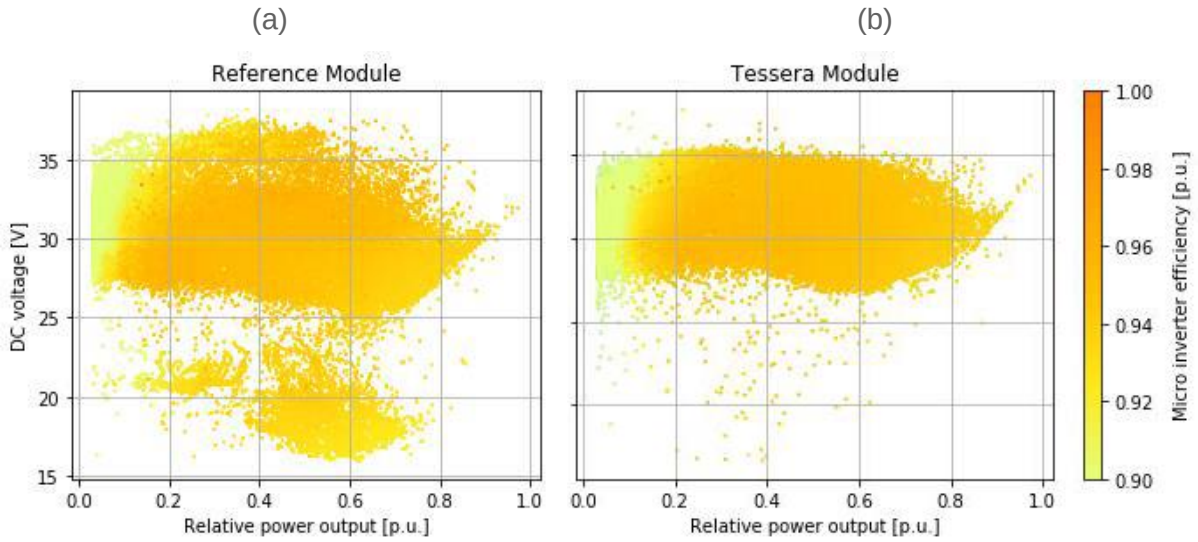


**Figure 25: Relation of voltage, power and efficiency of the micro inverters for the reference ((a) and Tessera ((b) system [42].**

A further comparison of measured data is shown in Table 7. This shows that in this test with the pole shade present in the afternoon (see Figure 24) micro inverters yield higher AC performance ratio than the string inverter. The higher MI efficiency for the Tessera module due to more stable voltage levels is also corroborated here. Based on these results, it is estimated that annual shading loss in residential systems with Tessera modules and microinverters would be similar to a module with one bypass diode per cell. Compared to standard modules with three bypass diodes, annual shading loss would be decreased from 9.3% to 3.3% [24].

**Table 7: AC performance ratio for the three modules systems [28].**

| **Module/inverter system** | **Months** | | | | | | | |
|---|---|---|---|---|---|---|---|---|
| | Feb | Mar | Apr | May | Jun | Jul | Aug | Sep |
| Tessera/MI | 0.91 | 0.88 | 0.85 | 0.84 | 0.83 | 0.81 | 0.76 | 0.84 |
| Standard/MI | 0.88 | 0.87 | 0.83 | 0.80 | 0.85 | 0.81 | 0.73 | 0.82 |
| Standard/SI | 0.76 | 0.84 | 0.81 | 0.77 | 0.84 | 0.78 | 0.68 | 0.78 |

The measurement protocol presented here is suitable to show advantages of the Tessera PV module configuration in specific shaded operation compared to standard PV modules. In order to provide information about the effect of shade resilient PV modules on the energy yield, or other performance indicators for specific PV systems operating under dynamic shading conditions in the course of a year a measurement protocol respecting dynamic shading has to be developed.

# 4 PERFORMANCE CHARACTERIZATION OF COMPLEX NEW SYSTEMS WITH PV

## 4.1 Transient PV Battery quotation according to the NESPRESSO$^{TM1}$-test

PV Battery systems show different transient behavior. System parameters are derived from the measured step response characteristics like dead-time, settling-time as it is commonly used in the technical field. This is in accordance with the German Energy Storage Association (BVES) and German Solar Industry Association (BSW) efficiency guidelines [43] described in section 4.4.

The end customers of a PV battery storage system in a single-family house require decision-making facts during the purchase phase that they understand. Thus, the Zurich University of Applied Science (ZHAW) Institute of Energy Systems and Fluid Engineering (IEFE) proposes a very practical transient figure to describe the speediness of that storage system to provide a standard coffee machine with stored solar power.

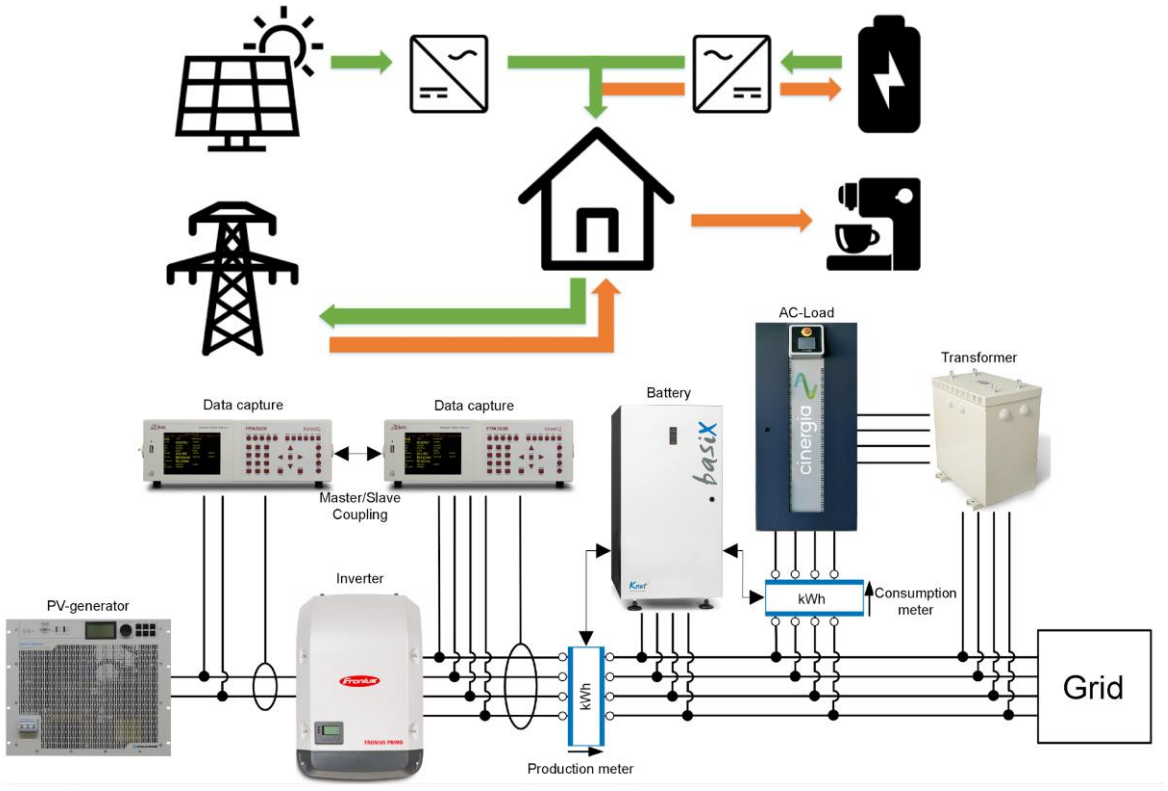


**Figure 26: Test setup to measure the amount of Energy coming from the battery to supply a Nespresso$^{TM1}$ coffee machine at ZHAW IEFE [44].**

[1] The trademarks, trade names, logos, service marks, domain names or other distinctive brand features of Nespresso ("Trademarks") displayed are the exclusive property of Nespresso and/or Nestlé.

During the NESPRESSO$^{TM1}$-test the quotation of used electricity coming from the battery compared to grid electricity is measured. A standard small single cup Nespresso$^{TM1}$ machine is used as consumer load which was connected to the test setup given in Figure 26.

To rate the speed of the battery storage control system a *Nespresso$^{TM1}$-ratio* with

$$Nespresso^{TM} - ratio = \frac{E_{Bat}}{E_{Nespresso^{TM}}} \quad (11)$$

was introduced. It is the ratio of $E_{Bat}$ the energy the battery storage system supplied during the coffee making process and the energy $E_{NespressoTM1}$ totally used for coffee making by the coffee machine.

Figure 27 shows during the 90 s it takes to brew one cup of coffee the used electrical power cycles between 1200 W and 0 W in red and the power delivered from the battery system in yellow. In this example the delivered power from the battery system lag vast behind the consumer need. So finally, the performance indicator *Nespresso $^{TM1}$-ratio* is only 1/8. One part of the used energy comes from the battery out of 8 energy units – illustrated by green and red Nespresso cup symbols.

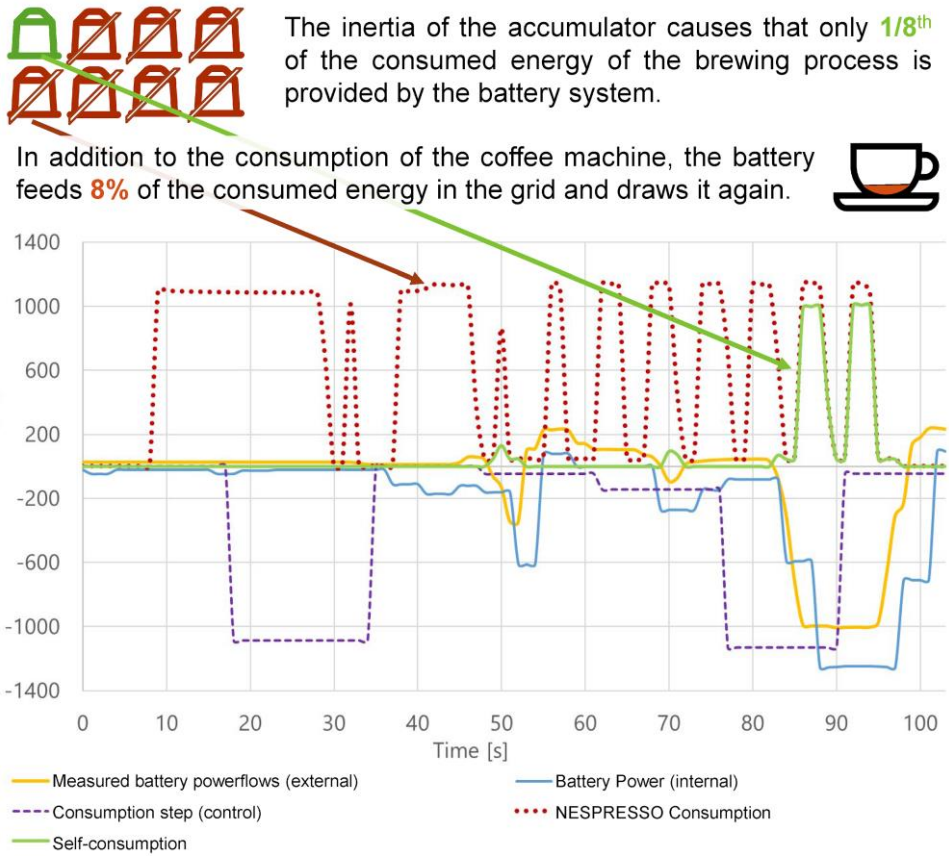


**Figure 27: Measurement results of the Nespresso Test of an AC coupled PV Battery System is given with the customer load of the coffee machine - in red - and the power delivered from the battery system – yellow, with the result of only 1/8 of the used energy coming from the battery [44].**

This Nespresso $^{TM1}$ use case shows how important meaningful key performance indicators for PV battery storage systems regarding real operating conditions are. Indicators like the nominal

battery capacity, or the maximum battery inverter efficiency as often found in data sheets are not meaningful. Besides the Nespresso ratio in section 4.4 regarding BVES/BSW efficiency guidelines further key performance indicators and measurement protocol for PV battery systems are described [43].

## 4.2 Using a dynamic system model to characterize a complex PV system

Characterizing a PV system component completely requires knowledge of each power flow path leading into and leaving this component, as well as the respective efficiency curves. At the Institute for Solar Energy Research Hamelin ISFH, a dynamic simulation model was developed for the evaluation of PV storage concepts. It calculates the electrical power flows between the system components PV generator, battery, electrical household load (HHL) and distribution grid. Thus, the losses occurring in the system can be localized for any load and irradiance conditions.

### 4.2.1 Simulation model

The simulation model only considers the active power flows of conversion paths shown in Table 8 in the PV storage system to determine the efficiency:

**Table 8: Conversion paths in PV storage systems.**

| Conversion paths | Description of power flows |
|---|---|
| PV2AC | PV power for direct load coverage and grid feed-in |
| PV2BAT | PV power for battery charging<br>(AC system: PV2BAT consists of PV2AC and AC2BAT) |
| BAT2AC | Discharge power from the battery to cover the load |

The described conversion paths are shown in Figure 28 for a DC- and AC-coupled PV storage system. The power-dependent efficiencies of the conversion paths are determined by measurements at the points sketched in light blue.

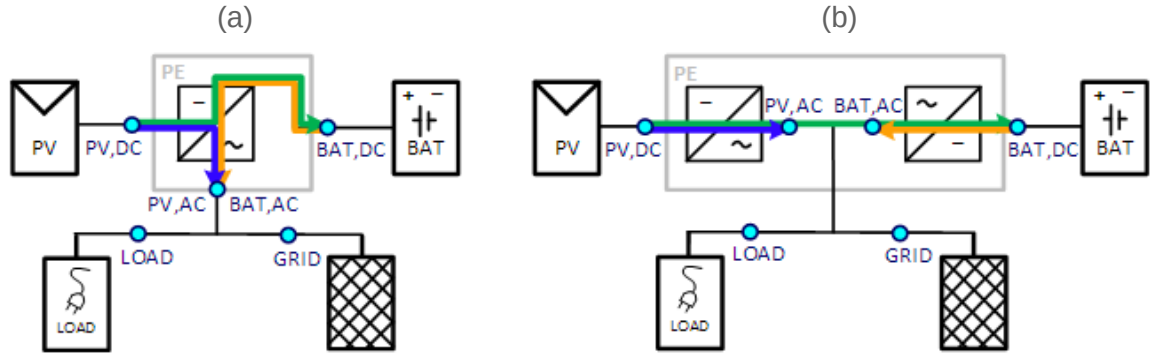


**Figure 28: Schemes depict the conversion paths in the DC-coupled (left) and AC-coupled PV storage systems (right) including the measurement points required for system characterization (light blue) [45].**

The amount of power flows between the system components depends primarily on the PV generator power, the electrical load and the dimensioning of the storage. The variable input variables for the simulation model are the irradiation intensity at PV module level, the module,

and the ambient temperature, as well as the electrical load $P_{LOAD}$. The power flows in the system are calculated according to four steps.

In the **1st step** the power for direct load coverage $P_{PV2LOAD}$ is calculated. The possible invertible ( ' for invertible) PV output $P_{PV,AC}$' results from the output of the PV generator $P_{PV,DC}$ and the conversion efficiency of the inverter $\eta_{PV2AC}$.

$$P_{PV,AC}\prime(t) = P_{PV,DC}(t) * \eta_{PV2AC}(P_{PV,DC}(t)) \quad (12)$$

$P_{PV2LOAD}$ corresponds to the smaller value of the total invertible PV power and the power value of the load profile, limited by the nominal power of the PV inverter:

$$P_{PV2LOAD}(t) = \min\left(P_{PV,AC}\prime(t), P_{Load}(t)\right). \quad (13)$$

The charging power $P_{PV2Bat}$ or discharging power $P_{BAT2AC}$ at the battery terminals in self-consumption-optimized operation is calculated in the **2nd step**. Two cases must be distinguished here:

(a) Calculating the charging power of the storage $P_{PV2Bat}$ for $P_{PV,AC'} > P_{LOAD}$, DC- and AC-coupled systems have to be distinguished. To determine the charging power $P_{PV2Bat}$, the excess PV power $P_{Bat,AC}$' (AC-side) and $P_{Bat,PV}$' (DC-side) are first determined by

$$P_{Bat,AC}\prime(t) = P_{PV,AC}\prime(t) - P_{Load}(t), \quad (14)$$

$$P_{Bat,PV}\prime(t) = P_{PV,DC}\prime(t) - P_{Load,DC}(t). \quad (15)$$

The auxiliary variable $P_{LOAD,DC}$ describes the DC PV power required to cover the load

$$P_{Load,DC} = \frac{P_{Load}}{\eta_{PV2AC}(P_{Load})}. \quad (16)$$

The excess PV power consumed by the battery is limited by the system-specific, charge condition-dependent maximum charge power ($P_{Bat,AC}$' limited by $P_{Bat,AC}$ and $P_{Bat,PV}$' limited by $P_{Bat,PV}$):

AC-coupling:
$$P_{PV2Bat,AC}(t) = P_{Bat,AC}\prime(t) * \eta_{AC2BAT}(P_{Bat,AC}\prime(t)), \quad (17)$$

DC-coupling:
$$P_{PV2Bat,DC}(t) = P_{Bat,PV}\prime(t) * \eta_{PV2BAT}(P_{Bat,PV}\prime(t)). \quad (18)$$

(b) For both system topologies the DC discharge power $P_{BAT2AC}$ for $P_{PV,AC'} < P_{LOAD}$ is:

$$P_{BAT2AC}(t) = \frac{P_{BAT,AC}(t)}{\eta_{BAT2AC}\left(\frac{P_{BAT,AC}(t)}{\eta_{BAT2AC}(P_{BAT,AC}(t))}\right)}. \quad (19)$$

In the **3rd step** the exchange power with the grid $P_{Grid}$ is calculated. If the battery is unable to compensate the residual load from PV feed-in and household load $P_{Load}$ the remaining power is fed into the grid ($P_{Grid}$ positive) or drawn from it ($P_{Grid}$ negative)

$$P_{\text{Grid}}(t) = P_{\text{PV,AC}}\prime(t)\, P_{\text{BAT,AC}}(t)\; P_{\text{Load}}(t) - P_{\text{VB}}(t). \tag{20}$$

In the DC-coupled system, while the battery is being charged, $P_{\text{Grid}}$ is modelled as

$$P_{\text{Grid,PV2BAT,DC}}(t) = (P_{\text{PV,DC}}(t) - \frac{P_{\text{PV2BAT,DC}}(t)}{\eta_{\text{PV2BAT}}}) * \eta_{\text{PV2AC}} - P_{\text{Load}}(t) - P_{\text{VB}}(t) \tag{21}$$

$P_{\text{VB}}$ describes the power consumption of the PV inverter, battery converter and power meter at the grid connection point (GCP) for the various operating modes "idle", "standby" and "sleep".

As a **4th step** the state of charge $C$ of the battery (in kWh) is calculated. It influences the maximum charging and discharging power in the next time step.

$$C(t+\Delta t) = C(t) + (P_{\text{PV2BAT}}(t) - P_{\text{BAT2AC}}(t) - P_{\text{SPV}}(t)) * \Delta t \tag{22}$$

The power $P_{\text{SPV}}$ describes the battery losses, determined from several charging cycles as a function of the charging power. E. g. Typical self-discharge rates are 20% per month for lead-acid storage and 2% per month for Li-ion [46].

For the evaluation of the PV storage systems the share of self-consumption and the degree of self-sufficiency are calculated as:

$$\varepsilon_{\text{self-sufficiency}} = \frac{\int P_{\text{PV2LOAD}}(t) + P_{\text{BAT2LOAD}}(t) * \eta_{\text{BAT2AC}}(P_{\text{BAT2AC}})\; \mathrm{d}t}{\int P_{\text{LOAD}}(t)\, \mathrm{d}t} \tag{23}$$

$$\varepsilon_{\text{self-consumption}} = \frac{\int P_{\text{PV2LOAD}}(t) + P_{\text{BAT2LOAD}}(t) * \eta_{\text{BAT2AC}}(P_{\text{BAT2AC}})\; \mathrm{d}t}{\int P_{\text{PV,DC}}(t)\, \mathrm{d}t} \tag{24}$$

The system efficiency $\eta_{\text{Sys}}$ describes the PV energy used to cover the load and fed into the grid in relation to the amount of energy fed into the system.

$$\eta_{\text{Sys}} = \frac{E_{\text{used}}}{E_{\text{supplied}}} = \frac{\int P_{\text{PV2LOAD}}(t) + P_{\text{PV2GRID}}(t) + (P_{\text{BAT2LOAD}}(t) + P_{\text{BAT2GRID}}(t)) * \eta_{\text{BAT2AC}}(P_{\text{BAT2AC}})\; \mathrm{d}t}{\int P_{\text{PV,DC}}(t) + P_{\text{VB}}(t)\; \mathrm{d}t} \tag{25}$$

### 4.2.2 Parameterization of the simulation model

The above introduced simulation model is parameterized with the usable storage capacity, the performance-related storage losses and the efficiency characteristics of the paths PV2AC, PV2BAT and BAT2AC measured in a laboratory [47] or taken from data sheets. The efficiency of the PV2BAT conversion path for an AC-coupled PV storage results from the partial conversions PV2AC and AC2BAT ($\eta_{\text{PV2BAT}}=\eta_{\text{PV2AC}}*\eta_{\text{AC2BAT}}$). Additionally, the transfer functions of the entire PV storage systems must be considered. They strongly depend on the inertia and deviation of the MPP tracking of the PV inverter and of the Battery Management System. Based on laboratory measurements they are adjusted individually. Static control deviations were not considered in the model.

### 4.2.3 Validation of the simulation model

The model was tested on the basis of two systems in one-day comparison measurements. As a validation example, Figure 29 shows the modeled and measured power flows of an AC-coupled lithium-ion battery matching very well.

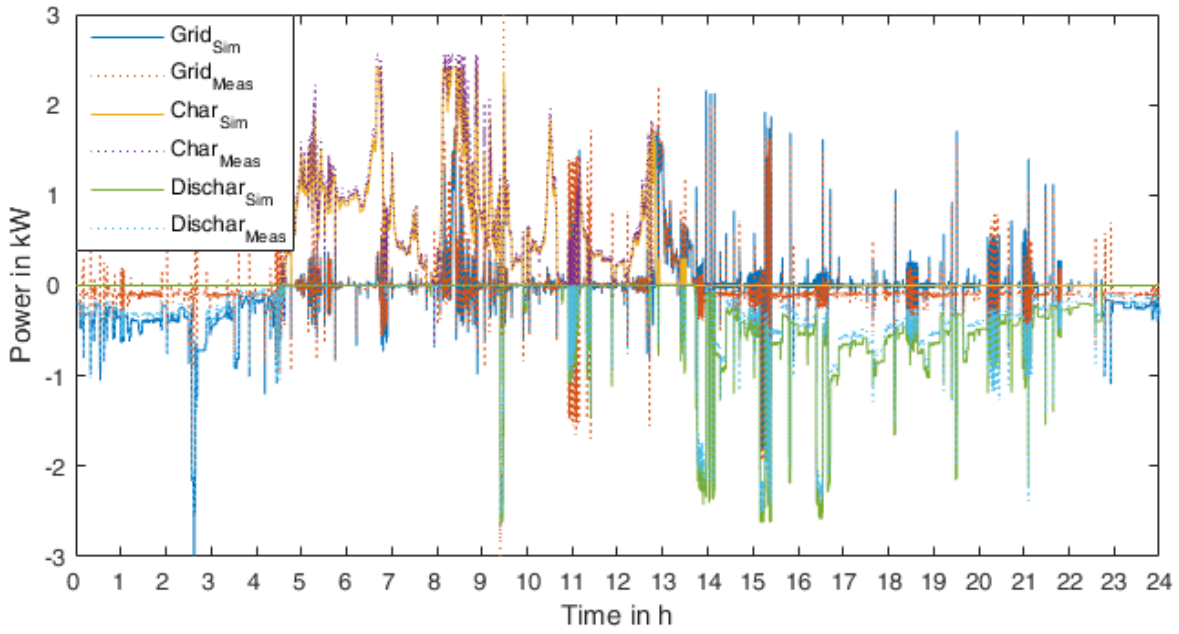


**Figure 29: Comparison of the simulated performance at the battery terminals and at the GCP with a one-day laboratory measurement (AC-coupled lithium-ion battery) [45].**

Table 9 shows the system parameters determined for simulation and measurement. The characteristic values for the DC system match even better.

**Table 9: Comparison of the calculated and measured assessment parameters.**

| | DC-System (Lead-Acid) | | AC-System (Lithium-Ion) | |
|---|---|---|---|---|
| | Model | Measurement | Model | Measurement |
| $\varepsilon_{Self\text{-}sufficiency}$ | 71.1% | 69.5% | 81.8% | 78.8% |
| $\varepsilon_{Self\text{-}consumption}$ | 65.6% | 65.3% | 74.6% | 71.7% |
| $\eta_{Sys}$ | 76.6% | 76.9% | 81.2% | 80.8% |

### 4.2.4 System evaluation

For the evaluation of the measured PV battery storage systems, yearly simulations with secondly weather data [48] and secondly HHL profiles (3.5 MWh/a to 8.6 MWh/a) [49] [50] were carried out. The simulated 11 kWp PV generator is inclined by 30°, oriented south and connected to a 10 kW PV inverter. The simulations show that, as expected, the degree of autarky and the share of self-consumption depend strongly on the season (Figure 30).

Regardless of the HHL profile, the autarky of both systems is often below 10% in winter and almost continuously above 90% in summer. With self-consumption it is the other way around. At least 10% of the PV output cannot be used in the system in winter due to conversion and storage losses.

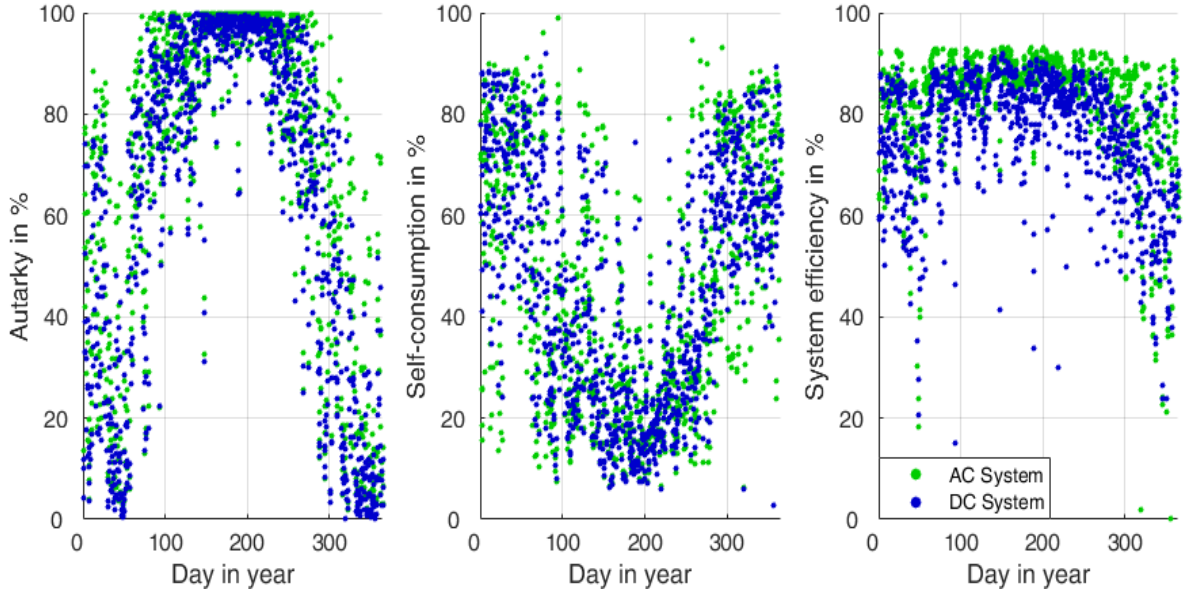


**Figure 30: Daily calculated system parameters (degree of self-sufficiency, share of self-consumption and system efficiency) in the course of the year [45].**

Throughout the year and averaged over 3 different HHL profiles and based on the amount of energy supplied to the system the average system efficiency for the lead-acid DC system is 83.2% and for the lithium-ion AC system 89%. Despite the slightly smaller storage capacity in the AC system, the calculated yearly self-consumption and degree of self-sufficiency is on average 3 to 4% higher than in the DC system. Depending on the selected HHL profile the yearly share of self-consumption lies between 38.3% and 49.2%, the degree of self-sufficiency between 62.3% and 75.8%. Including the system's consumption, the average daily losses in the DC (AC) system are 3.8 kWh (3.1 kWh) with an average daily energy supplied from the PV system of 30 kWh. An ideal system with 100% efficiency has 4 to 8% higher degree of yearly self-sufficiency and 10% higher share of self-consumption.

Section 4.1 and 4.3 to 4.4.8 show that for generating meaningful performance indicators for PV battery systems sufficient characterization of the respective components is essential. This requires knowledge of each power flow path leading into and leaving this component, as well as the respective efficiency curves. The described battery system model uses the figures measured accordingly to the efficiency guideline and enables to calculate any meaningful performance indicator regarding battery storage system operation in a household environment use case.

## 4.3 Hardware-in-the-Loop tests on complete systems with heat pumps and PV for the supply of heat and electricity

For the evaluation of the performance of heating and electric supply systems for buildings an overall system test method called Concise Cycle Test (CCT) was developed at the Institute for Solar Technology, Rapperswil SPF [51]. These tests comprise typical boundary conditions of climate and load in a test cycle and test realistic dynamic operation with a hardware-in-the-

loop approach. During a CCT, the tested system runs autonomously to cover the demand of a virtual building. One type of energy system is a combination of PV with heat-pump and heat storage or battery storage units.

### 4.3.1 Introduction

The performance of PV power systems as part of a complex energy system is depending on many parameters and difficult to forecast. To improve single components in such a system or the system constellation the Hardware-in-the-loop test is a method to have results under realistic conditions in a short time. To describe the method, we used a system with heat pumps and PV.

The complete systems were installed on a test rig that emulated a building with PV electricity production as well as the heat demand for domestic hot water and space heating and the electricity demand for household appliances. The test bench also emulated the environmental heat (air or ground source) as the source of the heat pump. The applied loads for space heating, hot water and household electricity are pre-defined to ensure an identical load and thus allow a direct comparison of the tested systems. In addition to insights into the performance of the tested systems, insights into the advantages and disadvantages of various key performance factors for these kinds of systems were gained. It is found that self-sufficiency and self-consumption are not suitable optimization parameters. The grid purchase ratio is proposed instead.

### 4.3.2 Methods

The CCT is a test method for testing complete heating systems under realistic conditions. The procedure for simulation and emulation can be outlined as follows: The test bench software transfers current measured values to the simulation software at the end of each time step. In the simulation, the behavior of the respective component is calculated according to the input data and communicated to the test bench software. During each time step, the test bench software controls the emulation while the simulation software pauses. Only at the end of the time step measured data is transferred to the simulation software, and the control target variables for the next time step are determined by the simulation software. Figure 31 shows the weather data of the 6-day test cycle of the CCT, which are representative of a whole year.

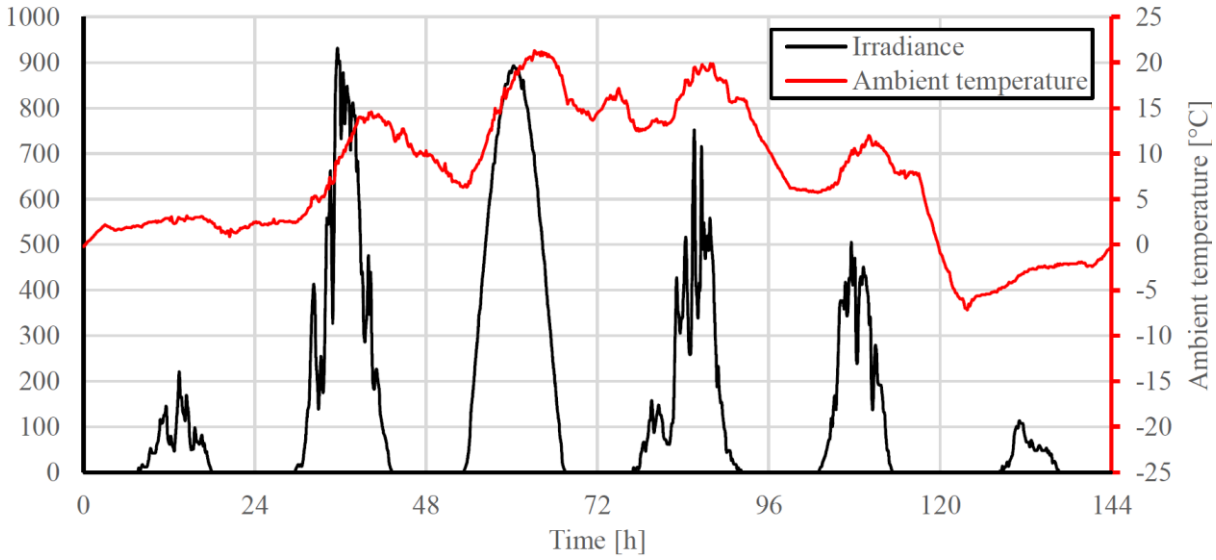


**Figure 31: Weather data of the 6-day test cycle for the CCT.**

In this example four tested systems include a PV system and a heat pump. The PV system size has been chosen such that its annual electricity yield corresponds roughly to the annual electricity consumption for the heat pump heating system and the household appliances. The storage concept differs considerably (thermal storage tanks like Drink Hot Water (DHW), heating buffers and electrical storage devices). Table 10 shows four tested system scenarios including a PV system and a heat pump.

**Table 10: Storage capacities of the tested systems (thermal and electric) and source of the heat pump [52].**

| Tested systems: | **2TankBrine** | **Combi BatAir** | **Combi Air** | **Combi BatBrine** |
|---|---|---|---|---|
| Thermal Energy Storage | DHW storage tank + heating buffer | Combistore | Combistore | Combistore |
| Volume | 500 l + 300 l | 600 l | 900 l | 900 l |
| Electrical Storage Device | No | Yes | No | Yes |
| Useable capacity | - | 6.5 kWh | - | 6.9 kWh |
| Heat pump source | Brine | Air | Air | Brine |

The common feature of all tested systems is a 5.8 $kW_p$ PV system and a heat pump.

Table 11 shows the common boundary conditions for the test method respectively the tested systems.

**Table 11: Boundary conditions of discussed CCTs.**

| PV System | Space Heating | Domestic Hot Water | Household Appliances | Comments |
|---|---|---|---|---|
| 5.76 $kW_p$<br>2x12 modules | heating floor<br>140m² | 4 persons | 4 persons | use of thermal mass excl. |
| orientation south | 7.4 MWh/a | 3.0 MWh/a | 3.3 MWh/a | |
| tilt angle 45° | respectively 120 kWh in a 6-day test | respectively 50 kWh in a 6-day test<br><br>max. flow rate 18 l/min | respectively 55 kWh in a 6-day test<br><br>max. power 5 kW | |

Both thermal and electrical power are measured in the system test. The thermal output is measured at the interface to the test bench via immersed temperature sensors in the flow and return lines and a volumetric flow meter. The important electrical variables for the energy balance are measured galvanically integrated as Figure 32 shows. Table 12 lists these variables.

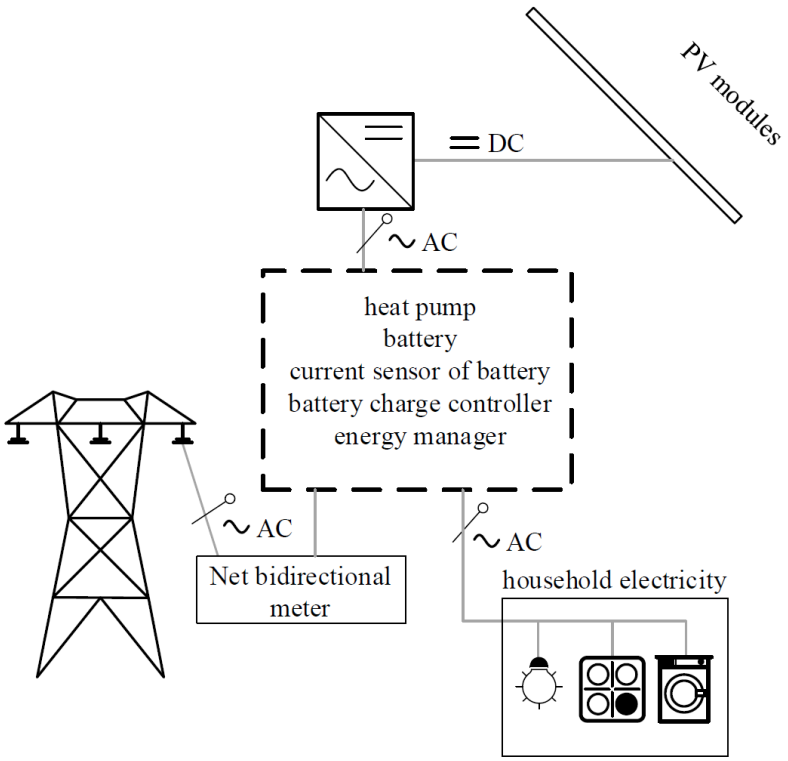


**Figure 32: Fixed (galvanically integrated) measuring points. In addition, non-contact measurements are carried out within the tested system.**

**Table 12: Important electrical variables for the energy balance.**

| Variable | Description |
|---|---|
| $E_{\text{PV-yield}}$ | Produced PV electricity, measurement on the DC and AC lines; the AC current measurement is used for the energy balance. |
| $E_{\text{HH}}$ | Household electricity (without heat pump). |
| $E_{\text{grid-purchase}}$ | Electric energy from the grid. |
| $E_{\text{grid-feed-in}}$ | Electric energy supplied to the grid. |

Various key figures are determined from the measurement data of the system test. The self-consumption ratio ($R_{\text{self-con}}$,eq. (26)) is the share of locally produced PV energy used on-site.

$$R_{\text{self-con}} = \frac{E_{\text{consumption}} - E_{\text{grid-purchase}}}{E_{\text{PV-yield}}} \quad \textbf{(26)}$$

The degree of self-sufficiency $R_{\text{suff}}$ in eq. (27) describes the level of independence from the external power grid.

$$R_{\text{suff}} = \frac{E_{\text{consumption}} - E_{\text{grid-purchase}}}{E_{\text{consumption}}} \quad \textbf{(27)}$$

The PV generation ratio ($R_{\text{gen}}$, eq. (28)) describes the ratio of PV yield to total electrical energy consumption. A system with $R_{\text{gen}} = 1$ corresponds to a net-zero energy building. Due to the different efficiencies of the different systems tested and thus different values for the total energy consumption ($E_{\text{consumption}}$), the PV generation ratio can vary despite the same size of PV system and the same useful energy demand in terms of heat for space heating and DHW and electricity for the household.

$$R_{\text{gen}} = \frac{E_{\text{PV-yield}}}{E_{\text{consumption}}} \quad \textbf{(28)}$$

The grid purchase ratio ($R_{\text{net}}$, eq. (29)) describes the ratio of energy purchased from the grid to total useful energy demand ($E_{\text{use}}$) for household electricity, domestic hot water ($Q_{\text{DHW}}$) and space heating ($Q_{\text{SH}}$, eq. (30)). In this way, a mixed calculation of thermal and electrical energy is used. The advantage, however, is that all variables are defined by the test method and are identical for all tests.

$$R_{\text{net}} = \frac{E_{\text{grid-purchase}}}{E_{\text{use}}} \quad \textbf{(29)}$$

$$E_{\text{use}} = E_{\text{HH}} + Q_{\text{SH}} + Q_{\text{DHW}} \quad \textbf{(30)}$$

### 4.3.3 System test and results

The installation of the systems on the test bench includes all hydraulic components as well as a complete electrical installation to supply the building with electricity. The tested systems had to work autonomously to meet the building's heat and electricity requirements. This also includes determining the current surplus of PV electricity and a strategy to utilize this energy.

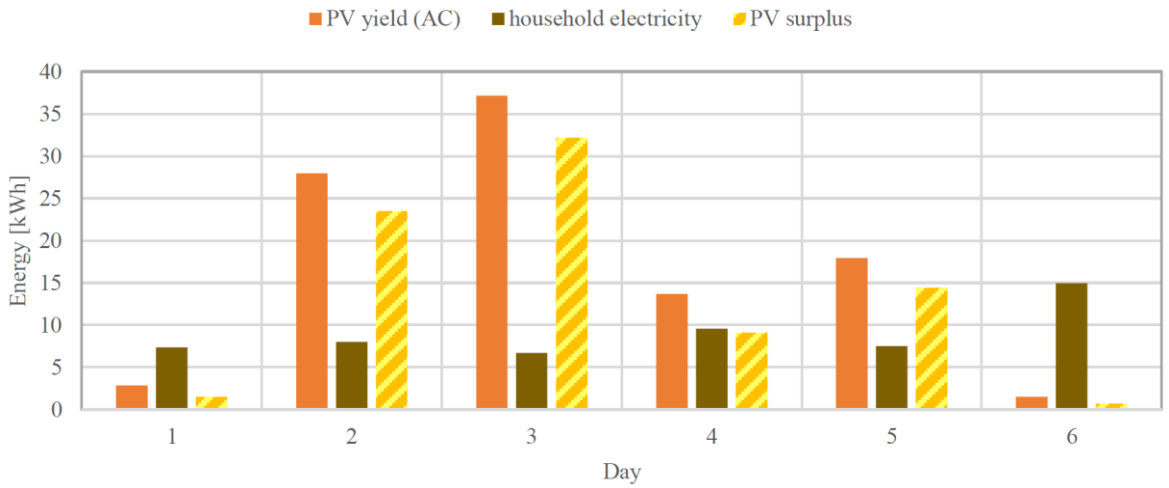


**Figure 33: PV yield and household electricity and PV surplus per day. The calculation of PV surplus is based on minutes.**

The systems that were tested aimed to increase self-sufficiency and decrease electricity costs for the household. This was done by a smart handling of the PV surplus and the storage capacities available in the system.

Figure 33 shows the PV yield and PV surplus, which are identical to all systems since they are the result of the yield that is predefined by the PV plant and weather and the equally predefined household electricity consumption (without heat pump). In the evaluation shown, the surplus is calculated on a per-minute basis, and shows the potential that is available for increasing self- consumption. Figure 34 shows how much of this PV surplus was fed to the grid by the different systems that were tested. Figure 35 shows the electric energy consumption from the grid for the same systems. Within the four tested Systems the CombiBatBrine-System uses the least electricity from the grid (45 kWh in total, Figure 35).

Due to the test method, the loads of space heating, domestic hot water and household electricity are equal for all systems. For this reason, the key figures of the tested systems can be compared directly with each other. The CombiBatBrine-System reaches in all categories shown in Figure 36 the best value. For the Key Performance Indicators (KPIs) self-consumption, self-efficiency and PV generation (grey to black bars) a higher value is better, for the grid purchase ratio (green bars) a lower value is better. The CombiBatAir-System achieves a comparatively high self-consumption ratio. However, the self-consumption ratio increases with higher overall consumption, and the purchase of electricity from the grid was thus also highest for the CombiBatAir-System, which shows the weakness of self-consumption and self-sufficiency as KPIs. The PV generation ratio can vary despite an identical PV system and identical useful energy demand. The CombiBatBrine-System achieves the highest yield ratio due to its lowest total consumption. A PV generation ratio of 1 indicates a Net Zero Energy building. In this case, internal consumption and self-sufficiency must be identical.

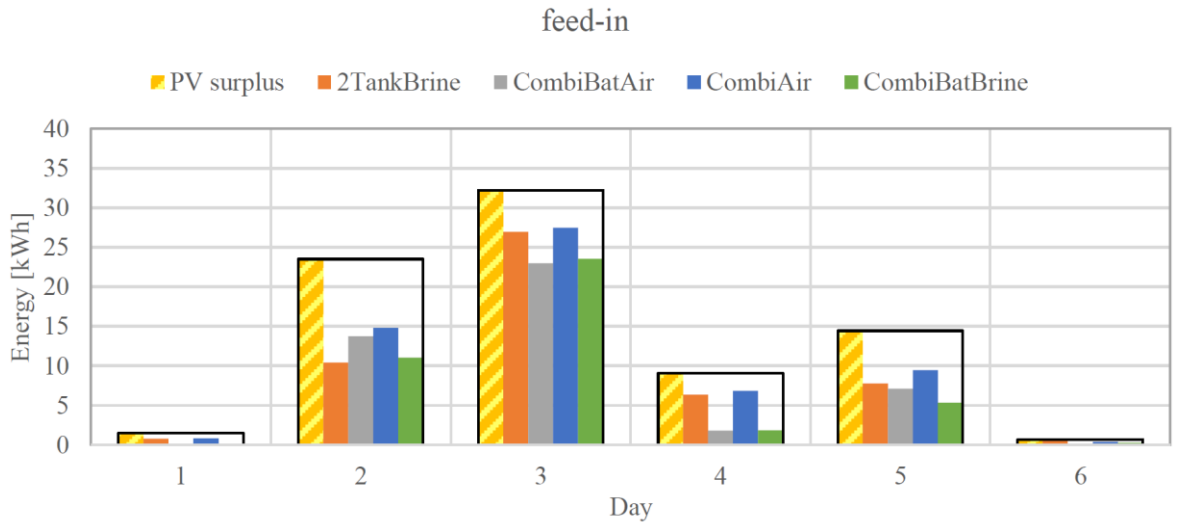


**Figure 34: Electric energy supplied to the grid per day.**

Figure 36 shows the key performance factor grid purchase ratio. It shows what proportion of total useful energy demand (the addition of DHW delivered, space heat delivered, and household electricity) had to be covered by electricity from the grid. This value should be as low as possible. The System CombiBatBrine achieves the lowest and thus the best value. A grid purchase ratio of 20% means that compared to the total useful energy demand, only 20% of electricity input from the grid was necessary. In other words, the system delivered five times more useful energy than it consumed electricity from the grid.

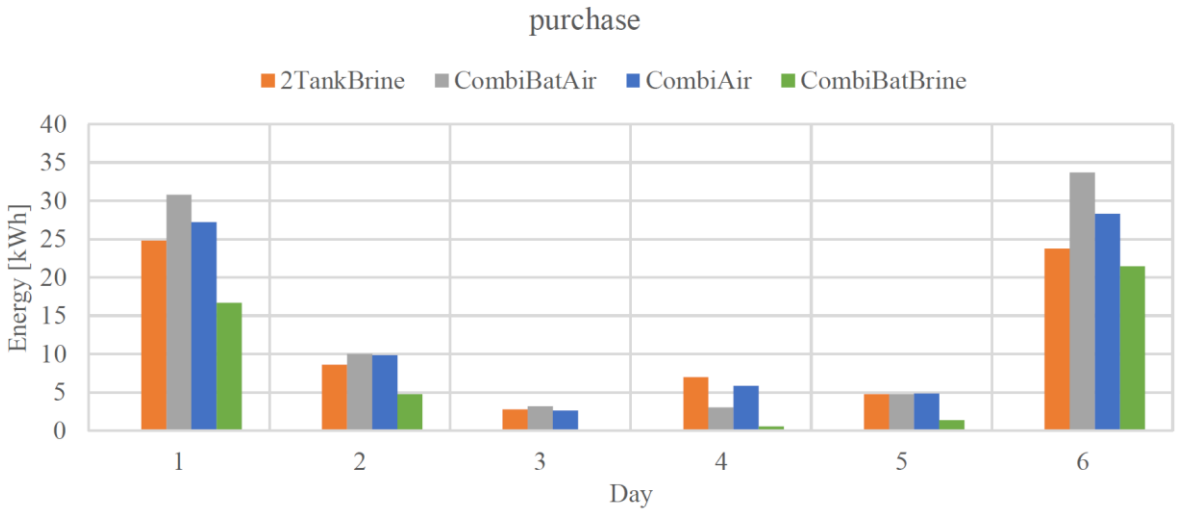


**Figure 35: Electric energy from the grid per day.**

The weakness of self-consumption and self-sufficiency as KPIs becomes apparent when electric or thermal storages are introduced with their respective losses. Losses of electric or thermal storages that are charged predominantly with PV electricity or with heat produced from PV electricity in combination with the heat pump, inevitably increase both KPIs. Therefore, a new KPI, the grid purchase ratio, has been introduced. This new KPI sets electricity purchase in proportion to useful energy demand. It has proven to be a more reliable indicator for the

quality of the system and its control, and it allows for a fairer comparison of the different systems.

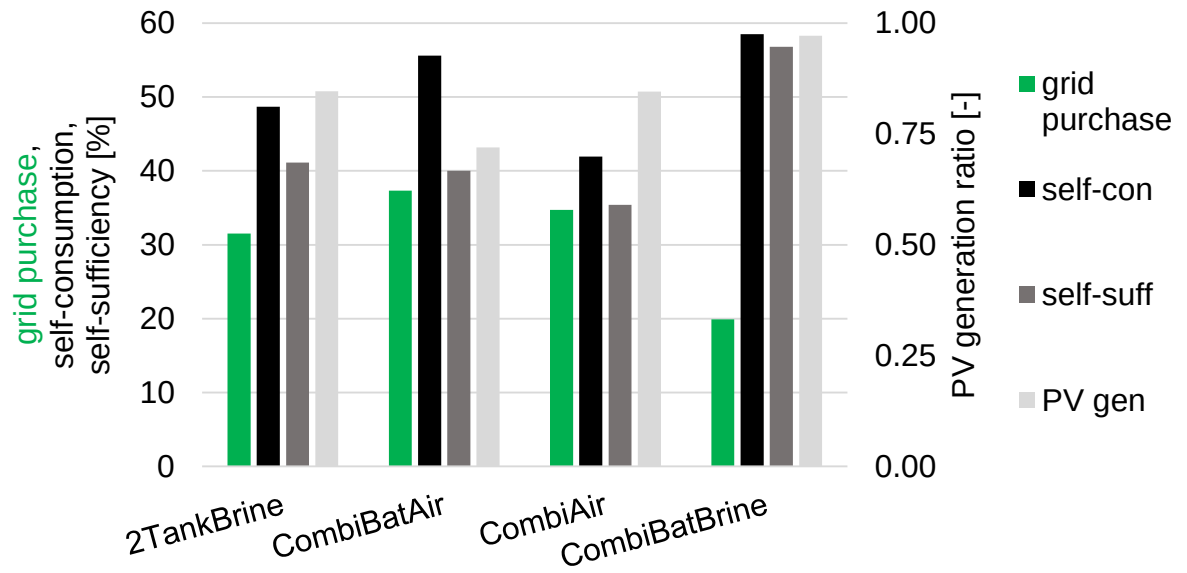


**Figure 36: New KPI grid purchase ratio, old KPIs self-consumption, self-sufficiency, PV generation ratio, data source** [52]**.**

### 4.3.4 Conclusion

The whole system test method CCT proved to be a valuable tool both for system development as well as for performance evaluation. The advantage of this kind of system test is that non-ideal component interactions and the influence of hydraulics and control under transient operating conditions can be detected and evaluated precisely. The test delivers within 6 days information about all operating conditions that may occur during a whole year and is thus much faster than field testing. Compared to field testing, the amount (number of sensors installed) and precision (high precision laboratory equipment used) of information that is obtained is much higher. Moreover, the results can be compared with tests of other systems that were performed under the same boundary conditions.

The CCT protocol proves that the grid purchase ratio assesses also for losses in PV and heating systems as combined systems which are ignored by other often used performance factors.

## 4.4 Performance of PV storage systems

### 4.4.1 State of the Art - Performance testing of PV storage systems

The state of the art for efficiency assessment of PV storage systems, is given by the German “Efficiency guideline for PV storage systems”, published by the German Energy Storage Association (BVES) and German Solar Industry Association BSW) first in April 2017 and in English language in April 2019 [43]. It addresses performance testing of the power conversion system, the battery and the control system. Despites the guideline also the international IEC 61427-2:2015 standard (Secondary cells and batteries for renewable energy storage - General requirements and methods of test - Part 2: On-grid applications) [53] includes methods for testing the battery roundtrip efficiency. As the power conversion and control system is not

addressed its applicability for PV storage systems is limited. The IEC 62933-2-1 (Electric energy storage (EES) systems - Part 2-1: Unit parameters and testing methods - General specifications) [54] provides simple test procedures for determination of the roundtrip efficiency and usable energy of electrical energy storage systems at the AC-connection point. The standard is limited applicable for DC-coupled systems, which are charging the battery directly from PV and not from the AC connection point.

Further efforts in standardization for residential storage systems are expected in Australia within the frame of a funded project by the Australian Renewable Energy Agency (ARENA lead by DNV GL. In Germany the working group AK 371.0.9 of the DKE (German Commission for Electrical, Electronic & Information Technologies) started 2019 its work for future standardization of key performance indicators of stationary battery storage systems.

### 4.4.2 Characteristics of PV storage systems

PV storage systems can be characterized by their power and capacity rating but also by their specific system topology as AC and DC coupled, single phase, three phase systems or low-voltage and high voltage battery system. A classification can be done according to the following specifications:

**Table 13: PV battery storage system classification.**

| | |
|---|---|
| Connection scheme | |
| Topology (AC or DC coupled) | Phases (single phase or three phase) |
| Power rating | |
| Maximum PV input power in case of a DC coupled system | Maximum output power (battery discharge and PV feed in) |
| Storage specifications | |
| Low voltage or high voltage battery system | Charge / discharge power or relation between power and capacity similar to the C-Rate |
| Battery capacity | |
| Usable energy of the battery, dischargeable with a certain power from the battery | |
| Usable energy of the system, which can be discharged at the AC connection point of the system (battery capacity reduced by inverter losses for a certain power level). | |

Two main system topologies, the AC and DC coupled system, exist. The principle of the AC coupled system is illustrated in Figure 37. The battery is connected over a bidirectional inverter to an AC connection point in the household. The DC coupled system is shown in Figure 38. The battery and PV array are connected to the DC-link (intermediate circuit) of the inverter. For the DC coupled system also a special type, the PV generator coupled system exists, which connects the battery over a converter directly to the PV array and a conventional PV inverter.

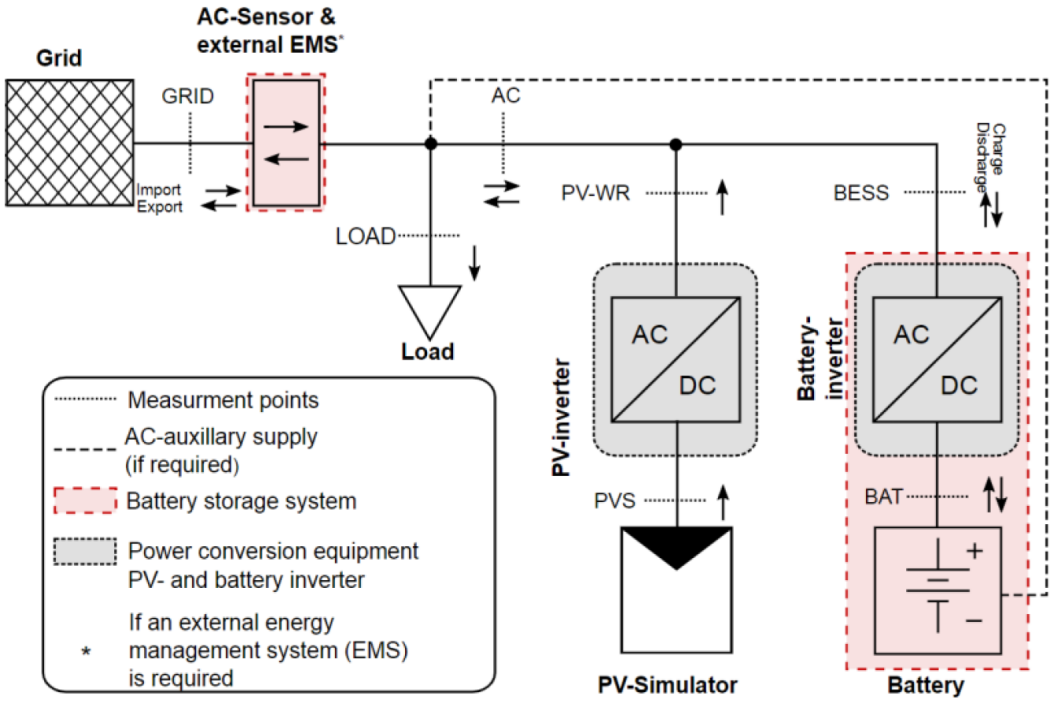


**Figure 37: Test setup for an AC coupled system [43].**

AC coupled and PV generator coupled systems are retrofittable and can be added to installations with conventional PV systems. An advantage of the AC coupled system is that the power rating of the battery inverter can be sized independently from the PV system size. This is usually not the case for DC coupled systems with a hybrid inverter. A smaller power of the battery inverter can be beneficial due to higher efficiencies in partial load operation and lower standby-losses under the assumption that most of the time the discharge power is below a certain level in residential homes. An advantage of the DC coupled system is that for battery charging no DC to AC conversion of the PV inverter and additional AC to DC conversion of the battery inverter is necessary. Hence, energy losses for charging are typically reduced.

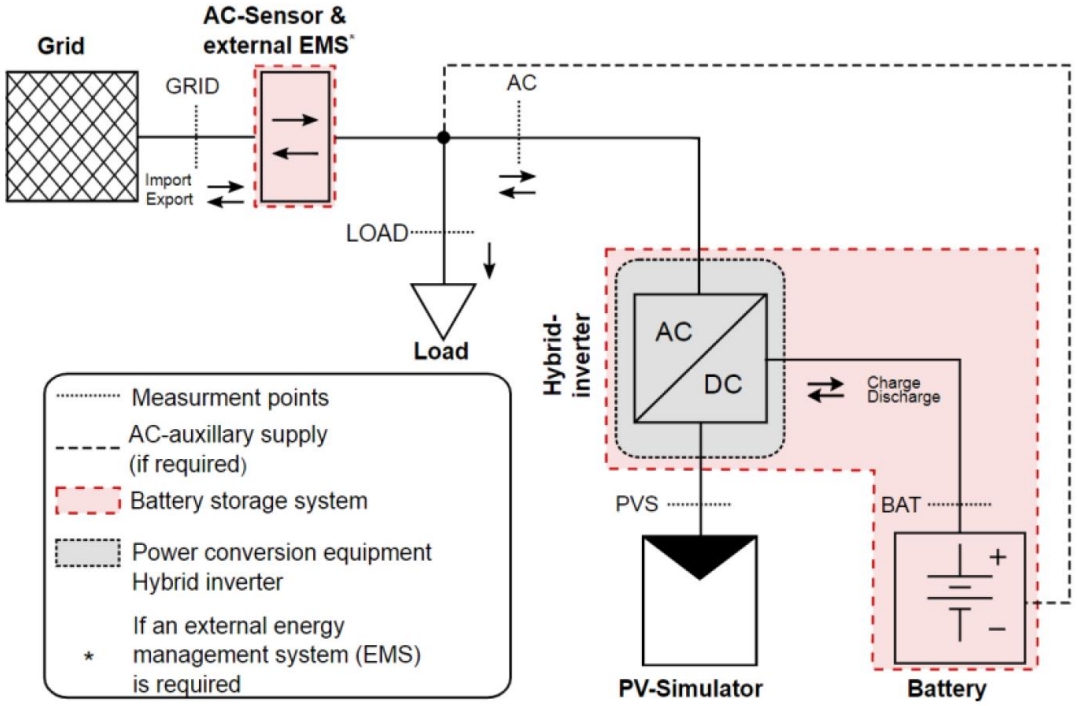


**Figure 38: Test setup for an DC coupled system [43].**

### 4.4.3 Efficiency assessment according to the BVES/BSW efficiency guideline for PV storage systems

The efficiency guideline provides test procedures for the efficiency assessment of the main three subsystems of PV storage systems.

- Power conversion system
- The battery system
- Performance of the control system.

The test setup for AC and DC coupled system corresponds to Figure 37 and Figure 38. The tests require adjusting a certain charge / discharge or grid-feed in power at a certain State of Charge (*SOC*) of the battery, which is done by controlling the PV power of a PV-Emulator and power of an adjustable load. For a sub clause of tests, it is also allowed to adjust power set points over a communication interface as Modbus e.g. Sunspec [43].

### 4.4.4 Power conversion system

Efficiency evaluation of the power conversion system determines the energy conversion losses and the standby consumption of the power converters. For PV storage systems different energy conversion paths can be distinguished. They are shown in Figure 39 for the different system topologies.

- PV direct grid feed-in
- Battery charging
- Battery discharging

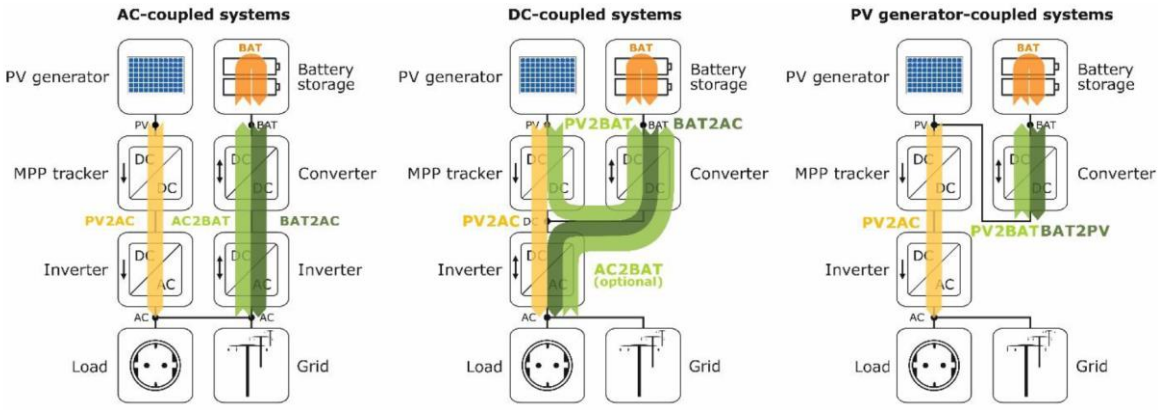


**Figure 39: Energy conversion pathways of the individual topologies of PV storage systems [43].**

For each energy conversion path, the efficiency is determined at full and partial load condition (100%, 75%, 50%, 30%, 25%, 20%, 10%, 5% of nominal power). For the AC- and PV-generator coupled system it is not necessary to measure also the efficiency of the PV inverter, which is usually a third-party device.

The standby consumption of the power conversion equipment is determined for a fully discharged (typically at the morning hours) and fully charged battery (typically the hours before sunset). The energy can be provided from the battery or AC grid if charged and must be provided from the AC grid when the battery is discharged.

### 4.4.5 Battery

The test procedure addresses the round-trip efficiency and net capacity of the battery. It is determined by fully discharging and recharging the battery several times (full cycles). The battery efficiency is the ratio between discharged to charged energy. The net capacity corresponds to the discharged energy. The efficiency is determined for 100%, 50% and 25% of nominal power and for each power level three full charge/discharge cycles are required.

### 4.4.6 Control System

The main objective of residential PV battery systems is to increase the self-sufficiency in homes. The basic control strategy is to reduce grid consumption and grid feed-in at the GCP to zero. It is done by charging the battery if PV generation is higher than the load demand (surplus) and discharging when the PV production is lower than the load demand (deficit). A surplus requires to feed-in the additional power to the utility grid, a deficit to import power from the utility grid. For most systems an AC energy meter is used at the GCP, which sends this information to the energy management system (EMS) of the PV storage system. The EMS starts to control the battery power to reduce the grid power to zero by charging the battery at a PV surplus and discharging it at a PV deficit. Limitations result due to the maximum charge/discharge power and instantaneous *SOC*. As an alternative to the energy meter at the GCP some systems use current transducers at the load and PV inverter output to measure the electric demand and generation for controlling the battery power.

The dynamic behavior is limited due to delays in the control loop as maximum data exchange speed from the energy meter to the EMS and the time period for the active power calculation. Hence the battery power is not adjusted-, and grid power is not reduced immediately after changes in PV generation or load demand. Furthermore, the energy measurement at the GCP

to the utility grid has a certain accuracy and resolution. Because of this a state error may result and the grid power is not reduced completely to zero.

The object of investigation is to test the speed and accuracy of the control system as important performance indicator. For assessment of the dynamic control behavior in total 140 load steps are performed. Figure 40 shows the response of a tested PV battery storage system to one of the 140 load steps. The delay time $t_d = t_2$ until the battery power starts to increase and the settling time $t_s = t_1$-$t_3$ until the battery power reaches and stays within a ± 5% tolerance band of the end value at which grid power is reduced best possible to zero. Evaluation of the steady state error is also done for several load steps and the deviation to zero grid power measured.

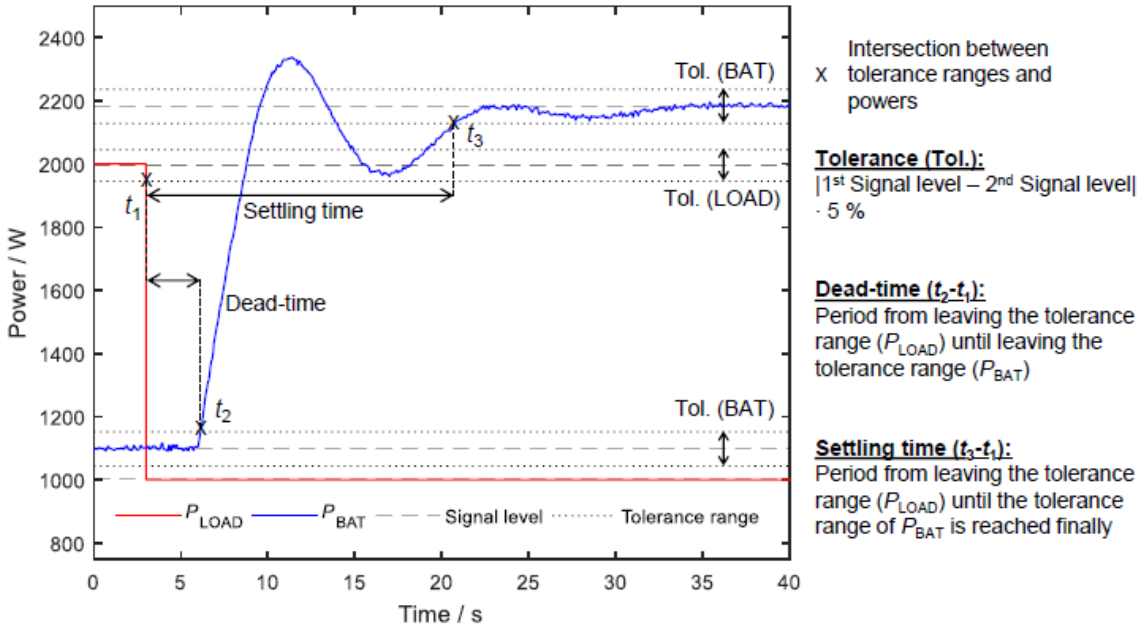


**Figure 40: Determination of the dead $t_d$ and settling time $t_s$ according to the BVES / BSW efficiency guideline [43].**

### 4.4.7 Test results of battery storage systems according to the BSW / BVES efficiency guideline

Within the “Energy Storage Inspection 2020” of the HTW Berlin [55] several manufacturers tested their system according to the efficiency guidelines and provided test results for the study. A brief overview of the results is given within this section.

In Figure 41 the discharge efficiency of the battery inverter for the tested AC coupled systems is shown in an efficiency chart.

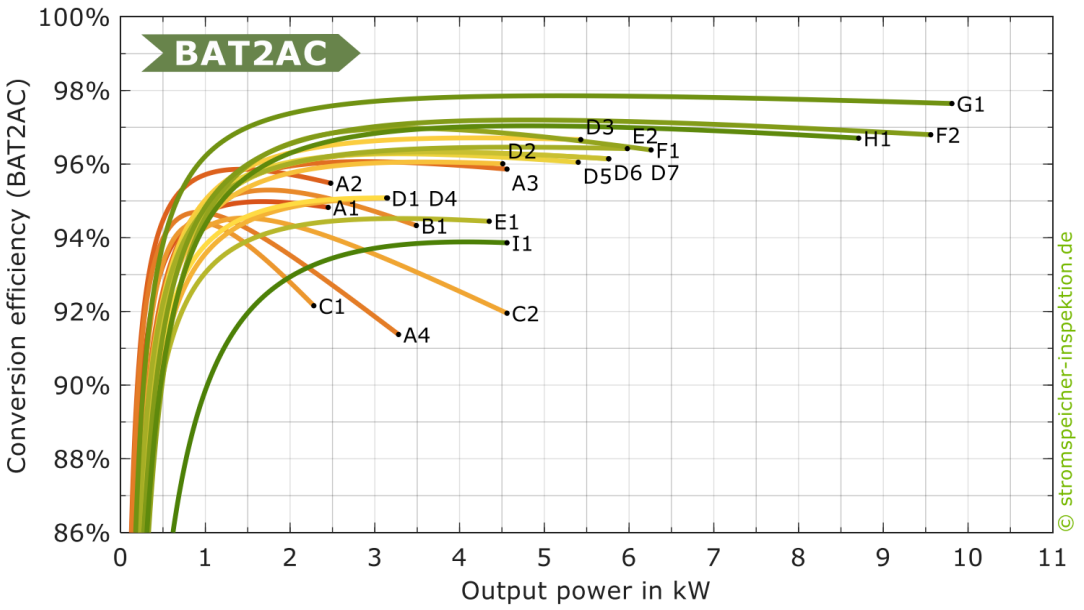


**Figure 41: Efficiency chart for battery discharge BAT2AC for AC coupled systems** [55]**.**

Table 14 lists the measured efficiency as the average over the eight tested power levels for each energy conversion path.

**Table 14: Average efficiency of nine AC coupled and seven DC coupled systems under test, based on "Energy Storage Inspection 2019" of the HTW Berlin** [55]**.**

| System or Config | | PV- grid feed in | PV battery charge | AC battery charge | AC battery discharge |
|---|---|---|---|---|---|
| 10 AC systems | Min.: | Not required for this topology | | 91.7% | 92.0% |
| | Median: | | | 93.5% | 93.7% |
| | Max.: | | | 95.1% | 95.4% |
| 11 DC systems | Min.: | 95.1% | 89.6% | 95.7% | 90.3% |
| | Median: | 96.1% | 95.5% | 95.9% | 95.2% |
| | Max.: | 97.6% | 98.2% | 96.9% | 97.3% |

Results for the battery round-trip efficiency from the Energy Storage Inspection 2019 are given in Table 15. The efficiency of the tested systems is between 91% and 97%. The charge/discharge power of the test is related to the nominal power of the system. As each system has its individual power the batteries were not charged and discharged with the same power/capacity ratio for a direct comparison e.g. which battery cell performs better. The battery cell efficiency usually increases with lower power/capacity rates due to lower thermal losses.

**Table 15: Average battery efficiency (mean of 100%, 50%, 25% nominal power) for different systems** [56]**.**

| System | A1 | A2 | A3 | A4 | B1 | C1 | C2 | D1 | D3 | D4 | D5 | D6 |
|---|---|---|---|---|---|---|---|---|---|---|---|---|
| $\eta_{Sys}$ [%] | 94.8 | 94.5 | 91.5 | 96.3 | 96.9 | 98.0 | 98.0 | 94.8 | 95.3 | 94.8 | 95.3 | 95.3 |

| System | D7 | E1 | E2 | F2 | G1 | H1 | I1 |
|---|---|---|---|---|---|---|---|
| $\eta_{Sys}$ [%] | 95.2 | 92.6 | 95.6 | 94.7 | 96.1 | 94.6 | 87.9 |

The time it takes until the battery power is increased after a load step (dead time) is determined for the tested systems between < 0.4 and 2 seconds. The settling time until the battery power is in a steady-state (± 5% of end value) is between 0.4 and 13 seconds.

The introduced measurement process provides reliable figures regarding battery system properties. They can be used as input parameters for battery system simulations of individual use cases, which can provide meaningful performance indicators as they are described in the next two section. A current research project conducts further tests and development of the measurement protocol of the efficiency guideline with the aim to start a standardization process [57].

### 4.4.8 Selected tests of the DC coupled RCT Power Storage DC 6.0-11.5 according to the efficiency guideline for storage systems

Here an example of laboratory test measurements on a PV Storage System at the PV-Lab of the Bern University of Applied Science (BFH) [58] is given.

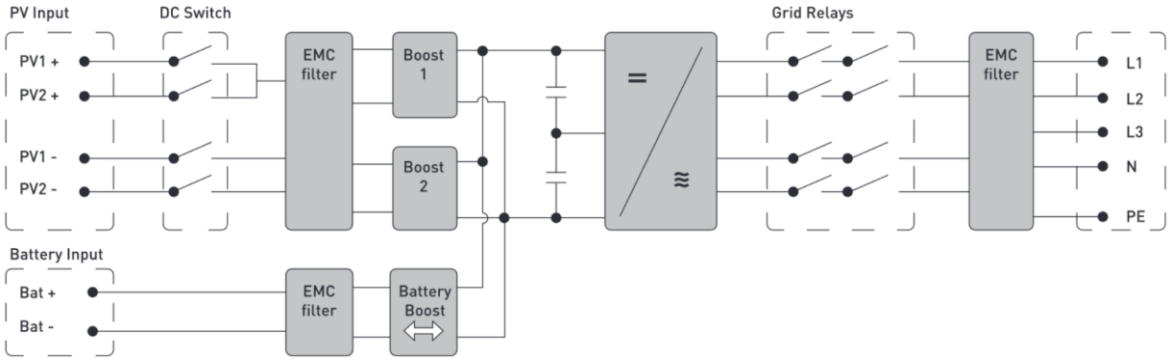


**Figure 42: Block-diagram from a PV battery storage system tested in the BFH testbench** [59]**.**

The system tested is the RCT power Storage 6.0 (PV in 9.9 kW, Battery charge 9.22 kW, Battery discharge 6 kW, AC output 6 kVa in combination with the RCT Power Battery 11.5 (11.5 kWh, charge power 9.22 kW, discharge power 6 kW), a $LiFePO_4$-battery for residential systems.

In this DC-coupled system a 3-phase grid connected hybrid inverter is working on a battery and on two PV inputs with independent MPP-trackers, as illustrated in Figure 42.

### 4.4.9 Tests of the Power Conversion system

According to the “Efficiency guideline for PV storage systems” [43] for DC-coupled systems the conversion efficiencies $\eta_{PV2AC}$, $\eta_{PV2BAT}$ and $\eta_{BAT2AC}$ must be tested.

All power tests have to be done at operation powers of 0.05, 0.2, 0.25, 0.3, 0.5, 0.75, and 1.0 times the nominal power of the components. PV related systems must be further tested at the three PV generator voltages $U_{MPP\ min}$, $U_{MPP\ nom}$ and $U_{MPP\ max}$ of the inverter input voltage window.

In battery related tests, the *SOC* of the battery for the test is specified. Further, the battery’s temperature is needed for the efficiency determination. The PV array’s characteristics are generated by a PV simulator with the fill factor for crystalline silicon technology of 0.72. The measurements have to be carried out according to the EN 50530 [1]. Figure 43 (a) shows the inverter (Power Storage 6.0) and battery unit (Power Battery) in the BFH test bench, which is depicted by Figure 43 (b). The test bench comprises a Solar simulator, a grid connection point (Grid electricity), Power analyzers and an AC load.

(a) (b)

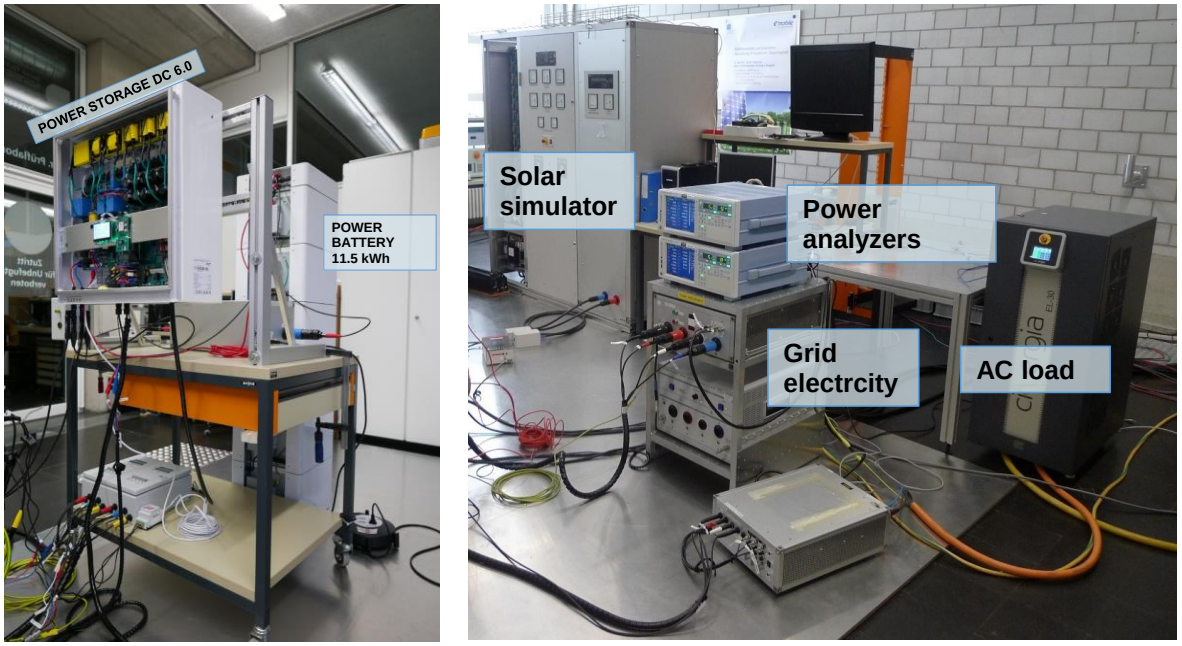


**Figure 43: (a) Power Storage DC 6.0-11.5 during the tests, (b) Simulation and measurement test bench for PV battery storage systems at BFH.**

In this DC-coupled system a 3-phase grid connected hybrid inverter is working on a battery and on two PV inputs with independent MPP-trackers, as can be seen in Figure 42.

### 4.4.10 Results of the conversion efficiencies tests

In Figure 44 (a)-(c) the results for the conversion efficiencies PV2AC, PV2BAT and BAT2AC are given. The three lines in PV2AC and PV2BAT represent the total conversion efficiencies for the three specified operation voltages $U_{MPP\ min}$ = 290 V, $U_{MPP\ nom}$ = 700 V, $U_{MPP\ max}$ = 780 V of the inverter as a function of the predefined relative power levels. In the test $U_{MPP\ max}$ was set at 780 V instead of 800 V, due to a limitation of the test infrastructure.

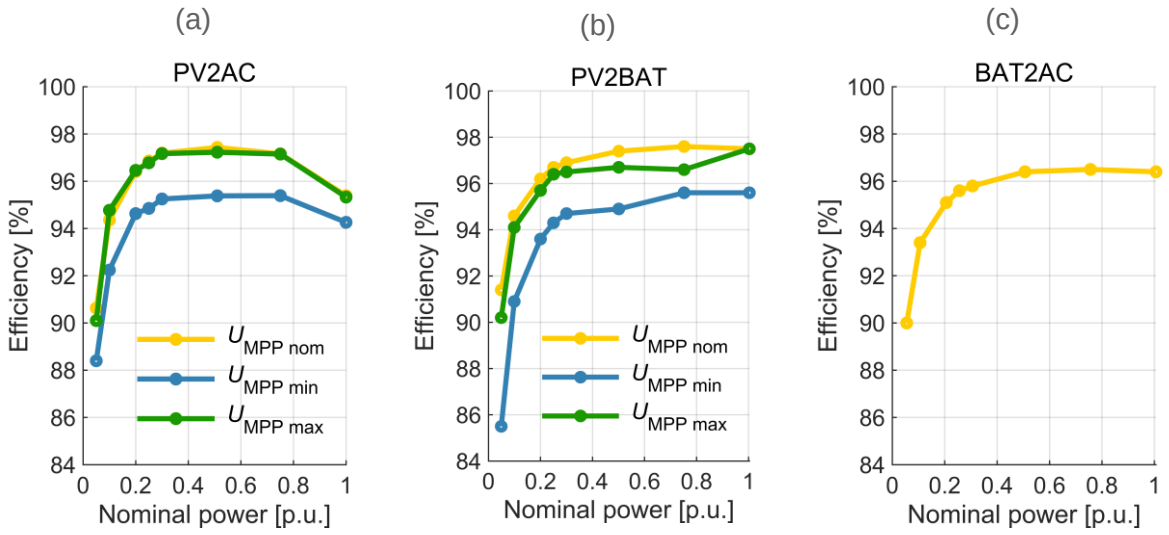


**Figure 44: Path conversion efficiencies of the tested PV battery storage system (a) PV2AC, (b) PV2BAT and (c) BAT2AC.**

The total efficiency $\eta_{PV2AC}$ (PV grid feed-in and direct use efficiency) had to be determined at the nominal power of 6 kW. During the test the battery was fully charged. The total efficiency $\eta_{PV2BAT}$ was tested at the nominal power of 9.9 kW for $U_{MPP\ nom}$ and $U_{MPP\ max}$ and at 6 kW for $U_{MPP\ min}$. During the test *SOC* was 55% +/- 10%. The efficiency $\eta_{BAT2AC}$ was determined at the nominal power of 6 kW. During the test *SOC* was 55% +/- 10%

### 4.4.11 Battery efficiency

The efficiency of batteries varies depending on their charging and discharging power. In a full cycle the battery is fully discharged by setting a constant load (grid-feed-in while zero generation) and then fully charged again by setting a constant generation and zero load consumption.

**Table 16: Operating points for the pathways BAT2AC and PV2BAT [43].**

| | Power cycle 1 | Power cycle 2 | Power cycle 3 |
|---|---|---|---|
| Discharge power | $P_{BAT2AC,nom}$ | 0.5*$P_{BAT2AC,nom}$ | 0.25*$P_{BAT2AC,nom}$ |
| Charging power | $P_{PV2BAT,nom}$ | 0.5*$P_{PV2BAT,nom}$ | 0.25*$P_{PV2BAT,nom}$ |
| Iterations | 3 | 3 | 3 |

The efficiency of a full cycle is determined by the ratio between the energy supplied and the energy withdrawn on the DC side. The battery efficiency tests have to be done for three iterations for three different powers in charge and discharge (power cycles 1 to 3) which depend on the nominal battery charging and discharging power as can be seen in Table 16.

### 4.4.12 Results of the battery efficiency tests

The battery was tested between system $SOC_{min}$ = 5% and $SOC_{max}$ = 97%. Because the maximal battery charge and discharge power are different for this battery, six different power levels have to be applied in the test.

In Figure 45 the charge and discharge power as a function of time is shown for the three power cycles or six half power cycles of the second iteration. From the integrated power over time of the two half power cycles the energies are determined, and the efficiency of a full power cycle is calculated.

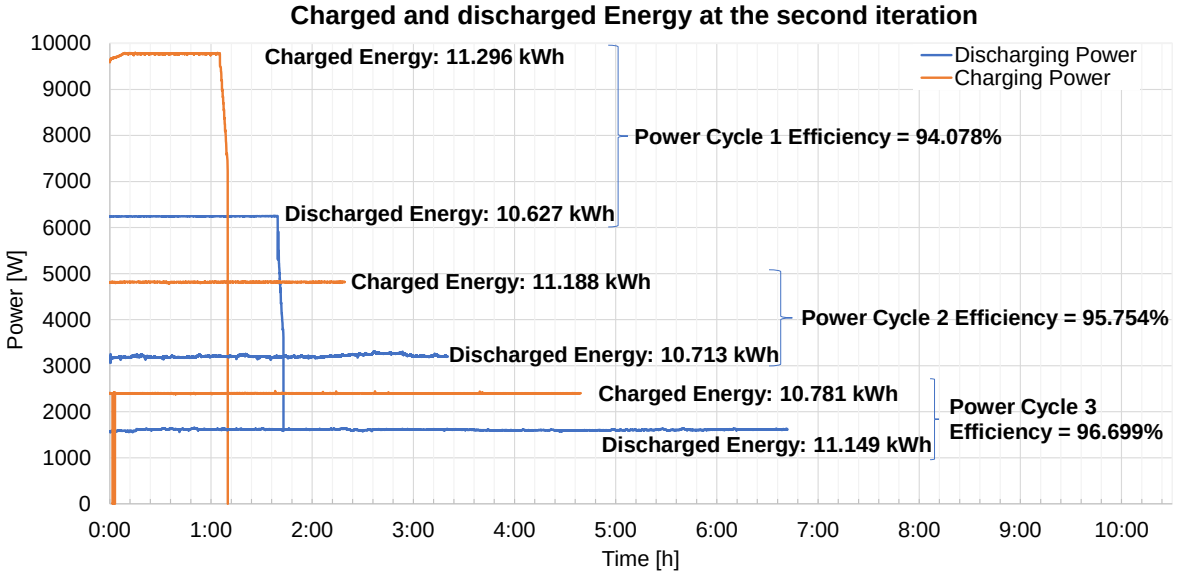


**Figure 45: Charge and discharge power curves as a function of time for the six half cycles of the second iteration. For each of the three cycles the charged and discharged energies and cycle efficiency values are given.**

### 4.4.13 No-load and Standby losses

The no-load consumption is measured when the battery is at $SOC_{max}$ and $SOC_{min}$ by switching off the load and PV generator. To measure the standby consumption, the conditions specified by the manufacturer for transition to standby mode are established.

The loss of the system is also measured when it is switched off. For this purpose, the system is deactivated according to the manufacturer's specifications and the energy consumption is measured. This is only done at maximum battery capacity.

**Table 17: No-load and standby losses at different battery charge states.**

| Losses | | $SOC_{max}$ | $SOC_{min}$ | |
|---|---|---|---|---|
| | | No-load | No-load | Stand-by |
| $P_{BAT2AC}$ | in W | 23.91 | 18.89 | 5.76 |
| $P_{Grid}$ (Purchase) | in W | 2.57 | 6.3 | 0.1 |

For the tested system the losses have been measured at $SOC_{min}$ = 7% and $SOC_{max}$ = 97%. In Table 17 the measured losses are given.

The chapters 4.4.3 to 4.4.7 show the general approach and the test protocols of the BVES / BSW efficiency guideline and give a broad overview of test results of battery storage systems according to the efficiency guidelines. Besides this overview the sections 4.4.8 to 4.4.13 show

the test protocols and measured data for a single battery storage to give detailed insights into the results a test according to the BVES / BSW efficiency guideline provides.

## 4.5 Performance indices for parallel agriculture and PV usage

Scarcity of land remains an arguable issue when comparing the performance of PV with other power generating technologies. In densely populated countries, particularly, the vast potential of utility scale ground-mounted PV (GM-PV) together with its large land use footprint is frequently discussed.

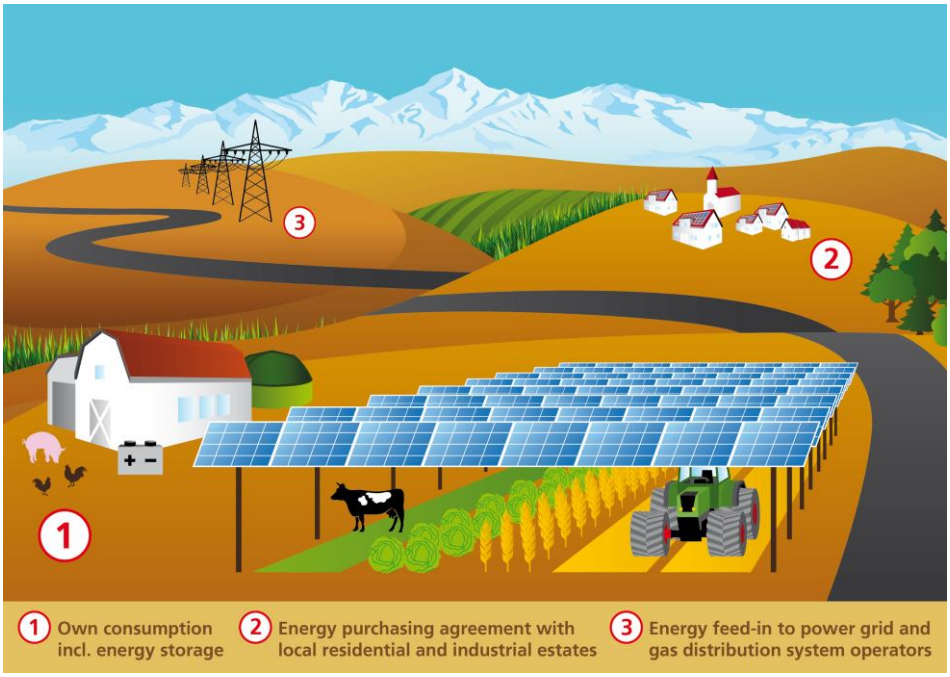


**Figure 46: Illustration of an APV system with different utilization options for the produced electricity.**

One approach of minimizing the land use footprint of GM-PV is agrivoltaics (APV), a dual use of land for food production and PV power generation [60]. While Goetzberger and Zastrow developed the concept already back in 1981 [61], today, APV gains in attention and political support in a growing number of countries accompanied by notable research activities in France, USA and Korea, amongst others.

### 4.5.1 Measuring land use efficiency of agrivoltaics

To quantify land use efficiency of intercropping systems, Mead and Willey [62] introduced the concept of the Land Equivalent Ratio (*LER*), which is frequently applied in agroforestry, aquaponics, and recently also APV [63].

The *LER* can be defined as the relative land area that is required for mono-production in order to achieve the yield of dual land use. Following Willey [64], the *LER* is specified as the sum of the respective yield ratios of dual land use to mono land use:

$$LER = \frac{Yield_a(\text{dual})}{Yield_a(\text{mono})} + \frac{Yield_b(\text{dual})}{Yield_b(\text{mono})} \quad (31)$$

For APV systems, *a* and *b* represent the cultivated crop and generated electricity, respectively. In field experiments, crop yields are typically measured comparing the yield of several test plots below the APV system with reference fields without shading from APV structures. Therefore, another factor to be considered is the land losses (*LL*) that occur if a part of the land cannot be cultivated due to the mounting structure of the APV system. When larger land machines are employed, *LL* are usually much larger than the built-up area itself.

$$LER = \frac{Yield_{agri}(\text{dual})}{Yield_{agri}(\text{mono})} + \frac{Yield_{elec}(\text{dual})}{Yield_{elec}(\text{mono})} - LL \qquad (32)$$

A *LER* < 1 indicates that combined crop and energy production is less productive than separate production, whereas a *LER* > 1 indicates increased productivity in the APV system as compared to mono production.

### 4.5.2 Land Equivalent Ratio of Fraunhofer ISE pilot system near Lake Constance

In 2016, Fraunhofer ISE installed Germany's largest APV research facility near Lake Constance with a capacity of 194.4 kWp. Experiments were deducted over a crop rotation of potato, celery, clover grass, and winter wheat. In the first year, the average results amounted to approximately 20% lower yields for both the agricultural and electrical layer leading to a LER of 1.6 or a rise of land use efficiency of 60% which is illustrated in Figure 47.

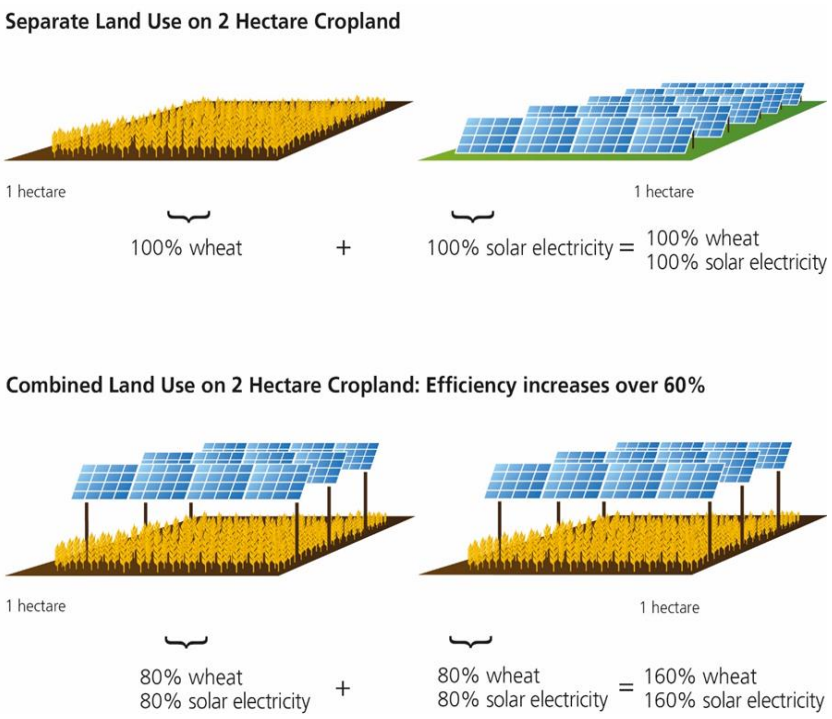


**Figure 47: Illustration of approximate land use efficiency of Fraunhofer ISE prototype in 2017.**

Since the installation of the pilot plant, with 1.87 the highest *LER* was observed in the dry and hot summer 2018 for celery, which indicated a 12% rise of yield compared to the reference area.

Regarding the electrical performance of the APV system, ZENIT, a software tool developed by Fraunhofer ISE [65], was employed to simulate the overall electrical yield of a standard GM-PV system implementing a chain of loss models. With 78.1 $kW_p/m^2$, the installed capacity of the reference scenario was 39% higher compared to the capacity of the APV system. Due to the application of bifacial modules in the APV system, though, the measured field results of the APV system were only 17% below the simulated results of the GM-PV system.

Regarding additional land losses of the mounting structure, only 0.23% of the total area was covered by mounting structure elements, whereas real *LL* amounted to 8.3% of the total area. Accordingly, the *LER* of celery in 2018 can be calculated as

$$LER_{\text{celery}} = \frac{1.12}{1} + \frac{0.83}{1} - 0.083 = 1.867 \quad \textbf{(33)}$$

### 4.5.3 Discussion

The average *LER* of 2017 and 2018 of the Fraunhofer ISE pilot plant was significantly higher than earlier results from other APV systems which were found to be in the range of 1.3 - 1.6. [66]. This was mainly triggered by both the hot and dry summer 2018 and the application of bifacial PV panels which were not considered for the PV reference scenario. Reasoning for this was, that in 2016 typical GM-PV systems did not use bifacial PV modules while, for the APV system, installing bifacial modules was recommendable for several reasons, e.g. a more equal light distribution due to an approx. 10% light transmission of the bifacial glass-glass modules, the safety glass of bifacial modules, and the much higher albedo due to larger row distance and south-west facing orientation of the module rows.

Beyond *LER*, also other performance indices have been applied to evaluate the efficiency of APV systems. E.g. in Massachusetts, the feed-in tariff of APV systems depends on the homogeneity of light distribution on the ground [67] while in Japan the governmental support scheme for APV foresees a minimum of 80% of agricultural yield compared to non-shaded agriculture [68].

## 4.6 Performance indices for double use installations of foldable PV generators

Innovation in the PV balance of system (BOS) area is created for decades to reduce PV module mounting costs and material. Most of the worldwide PV installations built today expose the PV modules in a fixed mounting position to extreme wind, snow, sand storms and other hazardous environmental conditions. According to the building codes these local mechanical load on the PV module is the base for the engineering of the mounting structure.

One other important aspect is the availability of space for PV power production, especially in densely occupied urban areas. Roof space is limited or only partially usable. A promising other application is PV power production on top of infrastructure installations like wastewater treatment basins or on top of urban carports on parking lots.

A newly developed PV plant which automatically stores the PV modules in a protection box in case of bad weather conditions was developed. Avoiding bad weather conditions implies that only a fraction of the mechanical load is present on the PV modules and the structure, enabling light weight structural design. First patents were filed in 2012 [69] and first results of the URBAN PLANT prototypes were presented in 2013 at the European PV conference [70].

(a) (b)

**Figure 48: The DHP's 640 kW HORIZON solar foldable PV plant on top of the wastewater retreatment basins in Chur, Switzerland operating since (Source: dhp technology AG).**

This newly developed PV plant folding the PV generator into a protection box and will pull out the PV generator, carried on supporting cables for operation during good weather conditions. An innovative autonomous control system to trigger the folding process was developed based on local meteo sensors and regional weather information.

**Figure 49: Parts of the PV foldable roof is opened to get access to regular service activities concerning the infrastructure of the wastewater treatment system (Source: dhp technology AG).**

The DHP Horizon system Chur (Figure 48 -Figure 50) consists of crystalline silicon PV generators grouped in sectors of 13 $kW_p$ each, moved by a single traction AC drive. This sub generator is segmented in forty 72 silicon 6" cells PV modules molded in a glass fiber reinforced plastic mounting. Each 13 $kW_p$ generator is moved a single AC motor into the safety box by a steering cable if automatically if the wind speed exceeds 15 m/s. In most of the regions in Switzerland this heavy wind will lead to PV performance losses of below 3% relative to a fixed PV installation [70].The manufacturer guarantees operation lifetime of 25 years for the PV generator in this application and 40,000 cycles of moving the folding system corresponding to roughly four movements a day.

(a) (b)

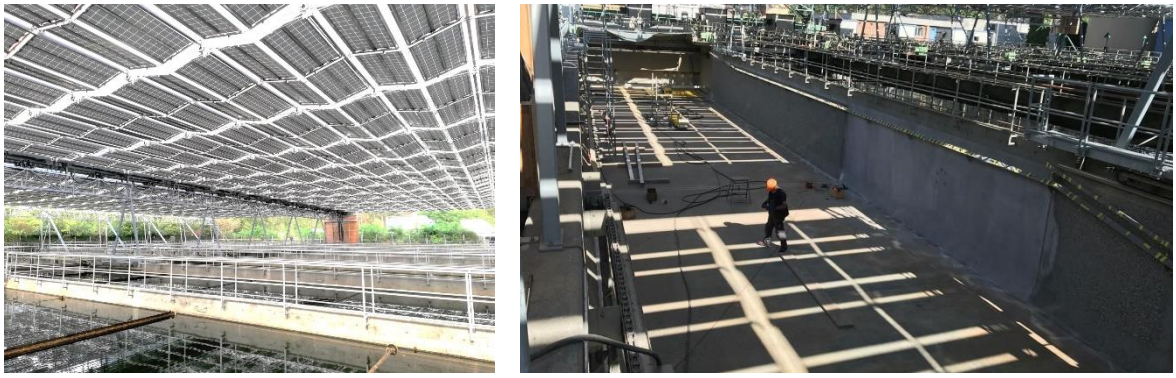

**Figure 50: View of the HORIZON PV plant on top of the filled basins (left) and (right) the cleaning of the basins during regular service activities. (Source: dhp technology AG)**

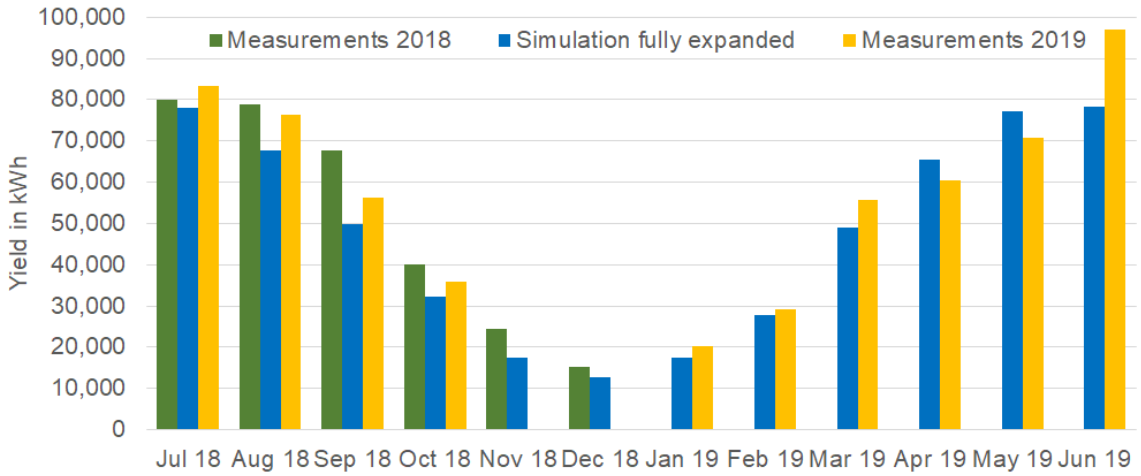


**Figure 51: The measured yield of HORIZON 640 kW in Chur was at specific 900 kWh/kW$_p$ and +/- 3% of similar fixed mounted horizontal PV plant close by in Chur** [71]**.**

The PV Horizon installation in Chur supplies about 20% of the total electricity needs of the wastewater treatment facility with a 95% PV self-consumption rate.

Beside the solar electricity supply the most valuable benefit in the wastewater system operation is the highly reduced growth rate of algae. Due to the shading of the basins by the solar modules the cost of the annual cleaning process is reduced. This is estimated to count for a financial benefit of about 0.02 €/kWh PV electricity produced.

In 2019 DHP has installed the first foldable HORIZON PV generator on top of a PV carport in Appenzell, Switzerland, see Figure 52. This will lead again to the advantage of the double use of land for PV and car parking purposes together with the shading effect for the car owners in summer time. Due to the reduced amount of used kg metal for the ground mounting system, the linked $CO_2$ emission of the BOS is drastically reduced compared to fixed PV module mounting solutions [70].

**Figure 52: Foldable PV System on top of a carport in Appenzell, Switzerland (Source: dhp technology AG).**

Due to the just starting market of Foldable PV installations no standards for characterizing their dual use performance are available, yet.

# 5 PERFORMANCE OF SHOW CASES OF COMPLEX PV SYSTEMS WITH MULTIPLE FUNCTION

## 5.1 Performance of showcases of net integrated PV system with battery storage

### 5.1.1 Description of the Showcase PV system

This showcase PV system is a hybrid generator comprising PV arrays, diesel generator, storage elements and a grid connection. This type of system is very popular in developing countries and is reminiscent of the current trend towards PV with storage coming of age in developed countries to alleviate stress on the distribution grid due to excessive PV production. There is however a fundamental difference between the two applications, aside from the addition of the generator, and that is the availability of the grid connection. The PV plus storage application in developed grid systems is primarily grid connected, following the grid and reacting to grid fluctuations and events as a subordinate producer as per the national and international standards for grid connected PV systems. Our showcase application is the opposite. The primary energy producer is the PV system with a generator backup, the grid connection is secondary and used on rare occasions when it is available and stable.

This particular system was built for a field school operating in a remote area unserved by the national utility in a developed country. It is designed to receive a grid connection, though the grid has yet to reach the field school.

The school is comprised of two classroom complexes with LED tube lighting, air-conditioning units, computer and projection equipment, coffee corner, restrooms and all the amenities one would expect of a modern educational installation. There are also three small apartment dwellings for teaching staff on site. These dwellings are outfitted as would be expected on any residential campus, with kitchen appliances, small air-conditioning units and household electronics.

The load profile developed for an average 24-hour period with seasonal allowance shows that the primary load is applied during the day light hours by the classrooms, while the residential loads are primarily drawn after the classrooms are shut down for the day.

Our system is comprised of the following generator components:

- 40.5 $kW_p$ of solar PV modules installed on 4 separate roof surfaces
- 35 kVA diesel generator
- 2,500 Ah of flooded lead acid batteries

The components that integrate the system include:

- Hybrid inverters
- Battery chargers
- Solar inverters

The heart and brain of the system is the hybrid inverter. This element faces the electrical distribution panel of the consumer and feeds the required energy on demand. The backend of the hybrid inverter receives the power inputs from the various generators.

The PV modules are divided into two groups. Since the major component of the load is during the daylight hours when the solar PV is working, most of the array is AC coupled directly into the consumer electric panel by a standard solar inverter programmed for grid connection, in parallel with the hybrid inverter. When the solar energy produced is greater than the consumption, the excess energy finds its way through the hybrid inverter to charge the battery bank.

If the batteries are charged, and excess power is flowing, the hybrid inverter raises the frequency of the system such that the solar inverters will reduce production using a simple control loop supported by the solar inverter software system.

A small 6.5 $kW_p$ array, about 15% of the total, sized for the night load, is DC coupled to the hybrid inverter by way of a battery charger. This small array is sized to charge the batteries during the day for use during the night while the AC coupled array feeds the main load. The DC coupled array is also necessary to enable a black start of the system in such a situation where there is no grid and no diesel fuel. The solar inverters are grid standard and will not operate in an island mode. For the solar inverters to operate after a total shutdown, the DC coupled array is necessary to energize the hybrid inverter and enable the solar inverter to couple with the load.

The division of the solar array between AC and DC coupling saves a lot of energy otherwise lost converting in two directions. In the case of the AC coupling, the only loss of conversion efficiency is in the solar inverter as it inverts the PV module DC power directly into the consumer electrical distribution panel. The DC coupled array would pass through the charger, the battery and the hybrid inverter with losses at each stage.

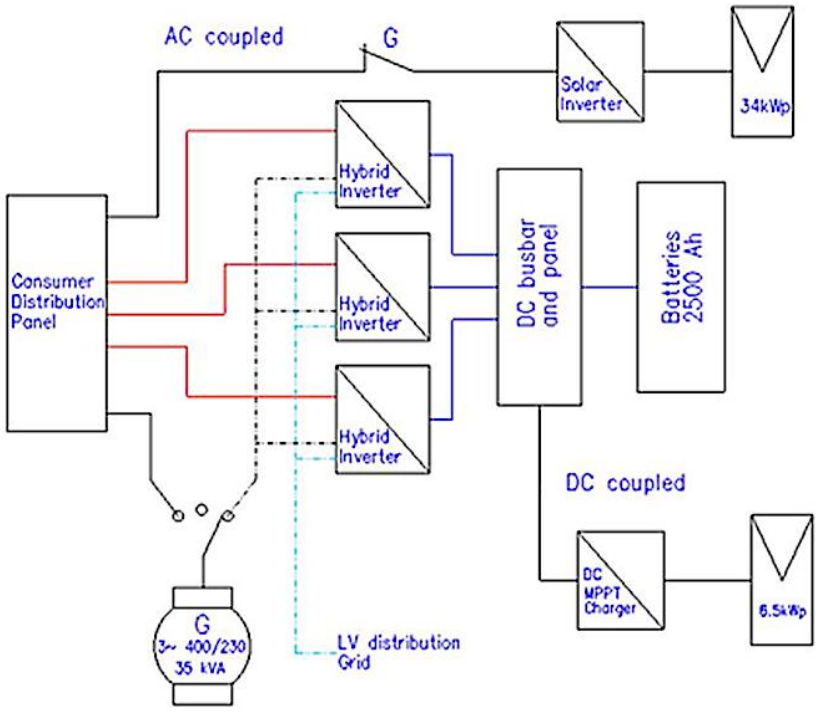


**Figure 53: System layout of PV hybrid show case with PV, diesel generator, battery and grid connection.**

When battery charge drops below the designated critical level, the diesel generator is automatically actuated by the hybrid inverter. Generator actuation automatically disconnects the solar array from feeding the consumer panel since a generator of this size as compared to

the PV array cannot easily fill in the variable PV energy flow. Figure 53 shows the complete PV hybrid system topology with all components introduced before.

A grid connection in this configuration would require an anti-islanding mechanism that would cut out the PV generator when the grid connection switch is closed and the grid parameters stray from the utility's standard requirements for power quality. The diesel generator will never be enabled to run when the grid switch is closed.

The system modes of operation are as follows:

1. PV array – DC coupled array charges the batteries, the AC coupled array feeds the load with excess power sent to charge batteries in parallel to the DC coupled charger. When batteries are full, DC coupled array maintains trickle charge while the AC coupled array continues to feed the load regulating power production in relation to the load by responding to varying frequency controlled by the hybrid inverter. The batteries feed the load after sundown and during the day if the AC coupled array is unable to meet the demand.
2. Battery Mode – As night falls, the batteries begin to supply the load in parallel to the AC coupled array, taking over fully as the array shuts down for the night. The battery bank is the sole power supply during the dark hours, until the charge obtained during the day is exhausted due to low solar irradiation earlier in the day or due to the connection of additional unauthorized load. At that point the system goes to diesel generator mode.
3. Diesel generator - During cloudy seasons, if the AC coupled array does not satisfy the load and at night when there is no solar radiation, if the load is increased beyond the design threshold levels, the diesel generator will automatically switch on and the AC coupled array will switch off. When batteries are fully charged the generator switches off, the AC coupled array switch is reclosed and the diesel generator is switched off. The diesel generator and the AC coupled PV array cannot work together.
4. Grid tied (designed, but not implemented due to lack of connection) – in this configuration. The grid supplies the load in parallel with the AC coupled PV array while the small DC coupled array charges the batteries. If the solar irradiation is not sufficient, to charge the batteries, the hybrid inverter connects grid power to the internal charging unit. If the grid parameters fail to meet Power Quality criteria or drops out, the hybrid inverter opens the grid Circuit Breaker to prevent PV energy from feeding the grid.

### 5.1.2 Qualifying Performance

The focus of solar PV energy in developed countries for the most part has been maximizing system energy output through increasing efficiency from the cell level down through the DC system, inverting process and grid connection. In an off-grid system, the definition of performance has added dimensions. Conversion efficiency is only one area of performance that must be considered. The defined purpose of system is not to achieve the highest energy yield possible with the chosen components, but to ensure that the consumer is continuously supplied with quality electrical power. Achieving highest energy yield possible is a performance metric, but only during the peak of the daily consumption and production cycle.

In a grid tied system, performance of the system is considered satisfactory if the performance meets the design criteria, almost always defined as meeting the designed PR every month. In a hybrid system, the *PR* is of no consequence as an ongoing performance qualifier, since the

solar inverter coupled to the AC load and the solar charger coupled to the battery bus-bar are regulated by demand, often curtailing even shutting down current flow in the system.

Upon completion of erecting any PV array a Performance Acceptance Test (PAT) is undertaken to ascertain that the system is performing to specification and to set the baseline for future comparison. A grid connected PV array is tested using the *PR*. In this test the array energy fed to the grid is compared to the solar energy absorbed by the modules as a ratio. This *PR* is then compared to the theoretical *PR* calculated at the outset of the design process. The residual power demand of the grid fed by the PV array is infinitely larger than the nominal power of the PV array itself, such that the grid absorbs all the energy supplied.

In a hybrid system the feed in method is problematic since the power demand of the grid to be fed by the system is very small. Its residual power demand is often less than the nominal power of the array. The PV array is often interrupted when the batteries are full and the consumer demands less energy than the array is currently producing, rendering such a method for defining the PV system efficiency as ineffectual.

The qualifying parameters in defining the performance of our system are the following:

- The straight-out *PR* of the system when consumption is at a maximum and the PV system is not being curtailed
- Number of battery system charging and discharging cycles
- Number of generator uptakes when batteries are exhausted
- Power quality in all modes of operation must be within the confines of internationally recognized parameters to ensure that the consumer load will not be damaged. In a grid tied system, this is not a concern since the PV system follows the grid. In this show case just, the PV systems sets up the grid by setting grid frequency and grid voltage itself. The diesel generator never operates with the AC coupled PV.

### 5.1.3 Performance Results

As discussed previously, the major performance matrix for a hybrid system in our configuration is uninterrupted power supply to the load and battery charge cycling such that depth of discharge is within the design parameters.

In Figure 54 we see the correlation between the three main parameters for defining performance in our system – Load consumption in kWh/d (red bars), PV production in kWh/d (yellow bars) and battery state of charge *SOC* in % (full blue line). The dashed blue lines represent the minimum and maximum battery state of charge *SOC* measured during the respective day.

Acceptable performance is defined as ensuring that the load is met while the *SOC* does not drop under the designed level of 70%.

The graph shows the solar energy produced by the DC coupled PV array opposite the consumption drawn by the load and in conjunction with the depth of discharge.

Performance in August is clearly high due to the solar resource available. The graph of December exhibits the challenge of the design. The first week of the December seems to have been somewhat overcast and the battery discharges to the lowest limit of the designed level. During the second week it appears that the clouds have moved on and the high levels of solar energy in contrast to the consumption from the 11$^{th}$ to the 13$^{th}$ of the month manage to charge the batteries back to maximum.

That the battery discharge level did not drop below the designed 70% during December is the most important performance indicator. So, 100 % of the evaluated days (August and December) met the performance requirements.

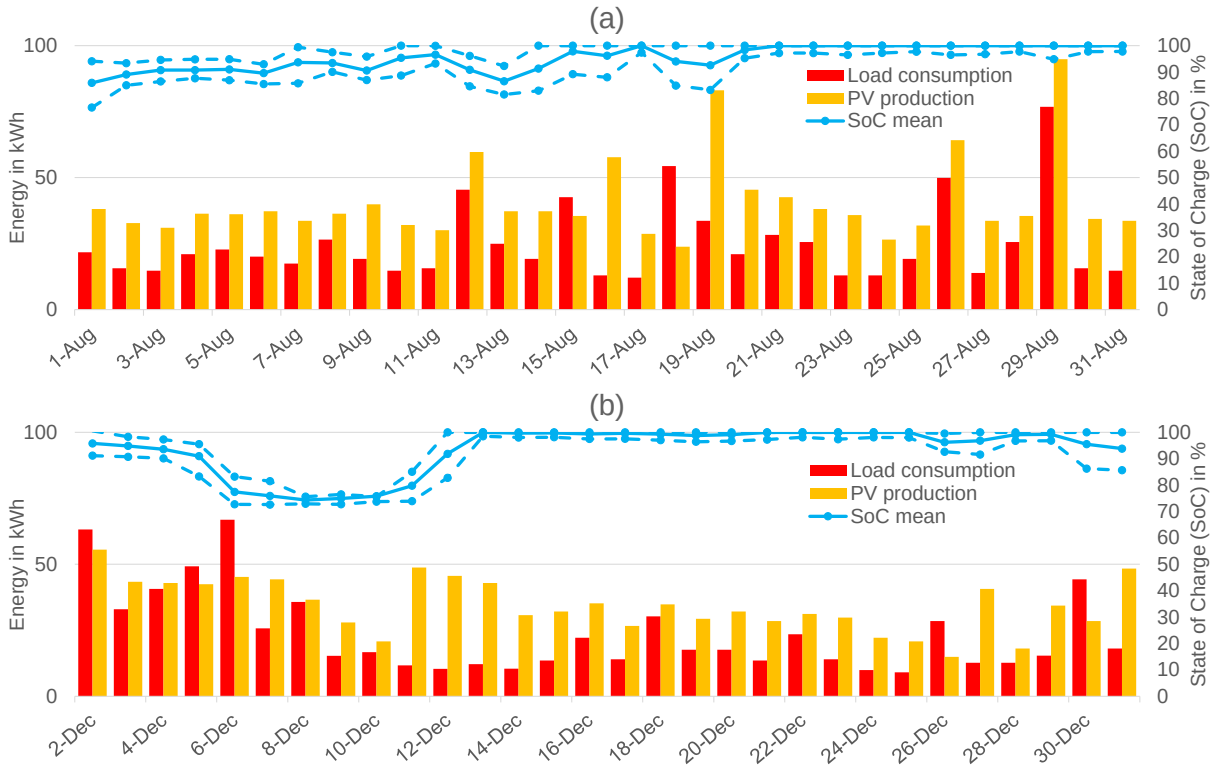


**Figure 54: Operating data of the PV hybrid system from (a) August and (b) December.**

## 5.2 Performance of floating PV systems

Massive tracks of land are used in the development of large utility-scale PV system installations, yet the demand for more solar energy continues to grow. Future large developments could be limited due to the cost and availability of land, [72]–[74]. This has prompted the development of floating PV systems (FPV), both on-shore, on inland bodies of water, and more recently off-shore [75]–[78]. FPV has the added advantages of increasing efficiency at high operating PV cell temperatures, and obviating potential environmental impact including biodiversity.

The combination of FPV with hydropower plants has been proposed to be able to provide constant power to the grid [79]. It has been reported that hydropower energy production may be increased by 65% when FPV plants are installed on a mere 10% of the area of 20 largest hydropower reservoirs [80]. The design of FPV systems is similar to designs used for land-based systems, as these inland water bodies are relatively quiet in terms of wind and waves [72].

An in-depth review of the complete FPV sector has been prepared recently [81]. Finally, FPV installation has been growing very fast, from 2 $MW_p$ installed in 2011 to an estimated 2.2 $GW_p$ at the end of 2019 [77], and this fast growth of the sector is expected to continue.

Installation of FPV systems on water saves land which may be otherwise implemented for agricultural use, and the natural cooling potential of the water body may enhance PV

performance, especially off-shore due to higher level of wind speeds, along with the presence of water. It was reported that due to this effect, the average efficiency of an FPV system in Korea is 11% relatively larger compared to a land-based PV system [82]. Additional advances are a lower number of obstacles that may cause shading loss and a lower amount of dust compared to land-based systems. Moreover, due to the fact that more than 50% of the entire world population lives within 100 km of an oceanic coast an off-shore FPV system can be conveniently located to supply energy to these regions [83].

There are many places around the world that do not have enough land for PV installations, such as Japan, Singapore, Korea, Philippines, and demand for FPV is growing at those locations. Floating solar systems can be installed in water bodies like oceans, lakes, lagoons, reservoirs, irrigation ponds, wastewater treatment plants, wineries, fish farms, dams and canals etc. showing also the potential for dual-use of water bodies.

FPV systems can be categorized in three main groups with respect to their supportive structures [84] (1) submerged: with or without pontoon, including special low weight thin film modules [85] and (2) surface mounted tilted arrays: needs rigid pontoons. Many examples are described in [78].

Systems built between 2007 and 2013 have been reviewed [86], [87]. The common benefits from these installations were identified as (i) reducing water evaporation from the reservoir/pond on which these systems are located, and (ii) decreased algal growth. It should be taken into consideration that none of the reviewed research projects was installed at sea or ocean. The following seven different factors that may indicate if an FPV system is designed optimally: modularity, flexibility, robustness, safety, optimum supportive structure size, simplicity of installation, and minimizing the final costs [77].

### 5.2.1 Challenges of floating PV

The first challenge facing the design of FPV is effective and safe grounding of the system due to failures like solar cables submerging or touching water, leading to electrical hazards and earth leakage. The inherent nature of the PV module, producing electrical voltage during the day even when disconnected makes total shutdown impossible. The effect of a partially or fully submerged damaged module must be examined for each specific reservoir and the components in use.

Aside from electrical safety issues that must be examined, the environment over water differs substantially from that over all different climates on land. Potential induced degradation of PV modules, or faster rates of corrosion of combiner boxes, inverters, and metal supporting structures are much more likely due to high moisture levels in the atmosphere over bodies of water.

From a logistic point of view, the design must be undertaken with forethought to maintenance. Safe access to the module mounting area can be challenging.

Soiling issues are of a different nature on FPV. Whereas the type of soiling typical to land based PV is less of a problem on bodies of water, there are other types of soiling that should be anticipated such as extraneous bird matter and water-based life forms of various sorts that can find their way onto the modules.

The mounting systems utilized for FPV have not yet matured. Hence, the actual life span of the various critical elements must be analyzed carefully. Operation and maintenance activities over 25 years of land-based PV system life can manage failure on almost all of its components. Many FPV systems, however, are based upon PVC plastic floats as their very foundation. The

inherent resistance to solar radiation of the plastic must be considered when calculating the business case for the project. Many manufacturer guarantees are for only 10 years. Their failure, e.g. sinking floats, will entail disassembling the entire array to replace the floats. Aftermarket UV or IR protection of plastic elements are not as readily available as those available for metal elements.

Furthermore, failure of anchoring and mooring and toxic element contamination of water bodies due to material degradation have to be considered amongst many others [88].

### 5.2.2 Overview of floating PV performance

As FPV is a relatively new branch in PV technology, high quality performance data is scarce. An early overview of FPV designs provided estimates of ~10% larger energy yields compared to similar installations on land [87], which is explained by the cooling effect of the underlying water body leading to lower PV module temperatures. As one of the first attempts to provide detailed performance data the Singapore Tengeh Reservoir test-bed has been developed [88]. In this test-bed, eight different commercial FPV technologies have been installed, and rigorous monitoring has been performed to study the potential cooling effect depending on the specific technology. Also, environmental impact studies have been performed, i.e. water evaporation and biodiversity. Figure 55 shows an aerial photograph of the test-bed. A reference system was installed on land. Main findings are that ambient temperatures over water typically are 2-3°C lower than on land, while wind speed on water is generally higher [88], [89]. Also, humidity above water is higher, and albedo on water is considerably lower (0.05 – 0.07) than on land (0.10 – 0.14). This leads to module temperatures that are about 5°C to 10°C lower than similar modules mounted on rooftops. As a result, annual performance ratios are found to be 10-15% larger than typical *PR* (75 – 80%) of rooftop systems in Singapore.

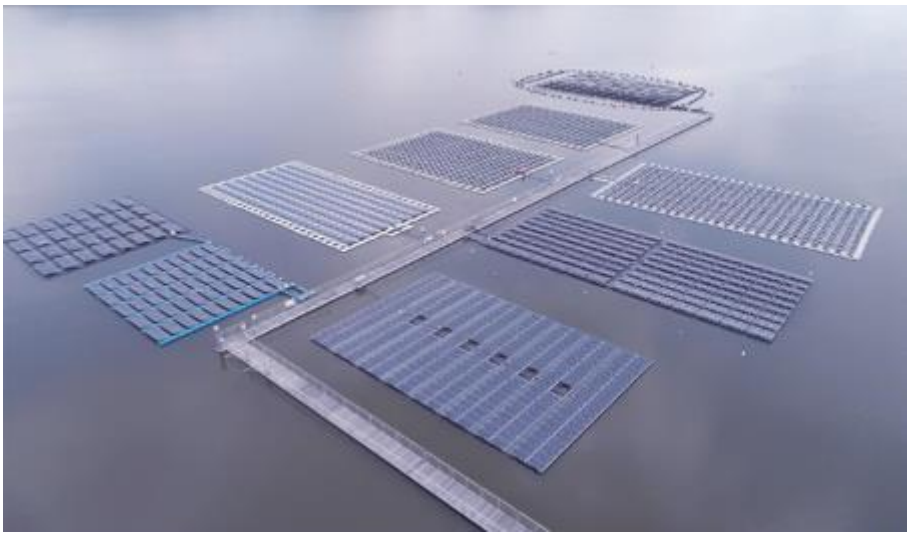

**Figure 55: Aerial photograph of the Singapore Tengeh Reservoir test-bed with different FPV technologies** [90]**.**

Figure 56 shows *PR* for the nine systems, from April 2017 to March 2018 [89]. Differences are mostly due to differences in cooling which depends on floating structure, location within the platform, and weather conditions. *PR* of system A is low due to excessive bird droppings and system B suffered from inverter downtime. The very high *PR* of the reference system is caused by the installed bi-facial modules which were also well ventilated. Two FPV systems consisted

of bi-facial modules, but no clear advantage is seen, due to the much lower albedo on water than on land.

Recent reports on FPV at the west coast of Norway shows similar energy yield advantages of 6 – 10% larger yield for an FPV system in direct contact with water compared to an comparable air-cooled FPV system [91]. A theoretical study for an FPV system with horizontally placed modules on the North Sea shows ~4% larger annual *PR* compared to a land-based system, where it is noted that this is due to cooling of the modules, and the effect of waves is limited, although weather and wind patterns have been considered [92]. Another theoretical study shows that energy loss to moving modules due to waves can range from 3% for medium wave intensity up to 9% for extreme wave intensity [93].

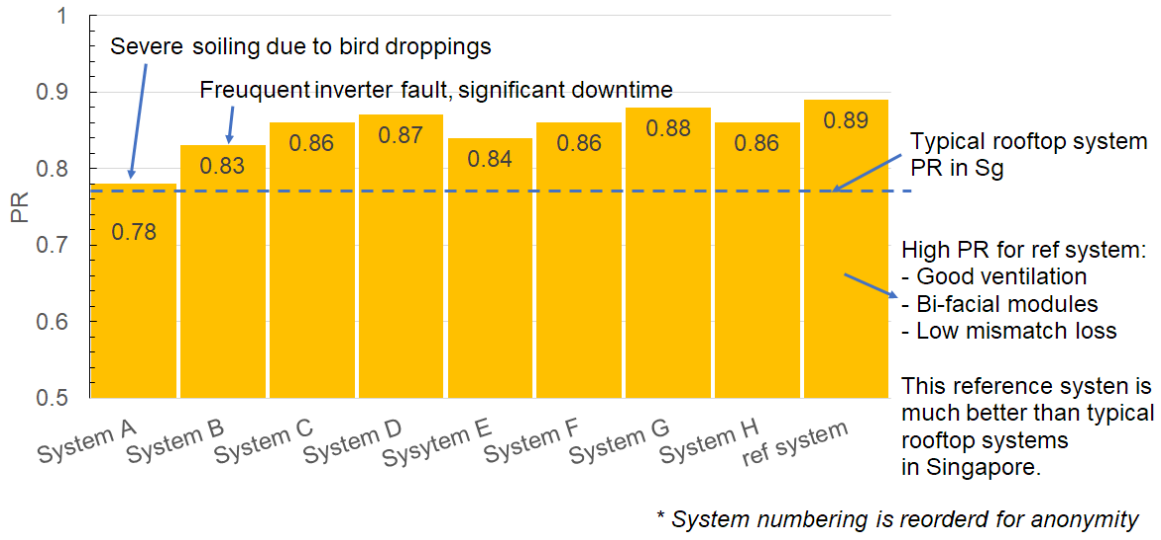


**Figure 56: Performance ratio of the FPV systems in the test-bed. Typical *PR* for rooftop systems in Singapore is indicated by the blue dashed line, data from** [89], [90]**.**

In summary, it can be concluded that FPV systems will show higher energy yields compared to similar systems on land, but this depends on the type of modules and the specific FPV design. Obviously, more measurements combined with modeling are needed. Even small-sized experiments can be useful in this respect [94]. Of special interest will be the effect of (salty) water on long-term reliability.

### 5.2.3 Examples

Korea Water Resources Corporation 100 $kW_p$ and 500 $kW_p$ floating PV systems, South Korea

Two research FPV systems have been installed on the Hapcheon dam water reservoir by Korea Water Resources Corporation starting already in 2011. The 100 $kW_p$ system was the first FPV demo system on a dam reservoir in the world. Both systems are built up using 240 $W_p$ c-Si modules and these are tilted by 33°; actual installed capacity is 99.36 $kW_p$ and 496.8 $kW_p$. The performance has been compared to a 1 $MW_p$ land-based PV system on a location 60 km southeast from Hapcheon, with similar irradiance and temperature. The land-based system comprises 250 $W_p$ modules, tilted by 30° [82], [87], [95].

Three years of monthly yield data are shown in Figure 57 [95]. The annual yields were 1297, 1364, and 1260 kWh/$kW_p$, for 2012, 2013, and 2015, respectively. The land-based system showed an annual yield of 1272 kWh/$kW_p$ (for 2012), which would lead to a 2% benefit for the floating system. However, due to missing data, blackouts, maintenance and data errors, only

half of the days in 2012 were useful for comparison. As a conclusion, it was found that the FPV system has 13.5% higher yield than the land-based system, which was attributed to the cooling effect of the water. This has been found to be more apparent in spring and summer.

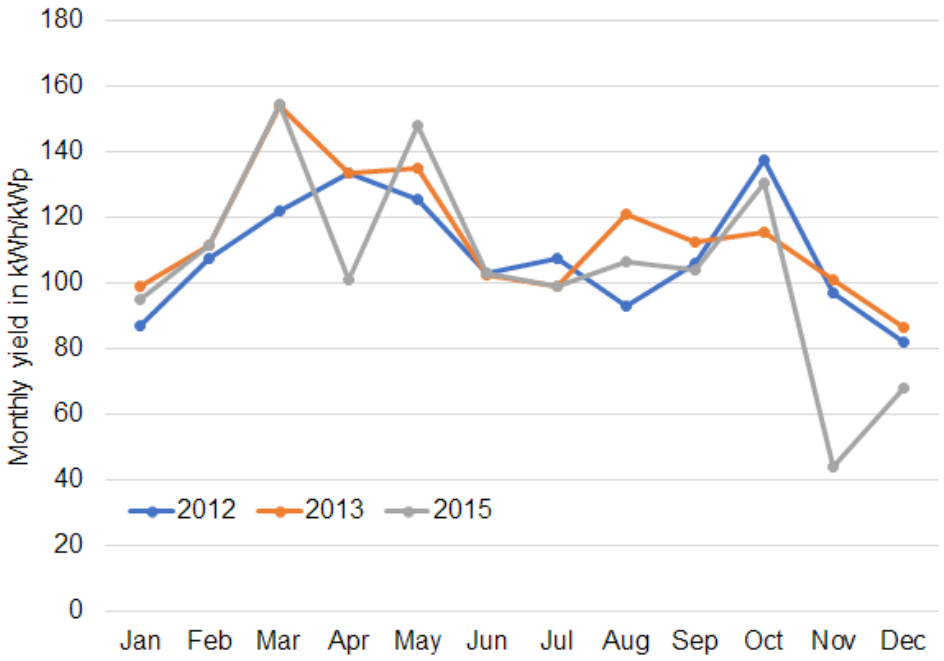


**Figure 57: Three years of monthly yield data for the 100 $kW_p$ FPV system at the Hapcheon dam water reservoir (data from** [95]**).**

Floating, tracking, cooling, concentrating systems

A special type of FPV systems denoted as Floating, Tracking, Cooling, Concentrating (FTCC) systems have been developed and deployed in Italy, a 30 $kW_p$ pilot system near Pisa and a 200 $kW_p$ grid-connected one in Livorno [96]. This includes reflectors on horizontally placed modules on a platform that is supported by polyethylene tube, and also allows for efficient vertical one-axis tracking. The system also includes a cooling system for modules, which is reported to increase energy yield by 15%. The FTCC system performance is reported to be 30% larger than a similar land-based PV system. A 30 $kW_p$ FTCC system was also installed in Cheongju-si, Korea [97].

(a) (b)

**Figure 58: Floating, Tracking, Cooling, Concentrating systems, (a) Colignola-Pisa, Italy** [98]**, (b) Cheongju-si, Korea** [98]

For the performance rating of FPV installation no standards exist. In this section performance factors were proposed, i.e. the wave intensity, wind speed, or the thermal inertia of the FPV installations. The presented results of the studies differ significantly regarding the cooling effect of the water body. The measurement protocols are similar but, the measured use cases differ significantly. The current status is that there is no commonly applicable use case for rating an FPV installation´s performance. Further research activities have to be carried out to find generally valid use cases for FPV performance characterization. Following a standardization process could be started.

## 5.3 Performance of agrivoltaic systems: a showcase from Germany

The question of whether to use valuable land for farming or solar power generation has been a subject of fierce debate in the green energy transition. But the two activities need not be in conflict with each other and, with a new generation of solar technologies, can in fact be mutually beneficial.

From an economic point of view, generating energy is typically more beneficial for farmers in Germany than producing food. Thus, about 18% of arable land in Germany is used for growing energy crops. And there is little doubt that Germany must allocate new land for the production of solar electricity in order to meet the urgent expansion of renewables needed for the energy transition.

**Figure 59: The pilot APV system uses bifacial glass-glass modules arranged in rows of two.**

A recent study of Fraunhofer ISE [99] shows that photovoltaic installations in the range of 360 $GW_p$ are required in order to meet the goal of reducing carbon emissions to zero until 2050. This will lead to a significant increase in the competition for land usage – “food versus fuel” – and at the same time presents an ethical dilemma: valuable, arable land is used to produce energy, while at the same time food is being imported from threshold and developing countries. As a result, these countries grow crops for export and less food is available for the indigenous population. But conflicts over land use are also arising in emerging and developing countries, as growing populations and rising living standards require more energy and food production.

Instead of being competitors, photovoltaics and photosynthesis can actually complement each other. APV systems make the efficient dual land usage possible: the farmer not only provides crop yields but also electricity – from the same piece of land – which dramatically increases the land use efficiency.

Today, numerous APV systems have been installed worldwide. Leading countries in the field are France, Japan, China, Korea and the United States, with support schemes for APV established. The overall installed capacity is estimated to be at least 2.4 $GW_p$, with approximately 1.9 $GW_p$ in China alone. Nevertheless, only a few research plants exist, and the full scope of applications is still to be investigated.

### 5.3.1 Case study Heggelbach: key facts and project structure

In the pilot project “agrophotovoltaics – A Contribution to Resource-Efficient Land Use” (March 2015 to December 2020), technical, social, ecological and economical dimensions of the technology were investigated in a pilot demonstration project. The seven partners of the model project, led by Fraunhofer ISE and financed by the German Federal Ministry of Education and Research and FONA (Research for Sustainable Development), also wanted to clarify the political and energy economical boundary conditions that are required to help the new technology break into the market.

The pilot APV system was installed at the organic Demeter farm in Heggelbach, near Lake Constance. On a test field covering one third of a hectare, 720 bifacial PV modules with a total power of 194.4 $kW_p$ were installed at a vertical clearance of five meters. This height makes sure that the use of versatile agricultural machinery is not restricted. The rows of semi-transparent glass-glass modules are placed at a slightly larger distance so that the crops growing underneath receive at least 60% of the total incoming irradiation. Modules are arranged in rows of two, with a gap between the rows to better distribute rainwater. The modules’ total surface measures 1206 $m^2$. The deviation from the south is 52°, with a fixed angle of inclination of 20°.

An important technical aspect was the possibility of deconstructing the plant without, for example, leaving foundations in the ground. The foundations were therefore laid using a spinning anchor system. In total, about 50 t of steel were used.

One of the Demeter farmers’ demands was that they could carry out their normal crop rotation under the plant: winter wheat, clover grass, celery and potatoes. The aim for the farmers was to achieve at least 80% of the usual yield. In order to be able to prove this, the same crops were cultivated on a reference area directly next to the test field.

From September 2016 to June 2019, the solar power and the agricultural yield were assessed.

### 5.3.2 Microclimatic effects and agricultural yields

Data on the microclimatic parameters such as photosynthetic active radiation (PAR), air and ground temperature as well as precipitation were collected. The analyses indicated that the PAR under the APV system is reduced by about 30%. In the first evaluated year, the local air temperatures under the APV system did not differ significantly to the reference plot. Washouts have been observed at single locations in the field, depending on the crop and its stage of development.

While the clover yield was reduced only slightly (-5.3%) due to shading from the APV, the yield decreases for potatoes (-18.2%), wheat (-18.7%) and celery (-18.9%) was higher. The winter wheat and the potatoes growing under the PV array showed a slightly slower development

than the same crops on the reference plot. Harvested at the same time, no mentionable delay in development was observable. The results from the first year of practice showed that all four crops were qualitatively good and marketable. In comparison to the crops from the reference plot, a lower yield was observed, but it was still within the target horizon determined in advance by the farmers (80% of reference yield). It has to be noticed that the harvest was about two weeks too early for some of the plants under the APV array. Normally the potatoes and celery plants should have been given about two more weeks to ripen. The second year, however, showed a different picture: In 2018, the yields from three of the four crops grown under the APV system were larger than the reference plot. The crop yields for celery profited the most by the system, with a gain of 12% compared to the reference. Winter wheat and potatoes produced a gain of 3 and 11% respectively, and clover a minus of 8%. In addition, in the case of potatoes, the marketable share (35-50 mm in size) was larger under the APV plant than in the reference area.

In spring and summer, the soil temperature under the APV system was less than on the reference field; while the air temperature was identical. In the hot, dry summer of 2018, the soil moisture in the wheat crop was higher than on the reference field, while in the winter months, it was less, as for the other crops. The agricultural scientists of the University of Hohenheim assume that the shade under the semi-transparent solar modules enabled the plants to better endure the hot and dry conditions of 2018. In their view, APV could mitigate climate change effects on agriculture in many regions.

For the research project, no particularly shadow-tolerant or even shade-loving plants were selected, but varieties normally marketed by the Demeter farm. It can be assumed that shade-loving plants such as hops, leafy vegetables, legumes or certain wine and fruit varieties would have shown significantly better yields. Further follow-up research projects are needed to investigate this in more detail.

### 5.3.3 PV performance and electrical storage system

As for the solar yield, the project results of the first year already exceeded expectations, at least with respect to the initial specifications. In the first 12 months of operation, the PV plant produced 245,666 kWh of electricity, or 1,266 kWh/$kW_p$ installed. The power output is mainly influenced by the use of bifacial module technology, but also by a larger distance from row to row which results in lower shading and temperature losses compared to conventional power plants. A detrimental factor with regard to the electrical yield is the orientation of the system, which is 52° off south.

In the second year of operation, the solar irradiation totaled 1,319.7 kWh/m², an increase of 8.4% compared to the previous year. The energy output of the APV system amounted to 249,857 kWh, corresponding to an extraordinarily good specific yield value of 1285.3 kWh/$kW_p$. Over the day, the power produced by the APV system was well matched to the power consumption on the Demeter farm. In the summer months, the load demand was covered almost fully by the APV system and in July close to 100%. The Demeter farmers use it primarily for processing their products and charging their electrical vehicle. With the subsequent installation of a 150-kWh battery storage system in 2018, the farm community could increase the own consumption rate for the solar power to approximately 70%. This shows that if the electricity is stored and used on site, for example for the use of electric agricultural vehicles, additional sources of income arise due to synergy effects.

While the expected capex costs of an APV plant are about one-third higher than for a conventional open space plant, mostly due to the higher racking system and higher logistics costs, the operational expenditure costs tend to be about a quarter lower. This is due to

synergy effects such as the avoided costs for mowing, surveillance or a fence. The electricity production costs of a typical APV system of 2 $MW_p$ today are competitive with a small PV rooftop system (<10 $kW_p$). Further cost reductions due to economies of scale and learning effects are to be expected.

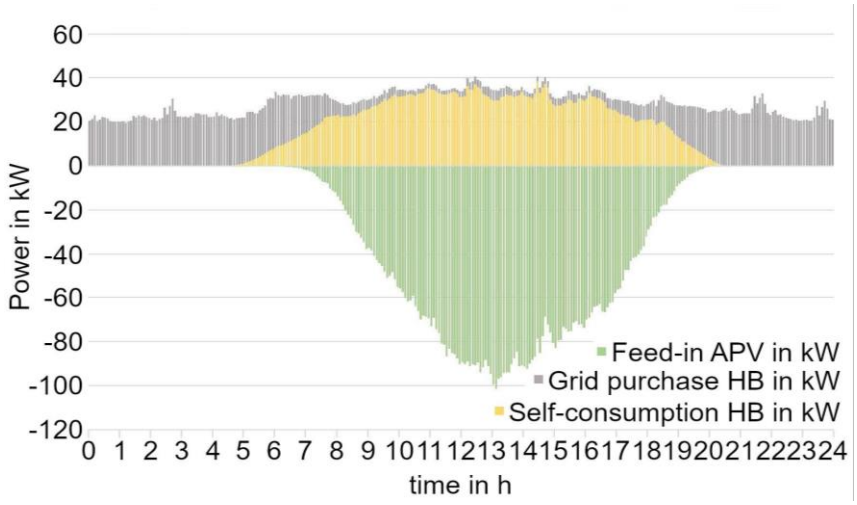


**Figure 60: During summer, the APV system covers the electricity load at the farm almost completely. The green area represents the feed-in of the solar power into the grid, the yellow area represents the own consumption, while the purchased power from the grid is plotted in grey. Source: BayWa r.e.**

### 5.3.4 Outlook

Now that evidence of increased land use efficiency and economic viability has been provided, to unlock the full potential of APV, a next step could be further horizontal technology development. To provide the necessary proof-of-concept before market entry, other techno-economic APV applications should be compared and larger systems in the MW range need to be realized. E. g. a high potential is expected for APV applications on fruits, berries, hops, and wine.

# 6 CONCLUSION

With this PVPS Task 13 report, a broad range of methods and protocols for the performance characterization and performance assessment of new PV system components up to complex new systems with PV is introduced. The report focuses on new PV components and systems of emerging and growing market segments, where standard characterization methods and protocols do not exist. The presented methods and protocols may overcome the lack of standardized performance characterization and assessment methods until such standards are available.

The state of performance characterizations presented in this report can be distinguished into three levels. In the first level, the introduced performance characterization is related closely to existing standards but provides significant additional information compared to the standard. In the second level of performance characterization, no standards for the performance characterization exist. Validated measurement protocols as well as performance indicators are introduced. Where besides the performance ratio *PR,* no characterization methods for multiple-usage benefits of the new PV components and installations are presented operating data of showcases are analyzed and discussed to point out possibly meaningful performance indicators.

*Performance characterization level one*

For the Multi-MPPT PV inverter, a new test procedure was introduced which enables to rate power losses due to inhomogeneous load conditions at each MPPT input. The proposed test profiles adjust existing test methods of the current standard EN 50530 [1] to make PV inverter efficiency a reliable performance indicator also for multi-MPPT PV inverter. Multi-MPPT PV inverter manufacturers can use this additional information to provide operators and investors with additional information regarding the efficient operation of their inverters under dynamic inhomogeneous conditions. This information can be used to calculate the additional economic benefit of multi-MPPT PV inverter and can push technological multi-MPPT PV inverter development as well as market development.

*Performance characterization level two*

For the DC/DC optimizers, the performance characterization of a single device can be conducted largely according to EN 50530 [1] and IEC 62891 [12]. However, it has been pointed out, that the voltage ratio *M* is not respected in the standardized characterization methods although it is crucial for meaningful performance figures of DC/DC optimizers with respect to the possible various operating conditions. Efficiency curves for various voltage ratios *M* in datasheets would help in choosing the most efficient PV module – DC/DC inverter combination. Furthermore, the shade mitigation factor was introduced as an indicator to quantify the additional yield of a DC/DC optimizer equipped PV system by mitigating shade induced losses compared to a shaded PV reference system. Laboratory tests with a DC/DC optimizer equipped PV system under dynamic inhomogeneous shading conditions showed higher energy yields than a standard PV system with string inverter but considerably less than the often claimed two-digit number percentage. The report provides methods and measurement protocols for rating DC/DC optimizers´ performance and enables the market to design PV systems with DC/DC optimizer more precisely and to quantify and rate their yield benefit for specific applications.

PV AC modules where PV module and microinverter are fully integrated have to be characterized as a whole, so established standards as IEC 61853 [18] and EN 50530 [1] for the individual characterization of a PV module and a (micro-) inverter are not applicable. The report presents a validated method comprising a measurement protocol and a simulation model for PV AC modules. It enables the market players to conduct simulations for individual PV AC module use cases and make them comparable to other PV-module-inverter combinations.

With the section of shade resilient PV module designs, the report provides information about the possible shade loss mitigation increasing the PV module granularity or even the PV cell granularity for PV modules under highly dynamic inhomogeneous operating conditions. The presented results show for which application cases the investigated granular PV module or PV cell concepts can gain valuable benefit.

With the presented “Efficiency guideline for PV storage systems” published by the German Energy Storage Association BVES and German Solar Industry Association BSW, manufacturers have a well-defined measurement protocol (not yet a standard) at hand to provide the market with reliable and comparable performance figures of their battery storage products. The presented showcase using the efficiency guideline´s measurement protocol, the PV battery storage simulation model and the concise cycle test makes performance characterization of PV battery storages in individual dynamic building energy systems with limited effort possible and comparable. Even in Germany, where in 2019 about 90 % of new private PV installations were equipped with a battery storage, the validated measurement protocols and methods, validated simulation models as well as new meaningful performance indicators, introduced and discussed in the report, can enhance the confidence in PV battery storages. This can lead to increasing the share of PV installations with battery storage, creating additional value and enhancing the energy transition where energy storage capacities are urgently needed.

*Performance characterization level three*

The performance characterization of agricultural PV systems (APV) is between level two and three of performance characterization. With the land equivalent ratio *LER,* one performance indicator exists besides the performance ratio *PR*. Nonetheless, more performance indicators such as the marketable crop size were proposed and evaluated for the introduced showcase. The showcase results in agricultural and energy yield pointed out that the combination of cultivated crops, weather and climate conditions on site and the specific PV system design have to be investigated as a whole to gain the most benefit of agricultural PV systems. With this information, the report gives the market valuable information at hand for further development of the APV sector, while scarcity of free areas for large PV generators and climate change with water shortage forces farmers to adapt their cultivation methods.

The performance of showcases of net integrated PV system with battery storage is assigned to level three of performance characterization. For these off-grid systems the *PR* does work as a performance indicator only when the produced PV energy is not curtailed. Under PV curtailment the number of battery system charging and discharging cycles, the number of generator uptakes when batteries are exhausted, the number of days with a battery state of charge below a certain limit and the number exceeding of power quality boundaries were proposed as performance indicators. By rating real operation data or system simulation results with the proposed performance indicators, system designers and operators are enabled to optimize their systems in terms of efficiency, reliability and maintenance efforts to improve their systems´ competitiveness and increase their market share.

Floating PV systems are an upcoming market with increasing growth, although further research on their performance characterization methods and performance indicators besides the *PR* is necessary. The introduced floating PV performance characterization methods and indicators can be assigned to level three as several indicators and measurement protocols in showcases have shown, but no uniform approach for rating floating PV systems is established or standardized yet. E. g. measurement protocols with comparative operation of floating PV systems and land-based reference systems to quantify yield differences and qualify the reason for them were introduced. That may give market players valuable advice which environmental conditions have to be considered most, to speed up the development of floating PV market.

This report as a compendium of performance characterization of new PV components and complex systems with PV shows that the performance characterization and the performance characterization indicators are as manifold as the additional benefits of the assessed systems are. To develop a uniform performance indicator for all kinds of new PV components or new complex systems with PV will hardly be possible. However, a frame work should be developed which allows the normalization of different performance indicators in order to make them comparable.

# REFERENCES


[1] "DIN EN 50530 (VDE 0126-12:2013-12):2013-12, Gesamtwirkungsgrad von Photovoltaik-Wechselrichtern; Deutsche Fassung EN 50530:2010 + A1:2013." Berlin, 2013.

[2] "IEC: „Photovoltaic systems - Power conditioners - Procedure for measuring efficiency", IEC 61683 ed.1 (1999-11)." 1999.

[3] "IEC 61724 Photovoltaic System Performance Monitoring—Guidelines for Measurement, Data Exchange and Analysis, 10th ed." Geneva, Switzerland, 1998.

[4] D. Gfeller, U. Muntwyler, and L. Borgna, "Testing of multi-MPPT PV inverters: approach and test results," *32nd European Photovoltaic Solar Energy Conference and Exhibition*. Munich, Germany, pp. 2138–2143, 2016.

[5] "IEC 60904-1:2006 Photovoltaic devices - Part 1: Measurement of photovoltaic current-voltage characteristics." 2006.

[6] S. M. MacAlpine, R. W. Erickson, and M. J. Brandemuehl, "Characterization of power optimizer potential to increase energy capture in photovoltaic systems operating under nonuniform conditions," *IEEE Transactions on Power Electronics*, vol. 28, no. 6. pp. 2936–2945, 2013.

[7] G. Ball and J. Fisher, "Rooftop PV Systems and Firefighter Safety, Proceedings," *2016 IEEE 43rd Photovoltaic Specialists Conference (PVSC 2016)*. Portland, Oregon, USA, pp. 1244–1250, 2016.

[8] Q. Gao, Y. Zhang, Y. Yu, and Z. Liu, "A direct current-voltage measurement method for smart photovoltaic modules with submodule level power optimizers," *Solar Energy*, vol. 167. pp. 52–60, 2018.

[9] Perry Tsao, Sameh Sarhan, and Ismail Jorio, "Distributed max power point tracking for photovoltaic arrays," *2009 34th IEEE Photovoltaic Specialists Conference (PVSC)*. pp. 2293–2298, 2009.

[10] C. A. Deline, "Deline unpublished." .

[11] "ASTM E1036 - 15(2019) Standard Test Methods for Electrical Performance of Nonconcentrator Terrestrial Photovoltaic Modules and Arrays Using Reference Cells." West Conshohocken, PA, 2019.

[12] "IEC 62891:2015-05 Overall efficiency of grid connected photovoltaic inverters." 2015.

[13] C. Deline and S. Macalpine, "Use conditions and efficiency measurements of DC power optimizers for photovoltaic systems," *2013 IEEE Energy Conversion Congress and Exposition, ECCE 2013*, no. October. pp. 4801–4807, 2013.

[14] C. Deline, J. Meydbray, and M. Donovan, "Photovoltaic Shading Testbed for Module-level Power Electronics: 2016 Performance Data Update," no. NREL Technical Report NREL/TP-5J00-62471. 2016.

[15] C. Deline, B. Sekulic, J. Stein, S. Barkaszi, J. Yang, and S. Kahn, "Evaluation of Maxim module-Integrated electronics at the DOE Regional Test Centers," *2014 IEEE 40th Photovoltaic Specialist Conference, PVSC 2014*, no. June. pp. 986–991, 2014.

[16] Solar Edge, “SolarEdge Efficiency of P Series Power Optimizers,” 2018.

[17] A. J. Hanson, C. A. Deline, S. M. MacAlpine, J. T. Stauth, and C. R. Sullivan, “Partial-Shading Assessment of Photovoltaic Installations via Module-Level Monitoring,” *IEEE Journal of Photovoltaics*, vol. 4, no. 6. pp. 1618–1624, Nov-2014.

[18] “IEC 61853-1:2011 Photovoltaic (PV) module performance testing and energy rating - Part 1: Irradiance and temperature performance measurements and power rating.” Berlin, 2011.

[19] D. M. Riley, C. W. Hansen, and M. Farr, “A Performance Model for Photovoltaic Modules with Integrated Microinverters,” no. January. Albuquerque, New Mexico, p. 55, 2015.

[20] C. Allenspach, V. Castro de Echavarri, S. Richter, C. Meier, F. Carigiet, and F. Baumgartner, “MODULE-LEVEL POWER ELECTRONICS UNDER INDOOR PERFORMANCE TESTS Scope / Objectives,” *37th European Photovoltaic Solar Energy Conference (EUPVSEC)*. Lisbonb, Portugal, 2020.

[21] F. P. Baumgartner, “Euro Realo inverter efficiency: DC-voltage dependency,” *20th European Photovoltaic Solar Energy Conference and Exhibition*, no. June. p. 2257, 2005.

[22] F. Baumgartner, “Photovoltaic (PV) balance of system components,” *The Performance of Photovoltaic (PV) Systems*. Elsevier, pp. 135–181, 2017.

[23] P. Moraitis, B. B. Kausika, N. Nortier, and W. Van Sark, “Urban environment and solar PV performance: The case of the Netherlands,” *Energies*, vol. 11, no. 6. 2018.

[24] K. Sinapis, T. T. H. Rooijakkers, L. H. Slooff, L. A. G. Okel, M. J. Jansen, and A. J. L. Carr, “Towards new module and system concepts for linear shading response.” 2017.

[25] S. Silvestre, A. Boronat, and A. Chouder, “Study of bypass diodes configuration on PV modules,” *Applied Energy*, vol. 86, no. 9. pp. 1632–1640, 2009.

[26] K. Sinapis *et al.*, “Annual Yield Comparison of Module Level Power Electronics and String Level PV Systems with Standard and Advanced Module Design,” *32nd European Photovoltaic Solar Energy Conference and Exhibition*. Munich, Germany, pp. 2011–2015, 2016.

[27] B. B. Pannebakker, A. C. de Waal, and W. G. J. H. M. van Sark, “Photovoltaics in the shade: one bypass diode per solar cell revisited,” *Progress in Photovoltaics: Research and Applications*, vol. 25, no. 10. pp. 836–849, 2017.

[28] K. Sinapis, T. T. H. Rooijakkers, and W. G. J. H. M. van Sark, “Effects of solar cell group granularity and modern system architectures on partial shading response of c-Si modules and systems,” *IEEE Journal of Photovoltaics*, vol. submitted. 2020.

[29] K. Sinapis *et al.*, “A comprehensive study on partial shading response of c-Si modules and yield modeling of string inverter and module level power electronics,” *Solar Energy*, vol. 135. pp. 731–741, 2016.

[30] S. K. Das, D. Verma, S. Nema, and R. K. Nema, “Shading mitigation techniques: State-of-the-art in photovoltaic applications,” *Renewable and Sustainable Energy Reviews*, vol. 78. pp. 369–390, 2017.

[31] D. Nguyen and B. Lehman, “An Adaptive Solar Photovoltaic Array Using Model-Based Reconfiguration Algorithm,” *IEEE Transactions on Industrial Electronics*, vol. 55, no. 7. pp. 2644–2654, 2008.

[32] G. Velasco-Quesada, F. Guinjoan-Gispert, R. Pique-Lopez, M. Roman-Lumbreras, and

A. Conesa-Roca, “Electrical PV Array Reconfiguration Strategy for Energy Extraction Improvement in Grid-Connected PV Systems,” *IEEE Transactions on Industrial Electronics*, vol. 56, no. 11. pp. 4319–4331, Nov-2009.

[33] A. Bidram, A. Davoudi, and R. S. Balog, “Control and Circuit Techniques to Mitigate Partial Shading Effects in Photovoltaic Arrays,” *IEEE Journal of Photovoltaics*, vol. 2, no. 4. pp. 532–546, 2012.

[34] S. Z. M. Golroodbari, A. C. De Waal, and W. G. J. H. M. Van Sark, “Improvement of shade resilience in photovoltaic modules using buck converters in a smart module architecture,” *Energies*, vol. 11, no. 1. 2018.

[35] B. Burger, B. Goeldi, S. Rogalla, and H. Schmidt, “25th European Photovoltaic Solar Energy Conference and Exhibition / 5th World Conference on Photovoltaic Energy Conversion, 6-10 September 2010, Valencia, Spain,” *25th European Photovoltaic Solar Energy Conference and Exhibition*, no. September. Valencia, Spain, pp. 3700–3707, 2010.

[36] C. Olalla, D. Clement, M. Rodriguez, and D. Maksimovic, “Architectures and Control of Submodule Integrated DC–DC Converters for Photovoltaic Applications,” *IEEE Transactions on Power Electronics*, vol. 28, no. 6. pp. 2980–2997, 2013.

[37] M. Uno and A. Kukita, “Current Sensorless Equalization Strategy for a Single-Switch Voltage Equalizer Using Multistacked Buck–Boost Converters for Photovoltaic Modules Under Partial Shading,” *IEEE Transactions on Industry Applications*, vol. 53, no. 1. pp. 420–429, Jan-2017.

[38] S. Z. M. Golroodbari, A. C. De Waal, and W. G. J. H. M. Van Sark, “Proof of concept for a novel and smart shade resilient photovoltaic module,” *IET Renewable Power Generation*, vol. 13, no. 12. pp. 2184–2194, 2019.

[39] A. J. Carr, M. J. Jansen, M. de Bruijne, L. Okel, M. Kloos, and W. Eerenstein, “High voltage MWT module with improved shadow performance,” *2014 IEEE 40th Photovoltaic Specialist Conference (PVSC)*. pp. 2685–2688, 2014.

[40] A. J. Carr *et al.*, “Tessera: Scalable, shade robust module,” *2015 IEEE 42nd Photovoltaic Specialist Conference (PVSC)*. pp. 1–5, 2015.

[41] L. H. Slooff *et al.*, “Shade response of a full size TESSERA module,” *Japanese Journal of Applied Physics*, vol. 56, no. 8S2. IOP Publishing, p. 08MD01, Jul-2017.

[42] K. Sinapis, R. Pacheco Bubi, L. H. Slooff, W. Folkerts, L. A. G. Okel, and M. J. Jansen, “Outdoor performance characterization of a novel shadow tolerant module,” *35th European Photovoltaic Solar Energy Conference (EUPVSEC)*. Brussels, Belgium, pp. 1169–1171, 2018.

[43] German Energy Storage Association (BVES) and German Solar Industry Association (BSW), “Efficiency guideline for PV storage systems.” Berlin, Germany, 2019.

[44] C. Allenspach, R. Koch, E. Kinigadner, F. Carigiet, and F. Baumgartner, “Solarbatteriesystem und transienter ‘NESPRESS-Test’ in der ZHAW Bachelorausbildung,” *österreichischen Fachtagung für Photovoltaik & Stromspeicherung*. Vienna, Austria, 2019.

[45] M. Knoop and M. Littwin, “MATLAB-basiertes Simulationsmodell zur Berechnung der elektrischen Leistungsflüsse im PV-Speichersystem,” *32. Symposium Photovoltaische Solarenergie*. OTTI e.V., Bad Staffelstein, Germany, 2017.

[46] D. Linden and T. B. Reddy, “Handbook of Batteries, third edition,” *McGraw-Hill*. 2002.

[47] M. Littwin and M. Kesting, “Experimentalanlage zur Untersuchung interaktiver Strom- und Wärmeversorgungssysteme in Gebäuden Universelle und flexible Untersuchungsmöglichkeiten mit der Experimentalanlage für integrierte Gesamtenergiesysteme,” *30. Symposium Photovoltaische Solarenergie*. 2015.

[48] J. Kalisch and et al, “Continuous meteorological observations in high-resolution (1Hz) at University of Oldenburg in 2014.” Carl-von-Ossietzky University of Oldenburg, Oldenburg, 2015.

[49] Bundesverband der Energie- und Wasserwirtschaft e.V, “Energie-Info: Stromverbrauch im Haushalt.” Berlin, p. 34, 2013.

[50] Hochschule für Technik und Wirtschaft HTW Berlin, “Repräsentative elektrische Lastprofile für Einfamilienhäuser in Deutschland auf 1-sekündiger Datenbasis.” Berlin, 2015.

[51] P. Vogelsanger, “The Concise Cycle Test Method - a Twelve Day System Test,” *A Report of IEA SHC - Task 26 Solar Combisystems A technical report of Subtask B*, no. November. 2002.

[52] R. Haberl, A. Reber, E. Bamberger, and M. Haller, “Hardware-in-the-Loop Tests on Complete Systems with Heat Pumps and PV for the Supply of Heat and Electricity.” 2018.

[53] “IEC 61427-2:2015 Secondary cells and batteries for renewable energy storage - General requirements and methods of test - Part 2: On-grid applications.” p. 108, 2015.

[54] “IEC 62933-2-1:2017 Electric energy storage (EES) systems - Part 2-1: Unit parameters and testing methods - General specifications Edition 1.0.” p. 85, 2017.

[55] J. Weniger, S. Maier, N. Orth, and V. Quaschning, “Energy Storage Inspection 2020 (English summary).” Berlin, Germany, 2020.

[56] J. Weniger, N. Orth, N. Böhme, and V. Quaschning Forschungsgruppe Solarspeichersysteme, “Stromspeicher-Inspektion 2Q19 (Präsentation deutsch).” Berlin, Germany, 2019.

[57] “Testbench Testverfahren zur Bestimmung der Effizienz von PV-Speichersystemen – Vom Leitfaden zum Standard.” 2020.

[58] L. Borgna, “Prüfbericht POWER STORAGE DC 6.0-11.5.” Bern, Switzerland, 2019.

[59] “POWER STORAGE DC 4.0 | 5.0 | 6.0.” RCT Power GmbH, Constance, Germany, 2019.

[60] C. Dupraz, H. Marrou, G. Talbot, L. Dufour, A. Nogier, and Y. Ferard, “Combining solar photovoltaic panels and food crops for optimising land use: Towards new agrivoltaic schemes,” *Renewable Energy*, vol. 36, no. 10. pp. 2725–2732, 2011.

[61] A. GOETZBERGER and A. ZASTROW, “On the Coexistence of Solar-Energy Conversion and Plant Cultivation,” *International Journal of Solar Energy*, vol. 1, no. 1. Taylor & Francis, pp. 55–69, 1982.

[62] R. Mead and R. W. Willey, “The Concept of a ‘Land Equivalent Ratio’ and Advantages in Yields from Intercropping,” *Experimental Agriculture*, vol. 16, no. 3. Cambridge University Press, pp. 217–228, 03-Jul-1980.

[63] H. Marrou, L. Guilioni, L. Dufour, C. Dupraz, and J. Wery, “Microclimate under agrivoltaic systems: Is crop growth rate affected in the partial shade of solar panels?,” *Agricultural and Forest Meteorology*, vol. 177. Elsevier B.V., pp. 117–132, 15-Aug-2013.

[64] R. W. Willey, “Evaluation and Presentation of Intercropping Advantages,” *Experimental Agriculture*, vol. 21, no. 2. Cambridge University Press, pp. 119–133, 1985.

[65] B. Müller, L. Hardt, A. Armbruster, K. Kiefer, and C. Reise, “Yield predictions for photovoltaic power plants: empirical validation, recent advances and remaining uncertainties,” *Progress in Photovoltaics: Research and Applications*, vol. 24, no. 4. pp. 570–583, 2016.

[66] D. Majumdar and M. J. Pasqualetti, “Dual use of agricultural land: Introducing ‘agrivoltaics’ in Phoenix Metropolitan Statistical Area, USA,” *Landscape and Urban Planning*, vol. 170. pp. 150–168, 2018.

[67] J. Weaver, “Agrovoltaics: a solar-powered safety net for Massachusetts farmers – pv magazine USA,” *pv magazine USA*. Aug-2018.

[68] J. Movellan, “Japan Next-Generation Farmers Cultivate Crops and Solar Energy - Renewable Energy World.” 08-Oct-2013.

[69] A. Bluechel and F. Baumgartner, “SOLAR SYSTEM WITH CLEANING DEVICE WO20141798934 (A1) und WO2014179893 (A1) — 2014-11-13.” p. 26, 2014.

[70] F. Baumgartner *et al.*, “‘Urban Plant’ Light-Weight Solar System for Parking and other Urban Double Use Applications,” *28th European Photovoltaic Solar Energy Conference and Exhibition*. Paris, France, pp. 2897–2901, 2013.

[71] G. A. Diem and A. Hügli, “Operating data fom a 640 kW HORIZON solar foldable PV plant on top of the wastewater retreatment basins in Chur, Switzerland.” Zizers, Switzerland, 2019.

[72] A. Sahu, N. Yadav, and K. Sudhakar, “Floating photovoltaic power plant: A review,” *Renewable and Sustainable Energy Reviews*, vol. 66. pp. 815–824, 2016.

[73] R. Cazzaniga, M. Cicu, M. Rosa-Clot, P. Rosa-Clot, G. M. Tina, and C. Ventura, “Floating photovoltaic plants: Performance analysis and design solutions,” *Renewable and Sustainable Energy Reviews*, vol. 81. pp. 1730–1741, 2018.

[74] P. Ranjbaran, H. Yousefi, G. B. Gharehpetian, and F. R. Astaraei, “A review on floating photovoltaic (FPV) power generation units,” *Renewable and Sustainable Energy Reviews*, vol. 110. pp. 332–347, 2019.

[75] K. Trapani and D. L. Millar, “Proposing offshore photovoltaic (PV) technology to the energy mix of the Maltese islands,” *Energy Conversion and Management*, vol. 67, no. March. pp. 18–26, 2013.

[76] I. Kougias *et al.*, “The potential of water infrastructure to accommodate solar PV systems in Mediterranean islands,” *Solar Energy*, vol. 136. Elsevier Ltd, pp. 174–182, 15-Oct-2016.

[77] M. Rosa-Clot and G. M. Tina, Eds., “Floating PV Plants.” Academic Press, p. 138, 2020.

[78] M. Rosa-Clot and G. M. Tina, “Submerged and Floating Photovoltaic Systems Modelling, Design and Case Studies.” Academic Press, p. 262, 2017.

[79] J. Haas, J. Khalighi, A. De La Fuente, S. U. Gerbersdorf, W. Nowak, and P.-J. Chen, “Floating photovoltaic plants: Ecological impacts versus hydropower operation flexibility.” 2019.

[80] R. Cazzaniga, M. Rosa-Clot, P. Rosa-Clot, and G. M. Tina, “Integration of PV floating with hydroelectric power plants,” *Heliyon*, vol. 5, no. 6. Elsevier Ltd, 01-Jun-2019.

[81] World Bank Group, ESMAP, and SERIS, “Where Sun Meets Water FLOATING SOLAR HANDBOOK FOR PRACTITIONERS.” Washington, DC, p. 155, 2019.

[82] Y.-K. Choi, “A Study on Power Generation Analysis of Floating PV System Considering Environmental Impact,” *International Journal of Software Engineering and Its Applications*, vol. 8, no. 1. pp. 75–84, 2014.

[83] Z. Wang, R. Carriveau, D. S.-K. Ting, W. Xiong, and Z. Wang, “A review of marine renewable energy storage,” *International Journal of Energy Research*, vol. 43, no. 12. pp. 6108–6150, 2019.

[84] A. M. Pringle, R. M. Handler, and J. M. Pearce, “Aquavoltaics: Synergies for dual use of water area for solar photovoltaic electricity generation and aquaculture,” *Renewable and Sustainable Energy Reviews*, vol. 80. pp. 572–584, 2017.

[85] K. Trapani and D. L. Millar, “The thin film flexible floating PV (T3F-PV) array: The concept and development of the prototype,” *Renewable Energy*, vol. 71. pp. 43–50, 2014.

[86] K. Trapani, “No TitleFlexible floating thin film photovoltaic (PV) array concept for marine and lacustrine environments.” pp. 1–217, 2014.

[87] K. Trapani and M. Redón Santafé, “A review of floating photovoltaic installations: 2007–2013,” *Progress in Photovoltaics: Research and Applications*, vol. 23, no. 4. pp. 524–532, 2015.

[88] H. Liu, V. Krishna, J. Lun Leung, T. Reindl, and L. Zhao, “Field experience and performance analysis of floating PV technologies in the tropics,” *Progress in Photovoltaics: Research and Applications*, vol. 26, no. 12. pp. 957–967, 2018.

[89] T. Reindl, “World’s largest Floating Solar Testbed - Overview and Findings,” *ACEF Deep Dive Workshop on Floating Solar*. Singapore, 2018.

[90] T. Reindl, “At the heart of floating solar: Singapore,” *PV Tech Power*, vol. 14, no. Buoyant Market. pp. 18–23, 2018.

[91] J. H. Selj *et al.*, “THE PERFORMANCE OF A FLOATING PV PLANT AT THE WEST COAST OF NORWAY,” *36th European Photovoltaic Solar Energy Conference and Exhibition*, vol. 46, no. 3. Marseilles, France, pp. 1763–1767, 2019.

[92] S. Z. Golroodbari and W. van Sark, “Simulation of performance differences between offshore and land-based photovoltaic systems,” *Progress in Photovoltaics: Research and Applications*, vol. n/a, no. n/a. .

[93] M. Dörenkämper, D. van der Werf, K. Sinapis, M. M. de Jong, and W. Folkerts, “INFLUENCE OF WAVE INDUCED MOVEMENTS ON THE PERFORMANCE OF FLOATING PV SYSTEMS,” *36th European Photovoltaic Solar Energy Conference and Exhibition*. Marseiles, France, pp. 1759–1762, 2019.

[94] M. Kumar and A. Kumar, “Experimental characterization of the performance of different photovoltaic technologies on water bodies,” *Progress in Photovoltaics*. p. 24, 2019.

[95] J. Suh, Y. Jang, and Y. Choi, “Comparison of electric power output observed and estimated from floating photovoltaic systems: A case study on the hapcheon dam, Korea,” *Sustainability*, vol. 12, no. 1. p. 14, 2020.

[96] R. Cazzaniga, M. Rosa-Clot, P. Rosa-Clot, and G. M. Tina, “Floating tracking cooling concentrating (FTCC) systems,” *2012 38th IEEE Photovoltaic Specialists Conference*. pp. 514–519, 2012.

[97] S. H. Kim, S. J. Yoon, W. Choi, and K. B. Choi, “Application of floating photovoltaic energy generation systems in South Korea,” *Sustainability*, vol. 8, no. 12. pp. 1–9, 2016.

[98] Koiné Multimedia, “Floating Tracking Cooling Concentrator.” [Online]. Available: http://www.koinemultimedia.eu/wp/sample-page/. [Accessed: 06-Oct-2020].

[99] P. Sterchele *et al.*, “WEGE ZU EINEM KLIMANEUTRALEN ENERGIESYSTEM Die deutsche Energiewende im Kontext gesellschaftlicher Verhaltensweisen.” Freiburg i.B., p. 66, 2020

ISBN 978-3-907281-04-8